INVESTIGATION OF THERMAL CHARACTERISTICS OF NAPHTHOXAZINES AND POLYNAPHTHOXAZINES VIA PYROLYSIS MASS SPECTROMETRY

A THESIS SUBMITTED TO
THE GRADUATE SCHOOL OF NATURAL AND APPLIED SCIENCES
OF
MIDDLE EAST TECHNICAL UNIVERSITY

BY

ZEYNEP KOYUNCU

IN PARTIAL FULFILLMENT OF THE REQUIREMENTS
FOR
THE DEGREE OF MASTER OF SCIENCE
IN
CHEMISTRY

MAY 2009

Approval of the thesis:

INVESTIGATION OF THERMAL CHARACTERISTICS OF NAPHTHOXAZINES AND POLYNAPHTHOXAZINES VIA PYROLYSIS MASS SPECTROMETRY

submitted by **ZEYNEP KOYUNCU** in partial fulfillment of the requirements for the degree of **Master of Science in Chemistry Department, Middle East Technical University** by,

Prof. Dr. Canan Özgen ______________________
Dean, Graduate School of **Natural and Applied Sciences**

Prof. Dr. Ahmet M. Önal ______________________
Head of Department, **Chemistry**

Prof. Dr. Jale Hacaloğlu ______________________
Supervisor, **Chemistry Dept., METU**

Examining Committee Members:

Prof. Dr. Duygu Kısakürek ______________________
Chemistry Dept., METU

Prof. Dr. Jale Hacaloğlu ______________________
Chemistry Dept., METU

Prof. Dr. Ahmet M. Önal ______________________
Chemistry Dept., METU

Prof. Dr. Zuhal Küçükyavuz ______________________
Chemistry Dept., METU

Assist. Prof. Dr. Tamer Uyar ______________________
Materials Science and Nanotechnology Institute, Bilkent University

Date: 20/05/2009

I hereby declare that all information in this document has been obtained and presented in accordance with academic rules and ethical conduct. I also declare that, as required by these rules and conduct, I have fully cited and referenced all material and results that are not original to this work.

Name, Last name: Zeynep Koyuncu

Signature:

ABSTRACT

INVESTIGATION OF THERMAL CHARACTERISTICS OF NAPHTHOXAZINES AND POLYNAPHTHOXAZINES VIA DIRECT PYROLYSIS MASS SPECTROMETRY

KOYUNCU, Zeynep
M.Sc., Department of Chemistry
Supervisor: Prof. Dr. Jale Hacaloğlu

May 2009, 78 pages

In this study, polymerization mechanisms of aromatic (C_6H_5 or C_6F_5) and alkyl (CH_3, C_2H_5, C_3H_7, C_6H_{13}, $C_{12}H_{25}$ or $C_{18}H_{37}$) amine based naphthoxazine monomers (15-Na, 15Na-C1, 15Na-C2, 15Na-C3, 15Na-C6, 15Na-C12 and 15Na-C18) and thermal degradation mechanisms of polynaphthoxazines synthesized by curing the naphthoxazine monomers (P-15-Na, P-15NaF, P-15Na-C1, P-15Na-C2, P-15Na-C3, P-15Na-C6, P-15Na-C12 and P-15Na-C18) were studied by direct pyrolysis mass spectrometry.

During the curing process, the evolutions of monomer and low mass aromatic or alkyl amines were detected below the curing temperature. The mass spectrometry findings indicated that the monomers were subjected to evaporation and degradation to a certain extent but also to polymerization during the curing process.

It has been determined that the polymerization of aromatic amine based naphthoxazine monomer proceeded through the aniline units, either by coupling of the radicals produced by the ring opening of the side chains or by substitution to the benzene ring of aniline. However, even if no direct evidence to confirm polymerization by attack of $-NCH_2$ groups to naphthalene ring was detected, it is not possible totally eliminate its existence.

The evolution of aniline, the main thermal degradation product for this polymer was observed at relatively low temperatures indicating that thermal decomposition started by elimination of aromatic amine involving linkages. Coupling of $-CH_2$ groups generated by loss of aniline, yielded naphthoxazines with unsaturated linkages that can recombine and form a crosslinked structure with higher thermal stability.

Similarly, the polymerization of naphthoxazines based on alkyl amines followed opposing paths. The mass spectral data indicated that the coupling of alkyl amine radicals was the main polymerization pathway.

Again, thermal decomposition of alkyl amine based naphthoxazines was started by loss of alkyl amines and diamines. The crosslinked structures produced by coupling of the radicals generated by lose of alkyl amines decomposed at relatively high temperatures.

Keywords: aromatic amine based naphthoxazine, alkyl amine based naphthoxazine, direct pyrolysis mass spectrometry, polymerization, thermal degradation

ÖZ

NAFTOKSAZİNLERİN VE POLİNAFTOKSAZİNLERİN ISIL ÖZELLİKLERİNİN DİREKT PİROLİZ KÜTLE SPEKTROMETRESİ İLE İNCELENMESİ

KOYUNCU, Zeynep
Yüksek Lisans, Kimya Bölümü
Tez Yöneticisi: Prof. Dr. Jale Hacaloğlu

Mayıs 2009, 78 sayfa

Bu çalışmada, direkt piroliz kütle spektometre ile aromatik (C_6H_5 veya C_6F_5) ve alkil (CH_3, C_2H_5, C_3H_7, C_6H_{13}, $C_{12}H_{25}$ veya $C_{18}H_{37}$) amin bazlı naftoksazin monomerlerin (15Na-C1, 15Na-C2, 15Na-C3, 15Na-C6, 15Na-C12 ve 15Na-C18) polimerizasyon mekanizmaları ve naftoksazin monomerlerinin pişirilmesi ile sentezlenen polinaftoksazinlerin (P-15Na, P-15Na-C1, P-15Na-C2, P-15Na-C3, P-15Na-C6, P-15Na-C12 ve P-15Na-C18) ısıl bozunum mekanizmaları çalışılmıştır.

Pişirme işlemi esnasında, monomerin ve düşük kütleye sahip aromatik veya alkil aminlerin pişirme sıcaklığından önce buharlaştıkları belirlenmiştir. Kütle spektrometre bulguları pişirme işlemi esnasında monomerlerin bir miktar buharlaştığını ve bozunduğunu bununla beraber aynı zaman da polimerleştiğini göstermiştir.

Anilin bazlı naftoksazin monomerin polimerizasyonunun anilin birimleri üzerinden, ya yan grupların halka açılımı ile oluşan radikallerin birleşmesi ya da anilinin benzen halkasına tutunması ile olduğu belirlenmiştir. Ancak, $-NCH_2$ gruplarının naftalin halkasına saldırması ile polimerizasyon gerçekleştiğini doğrulayan doğrudan bir kanıt bulunmamış olsa bile, bunun varlığını tamamen yok saymak da mümkün değildir.

Bu polimer için ana bozunum ürünü olan anilinin göreceli olarak düşük sıcaklıklarda buharlaştığının gözlemlenmesi, ısıl parçalanmanın aromatik amin içeren halkaların çıkması ile başladığını göstermektedir. Anilinin kopması ile üretilen $-CH_2$ gruplarının birleşmesi, tekrar birleşebilen ve yüksek ısıl kararlılığa sahip çapraz bağlanmış bir yapı oluşturabilen doymamış bağları olan naftoksazinlerin oluşmasını sağlamıştır

Benzer şekilde, alkil amin bazlı naftoksazinlerin polimerizasyonu farklı yollar takip etmiştir. Kütle spektral veriler ana polimerizasyon yolunun alkil amin radikallerinin birleşmesi olduğunu göstermiştir.

Yine, alkil amin bazlı naftoksazinlerin parçalanması alkil amin ve diaminlerin kopması ile başlamıştır. Alkil aminlerin kopması ile üretilen radikallerin birleşmesi sonucunda oluşan çapraz bağlanmış yapılar göreceli olarak yüksek sıcaklıklarda parçalanmıştır.

Anahtar kelimeler: aromatik amin bazlı naftoksazin, alkil amin bazlı naftoksazin, direkt piroliz kütle spektometrisi, polimerizasyon, ısıl bozunum

TO MY FAMILY

ACKNOWLEDGEMENT

Firstly I would like to express my gratefulness to my supervisor Prof. Dr. Jale Hacaloğlu for her guidance, understanding, encouragements, patience and valuable comments throughout my thesis. Also, I would like to express my special thanks to Assist. Prof. Dr. Tamer Uyar and Prof. Dr. Hatsuo Ishida for sharing information related to my study.

I would also express my special thanks to Şafak Kaya and Yusuf Nur for their friendship, patience, technical support and encouragements throughout my study. I would like to thank to my lab-mate Ayşegül Gediközer Elmacı for her friendship and encouragements.

I would also like to give my special thanks to Demet Asil, Buket Bezgin, Merve İçli for their friendship and support.

Finally, I would like to thank to my family for their love, supporting all my decisions and being always behind me.

TABLE OF CONTENTS

ABSTRACT iv
ÖZ vi
ACKNOWLEDGEMENT ix
TABLE OF CONTENTS x
LIST OF FIGURES xii
LIST OF SCHEMES xv
ABBREVIATIONS xvi
CHAPTERS 1

1. INTRODUCTION 1
 1.1 Thermosets 1
 1.2 Phenolic resins 1
 1.3 Benzoxazines 2
 1.4 Naphthoxazines 5
 1.5 Thermal Degradation 7
 1.6 Pyrolysis 7
 1.7 Pyrolysis Mass Spectrometry Techniques 8
  1.7.1 Pyrolysis GC/MS 9
  1.7.2 Direct Pyrolysis-MS 9
  1.7.3 Applications of Pyrolysis Mass Spectrometry Techniques 10
 1.8 Aim of the study 10

2. EXPERIMENTAL 12
 2.1. Materials 12
 2.2 Mass Spectrometry 14

3. RESULTS AND DISCUSSION 16
 3.1 Polymerisation and degradation mechanism of aromatic amine-based naphthoxazine (15-Na) 17
  3.1.1 Curing of aromatic amine-based naphthoxazine monomer (15-Na). 17
  3.1.2. Pyrolysis of aromatic amine-based polynaphthoxazine 21
  3.2.1 Curing of alkyl-functional naphthoxazine monomers 32
   3.2.1.1 Curing of 15Na-C1 monomer 32
   3.2.1.2 Curing of 15Na-C2 monomer 34
   3.2.1.3 Curing of 15NaC3 monomer 36

3.2.1.4 Curing of 15Na-C6 monomer 38
3.2.1.5 Curing of 15Na-C12 monomer 40
3.2.1.6 Curing of 15Na-C18 monomer 42
3.2.2 Pyrolysis of alkyl-functional polynaphthoxazines 52
3.2.2.1 Pyrolysis of 15Na-C1 polymer (P15Na-C1) 52
3.2.2.2 Pyrolysis of 15Na-C2 polymer (P15Na-C2) 54
3.2.2.3 Pyrolysis of 15Na-C3 polymer (P15Na-C3) 56
3.2.2.4 Pyrolysis of 15Na-C6 polymer (P15Na-C6) 58
3.2.2.5 Pyrolysis of 15Na-C12 polymer (P15Na-C12) 60
3.2.2.6 Pyrolysis of 15Na-C18 polymer (P15Na-C18) 62
4. CONCLUSIONS 73
REFERENCES 75

LIST OF FIGURES

Figure 1: a. The total ion current (TIC) curve and the pyrolysis mass spectra recorded at b. 100 °C c. 210 °C and d. after 3.6 minute at 210 °C during the heating process of 15-Na 17

Figure 2: Single ion evolution profiles of some characteristic products detected during the curing process of 15-Na (Note: the intensities are normalized by a number factor as shown in the figure) 20

Figure 3: The TIC curve and the pyrolysis mass spectra recorded during the heating process of the cured monomer, poly15-Na 22

Figure 4: The single ion evolution profiles of fragments involving N-substituted anilines 23

Figure 5: The evolution profiles of some of the products involving naphthoxazine units or N-alkyne aniline 29

Figure 6: The single ion pyrograms of some characteristic products recorded during pyrolysis of cured naphthoxazine involving pentafluoroaniline 31

Figure 7: a. The total ion current curve and the mass spectra recorded at b. 210 °C and c. after 0.67 minute at 210 °C for 15Na-C1 monomer 33

Figure 8: Single ion evolution products of some characteristic products detected during the curing process of 15Na-C1 monomer 34

Figure 9: a. The total ion current curve and the mass spectra recorded at b. 170 °C and c. after 1 minute at 170 °C for 15Na-C2 monomer 35

Figure 10: Single ion evolution products of some characteristic products detected during the curing process of 15Na-C2 monomer 36

Figure 11: a. The total ion current curve and the mass spectra recorded at b. 150 °C and c. after 2 minute at 150 °C for 15Na-C3 monomer 37

Figure 12: Single ion evolution products of some characteristic products detected during the curing process of 15Na-C3 monomer 38

Figure 13: a. The total ion current curve and the mass spectra recorded at b. 125 °C and c. after 3 minute at 150 °C for 15Na-C6 monomer 39

Figure 14: Single ion evolution products of some characteristic products detected during the curing process of 15Na-C6 monomer 40

Figure 15: a. The total ion current curve and the mass spectra recorded at b. 120 °C and c. after 8 minute at 150 °C for 15Na-C12 monomer 41

Figure 16: Single ion evolution products of some characteristic products detected during the curing process of 15Na-C12 monomer 42

Figure 17: a. The total ion current curve and the mass spectra recorded at b. 130 °C and c. after 8 minute at 150 °C for 15Na-C18 monomer 43

Figure 18: Single ion evolution products of some characteristic products detected during the curing process of 15Na-C18 monomer 44

Figure 19: TIC curves of alkyl amine based naphtoxazines 45

Figure 20: Single ion evolution profiles of some products generated during EI ionization of alkyl amine based naphthoxazine monomers 47

Figure 21: a. The total ion current curve and the mass spectra recorded at b. 440 °C and c. 390 °C d. 310 °C recorded during the pyrolysis of P15Na-C1 polymer 53

Figure 22: Single ion evolution products of some characteristic products detected during the curing process of P-15Na-C1 polymer 54

Figure 23: a. The total ion current curve and the mass spectra recorded at b. 430 °C and c. 310 °C during the pyrolysis of P15Na-C2 polymer 55

Figure 24: Single ion evolution products of some characteristic products detected during the curing process of P-15Na-C2 polymer 56

Figure 25: a. The total ion current curve and the mass spectra recorded at b. 440 °C and c. 320 °C and d. 270 °C during the pyrolysis of P15Na-C3 polymer 57

Figure 26: Single ion evolution products of some characteristic products detected during the curing process of P-15Na-C3 polymer 58

Figure 27: a. The total ion current curve and the mass spectra recorded at b. 430 °C and c. 320 °C and d. 270 °C during the pyrolysis of P15Na-C6 polymer 59

Figure 28: Single ion evolution products of some characteristic products detected during the curing process of P-15Na-C6 polymer 60

Figure 29: a. The total ion current curve and the mass spectra recorded at b. 440 °C and c. 325 °C and d. 240 °C during the pyrolysis of P15Na-C12 polymer 61

Figure 30: Single ion evolution products of some characteristic products detected during the curing process of P-15Na-C12 polymer 62

Figure 31: a. The total ion current curve and the mass spectra recorded at b. 440 °C and c. 330 °C and d. 270 °C during the pyrolysis of P15Na-C18 polymer 63

Figure 32: Single ion evolution products of some characteristic products detected during the curing process of P-15Na-C18 polymer 64

Figure 33: TIC curves of alkyl amine based polynaphthoxazines 65

Figure 34: Single ion evolution profiles of some products detected during pyrolysis of alkyl amine based polynaphtoxazines 70

LIST OF TABLES

Table 1. Heating profiles used in curing and thermal degradation behavior of polynaphthoxazines at a heating rate of 20 °C/min 13

Table 2. Peaks present in the low temperature pyrolysis mass spectra, the proposed structures and the temperatures at which the product yields were maximized 24

Table 3. Peaks present in the high temperature pyrolysis mass spectra and the proposed structures 30

Table 4. Peaks present in the pyrolysis mass spectra of polynaphthoxazines, the proposed structures and the temperatures at which the product yields were maximized 68

LIST OF SCHEMES

Scheme 1: Synthesis of naphthoxazines 5

Scheme 2: Difunctional naphthoxazines 6

Scheme 3: Formation of alkyl and aromatic amine based naphthoxazines 12

Scheme 4: The main fragmentation patterns proposed for 15-Na during EI ionization 19

Scheme 5: 1. The linkages formed during the polymerisation of aromatic amine-based bifunctional naphthoxazines 2. Generation of aniline and unsaturated linkages by thermal degradation of Poly15-Na 26

Scheme 6 . The linkages formed during the polymerisation of aromatic amine based bifunctional naphthoxazines 27

Scheme 7: The main fragmentation pattern proposed for alkyl amine-based naphthoxazine monomers during EI ionization 46

Scheme 8: Fragmentation patterns proposed for alkyl amine-based naphthoxazine monomers during EI ionization 48

Scheme 9: Fragmentation patterns proposed for alkyl amine-based naphtoxazine monomers during EI ionization 49

Scheme 10: Proposed polymerization mechanism for alkyl amine based naphthoxazines 71

Scheme 11: Coupling of the radicals generated by lose of alkyl amines from polynaphtoxazines 72

ABBREVIATIONS

T_g	Glass transition temperature
EI	Electron Impact
GC	Gas Chromatography
DSC	Differential Scanning Calorimetry
TGA	Thermal Gravimetric Analysis
MS	Mass Spectrometry
FTIR	Fourier Transform Infrared Resonance
Py	Pyrolysis
DP-MS	Direct Pyrolysis- Mass Spectrometry
TIC	Total Ion Current
Da	Dalton
M	Monomer

CHAPTER 1

INTRODUCTION

1.1 Thermosets

Thermosets are crosslinked polymers which are obtained through heat, irradiation or a chemical reaction. This process is called curing and after curing, thermosets become hard and rigid which cannot be reshaped. When cured thermosets are heated, they may soften but do not melt or flow. Phenolic resins and plastics are the origin of thermosets.

Different types of thermosets are present. Reinforced products are obtained by resins and modifiers, such as plasticizers, fibers. However, base polymers and raw materials do not include additives. These raw materials are present as powders, pellets, liquids or granules before curing. The curing process provides crosslinking and converts resins to plastics and rubbers. Crosslinking provides three dimensional (3-D) rigid structures with higher molecular weight and higher melting point. By this process material solidifies and the 3-D structure of thermosets makes them suitable for high temperature applications.

1.2 Phenolic resins

Phenolic resins are synthetic thermosetting resins formed by condensing phenol with various aldehydes. Phenolic resins have high carbon content and curing of these carbons yields durable char which maintains strengthening in severe heat applications.

In general, phenolics are obtained by the polymerization of the resin on a base material. The base material used, paper, glass or cotton, etc., depends on the intended application of the final product. Phenolic resins with high temperature stability and strong mechanical strength find applications in many fields of industry from commodity and construction materials to the high technology electronic and aerospace industry. It means that, cured phenolic resin provides the product rigidity necessary to maintain structural integrity and dimensional stability even if the conditions are very strong. However, besides these good properties these resins have weaknesses such as brittleness, release of by-products during curing, use of strong acids and alkalines as catalysts, and short shelf life. To eliminate these disadvantages, polybenzoxazines, a new class of phenolic resins with a similar main chain structure, have been developed [1].

1.3 Benzoxazines

Benzoxazines are synthesized from phenols, formaldehyde and amines. The chemical structure of benzoxazines can be changed by using different phenols and amines. Polybenzoxazines have better mechanical strength compared to other phenolic resins and have similar T_g (glass transition temperature) with high performance epoxy materials. Additionally, some carbon/polybenzoxazine composites show superb heat and mechanical properties, near to the properties of polyimide composites, but with better processability [2].

The use of variety of phenols and amines during the synthesis of polybenzoxazines provides structural design flexibility, thus, the specific properties of the resulting polymer can be adapted for the target application. Various types of high performance polybenzoxazines can be obtained by ring-opening polymerization of these cyclic benzoxazine monomers.

High thermal stability is one of the most important characteristic of polybenzoxazines. They can have a char yield nearly 80% (at 800° C under nitrogen) with retaining the ease of processing [3]. Polybenzoxazines also have other unique properties such as, high glass transition temperature, excellent thermal, mechanical and electrical properties, low melt viscosity, low water absorption and low coefficient of thermal expansion. In addition to these, during polymerization of benzoxazines by heat treatment, curing, no catalyst is needed and no byproducts and volatiles are generated. These provide void-free thermosets with excellent dimensional stability. These properties of polybenzoxazines make them a good alternative to high performance composites [1, 2, 4-6].

Benzoxazines were first synthesized by Cope and Holy in 1944 by using phenols, formaldehyde, and amines as starting materials through Mannich reactions [7]. Various types of benzoxazines were synthesized by Burke and his colleagues between 1950s and 1960s [8-16].

The first polybenzoxazines obtained by curing of benzoxazine monomers were done by Schreiber [17-18]. Riess and his colleagues studied the polymerization of mono functional benzoxazines with and without phenol as an initiator and they obtained linear polymers having molecular weight less than 4000 g/mol [19]. Several researches on different properties of polybenzoxazines showed that various types of polybenzoxazine can be synthesized by changing the structure of the benzoxazine monomers, curing conditions and initiators [2, 20-21]. Syntheses of polybenzoxazines are typically achieved above 200 ^{0}C where the benzoxazine ring opens by thermal energy and produce crosslinked polymers. Thermal decomposition depends on the molecular structure of the polymer, yet, in general, the first weight loss of polybenzoxazines is observed around 275 ^{0}C and the main degradation takes place in the range 300-450 ^{0}C.

Although, benzoxazines have molecular design flexibility as a result of possibility of using different starting materials, the majority of the benzoxazine monomers are in the form of powder and making thin films from these monomers may be quite difficult. These monomers can only be processed by melt molding process. Additionally, when benzoxazine monomers are cured to obtain polybenzoxazines they become brittle. To overcome these difficulties several strategies have been applied and several studies have been performed to alter the thermal and thermooxidative stability of benzoxazines [5, 22-26].

It was shown that chemical modification of novolac resins with benzoxazine rings or grafting of various phosphorous compounds to benzoxazine modified resins forms nonflammable coatings [27-28]. It was also reported that benzoxazine monomers with additional polymerizable functional groups form highly thermally stable cross-linked networks [29-30]. For this purpose, different curable functional groups to phenol and/or amine group were added and design flexibility for benzoxazines was obtained. Extra curable groups, acetylene, allyl, etc. [30-31], were integrated into the structure to enhance the thermal stability of benzoxazines [4, 32-35]. For example, Takeichi and Agag added propargyl [23] and allyl [5] groups to benzoxazines to obtain higher glass transition temperature and higher thermal stability. Acetylene [30], maleimide [36] and phenylphosphene oxide [37] were added to benzoxazine by Ishida and his coworkers in order to increase glass transition temperature and char ratio. Other examples for the curable groups added to the structure were ethynyl [3] and nitrile [30]. By this method high performance polybenzoxazines were obtained.

Yağcı and coworkers, proposed a macromonomer method for obtaining polybenzoxazines with polymer segments involving good mechanical properties by using Atom Transfer Radical Polymerization (ATRP) [38] and Ring Opening Polymerization (ROP) [39] methods. They added benzoxazines to conventional polymers such as polystyrene [38], poly(e-caprolacton) [39], poly(methylmethacrylate) [40], poly(propylene oxide) [41], poly(etherester) [42] and polymerized these macromolecules in order to obtain high performance polybenzoxazines. Recently, to increase the char yield, polybenzoxazines consisting polyetherester [42] and 1,2 triazol [43] have been synthesized.

Although several studies have been performed for synthesis and modification of polybenzoxazines, practical applications are still limited because of the difficulties in making thin films from these powdered polymers, brittleness of the materials and low molecular weight. Recently, researches on another group of phenolic resins, polynaphthoxazines were started to appear in the literature. By replacing the starting material, phenol of benzoxazines with naphtol naphthoxazines can be obtained.

1.4 Naphthoxazines

Polymers involving condensed polynuclear aromatic structure, for instance naphthalene, show high thermal stability because of the extended double bond conjugation.

Naphthalene ring has been integrated in many polymers. Epoxy [44-45], bismaleimides [46], phenolic resin [47-48], polyester [49], polyamides [50], poly(ester amide) [51], poly(ester-imide) [52], polyimides [53-54], poly(amideimide), [55-57] and poly(aryl ether ketone) [58] are some examples for these polymers.

Naphthoxazines were synthesized by reacting napthol, formaldehyde and amines (Scheme 1). The solvent used, the temperature applied and the basicity of the amine have important effects on the yield of the naphthoxazine monomer formed.

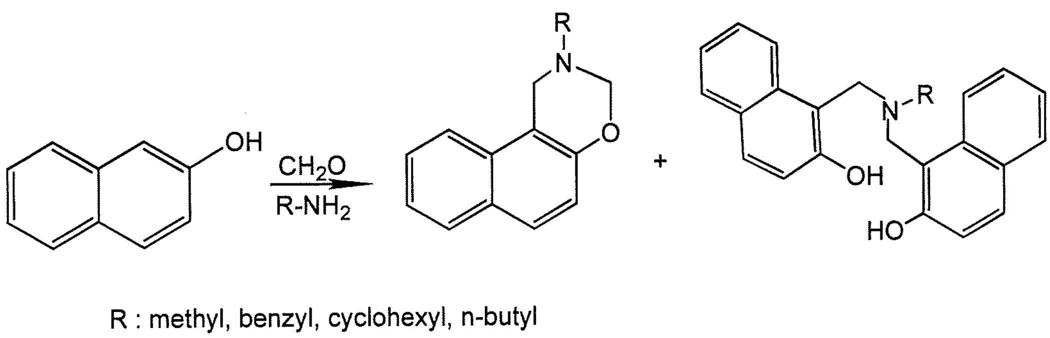

Scheme 1: Synthesis of naphthoxazines

Unexpectedly, naphthoxazines do not have as high thermal stability as benzoxazines. Moreover, it has been determined that naphthoxazine monomers evaporate during curing so the use of autoclave is needed.

Various difunctional naphthoxazines were synthesized in order to improve the thermal stability and char yield of polynaphthoxazines. Difunctional naphthoxazines were synthesized either by reacting difunctional amines, formaldehyde and napthol (2Na-a) or by reacting primary amines, formaldehyde and dihydroxynaphthalene (Scheme 2) [1, 9, 15-16, 32, 59-60].

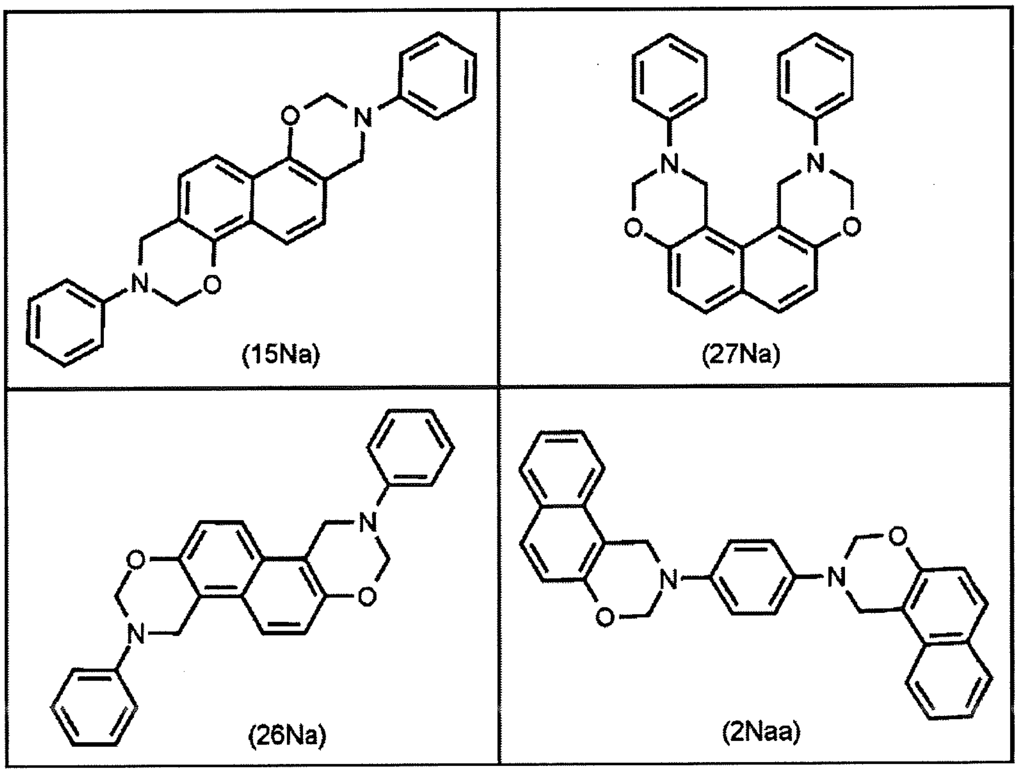

Scheme 2: Difunctional naphthoxazines

Aniline based difunctional naphthoxazine resins were synthesized by Shen and Ishida [32]. Agag synthesized a series of allylamine-based naphthoxazines with extended network via the polymerization of allyl functionality [61]. However, the thermal degradation/evaporation of the monomers again occurred below 200 ^{0}C [61]. The same group, as a result of curing, was able to obtain void-free resin structure from only one of the four different polyfunctional naphthoxazines [32]. Moreover, Ishida and his coworkers also prepared naphthoxazines by changing the phenolic precursor as hydroxynaphthalenes in order to increase the thermal stability and char yield [32, 61]. On the other hand, Yagci and his research group, again applied macromonomer method and prepared naphthoxazine terminated polymers of poly(propylene oxide)s and poly(3-caprolactone) (PCL) to improve both thermal and mechanical properties [39, 41].

The knowledge of curing and thermal degradation mechanisms of thermosets is very important not only to determine the necessary modifications but also to investigate the application areas. Yet, only few studies appeared in the literature on curing and thermal degradation mechanisms of naphthoxazines and polynaphthoxazines [32, 61-62].

1.5 Thermal Degradation

Thermal degradation is breaking of chemical bonds of materials by thermal energy. Various techniques are used to investigate the thermal degradation behavior, such as thermal stability, thermal degradation products and mechanisms.

In general, in order to detect thermal stability of materials, thermogravimetric analysis (TGA) and differential scanning calorimetry (DSC) techniques are used.

Thermogravimetric Analysis (TGA) is a technique which measures weight loss as a function of temperature isothermally or as a function of temperature by applying heat. TGA experiments can be performed under different conditions such as in an atmosphere of nitrogen, helium, air, other gas, or in vacuum. This technique is used to determine thermal characteristics of the sample such as polymers. TGA gives information on thermal stability, weight loss, decomposition temperature, etc. The technique can be combined with FTIR or mass spectrometer (MS) to identify the evaporated/decomposed products causing the weight loss.

Differential scanning calorimetry (DSC) is a technique which measures the heat flow between the sample and an inert reference material as a function of time and temperature. In this technique, the heat difference is detected as a peak. DSC gives information about phase transitions such as glass transition, melting, polymerization, curing, decomposition and polymerization. Heat capacity changes and energy changes show these transitions.

1.6 Pyrolysis

Pyrolysis is the thermal degradation of materials in an inert atmosphere or in vacuum. The relative strength of chemical bonds determines the thermal stability of that material. During heating, thermal energy is delivered to all excitation modes if the vibrational excitation is greater than the bond energy, the molecule will fragment into smaller fragments. Structure and fragmentation manner of the original molecule can be understood by analyzing these processes and fragments. Thermal degradation of a material at a specific temperature is always the same, in other words occurs in a reproducible way. Controlling the pyrolysis temperature is important for these analyses. If the temperature is under the pyrolysis temperature, process will be too slow to be analytically useful. When the temperature is higher than the pyrolysis temperature, fragments produced may be very small and nonspecific. Another parameter that should be controlled is the heating rate. If high heating rate is used thermal equilibrium may not be obtained among all vibrational modes and degradation may be more selective. For that reason, energy parameters, time, temperature and heating rate should be specific for a specific material to have a reproducible degradation pathway for that material.

Pyrolysis is applied to all types of samples gaseous, liquids or solids, particularly polymers. Moreover, this method is used to analyze big molecules that can not be easily analyzed by decomposing them into smaller molecules which can be detectable in an easier way. Pyrolysis is also applied for analysis of a multi component system by separating the components according to volalities and/or thermal stabilities. The resulting fragments are separated and analyzed via different techniques such as mass spectrometry (MS), gas chromatography (GC) and fourier-transform infrared (FT-IR) spectrometry. When compared to other techniques, mass spectrometry techniques, Py-GC/MS or DP-MS, are more advantageous because of their high reproducibility and sensitivity and rapid rate of analysis. Furthermore, very small amounts of samples are sufficient [63-69].

1.7 Pyrolysis Mass Spectrometry Techniques

Two types of pyrolysis mass spectrometry techniques are gas chromatography/ mass spectrometry (Py-GC/MS) and direct pyrolysis mass spectrometry (DP-MS) [70].

1.7.1 Pyrolysis GC/MS

In this technique, firstly, thermal degradation of the sample occurs in a pyrolyzer and then the fragments are separated by gas chromatograph and lastly analyzed via mass spectrometer.

Each pyrolyzate can be determined with its pyrogram based on their mass spectra. But, sometimes, because of their molecular weight and high polarity, some thermal degradation products are locked in pyrolytic zone, injection system or capillary column and may not be detected. Additionally, in some cases, even if polar pyrolyzates are produced, separation through the gas chromatography column shows low reproducibility, peak tailing properties, long elution times and sometimes no chromatographic peak. Derivatization of polar materials to nonpolar structures solves the problem totally.

1.7.2 Direct Pyrolysis-MS

In this technique, thermal degradation of the sample occurs inside the mass spectrometer and degradation products are forwarded towards the ion source and ionized there immediately [63]. The ionized thermal degradation products further fragments because of the excess energy and then all the ions are detected via mass spectrometer.

The high vacuum inside the mass spectrometer quickly transports the degradation products from the heating zone so condensation reactions and secondary reactions are blocked. Additionally, unstable degradation products can also be detected by the rapid detection system of the mass spectrometers. Thus, thermal stability, degradation products and decomposition mechanism of the compounds, mostly polymers can be determined. The data can also be used to characterize the structure of the compounds involved [63-66, 69, 71]. However, as thermal degradation products further dissociates inside the mass spectrometer during the ionization process, pyrolysis mass spectra of polymers are usually very complicated. Moreover, the fragments which have the same mass to charge ratio contributes to the intensity of the same peak in the mass spectrum. Therefore, interpretation of the mass spectra is quite difficult. In this technique, the total ion current (TIC), curve, the variation of total ion yield as a function of temperature, is recorded in real time. In the TIC curve presence of more than one peak indicates a multi-component sample or presence of units with different thermal stabilities. Additionally, degradation products can be separated as a function of volatility and/or thermal stability by scanning single ion pyrograms. In direct pyrolysis mass spectrometry technique, variation of peak intensity as a function temperature, evolution profile, is as crucial as detection of a peak. In order to identify the thermal degradation products and/or fragmentation pathway, the variations in the single ion evolution profiles can be compared.

1.7.3 Applications of Pyrolysis Mass Spectrometry Techniques

Pyrolysis mass spectrometry techniques are used in many fields such as science, industrial and technological areas. These techniques are mainly used in polymer science to determine the thermal characteristics and structure of homopolymers and copolymers, molecular weight distribution, order of monomers in the polymer, crosslinking, branching, end groups, chain substitution, grafting, additives and impurities [63-65, 72-74].

Pyrolysis MS techniques are also used to analyze coatings, paints, contamination, adhesives and unknown materials. Some other fields where pyrolysis MS techniques are used for analyses are environmental chemistry, biochemistry, clinical science, pathology, forensic science, toxicology, food science [11], wood science and extraterrestrial studies. In all these application areas, pyrolysis MS technique both jump the isolation and amplification steps needed for separating the component from the complicated chemical, clinical, or environmental matrix and provides fast identification [70].

1.8 Aim of the study

The aim of this study is to investigate:

1) The polymerization mechanisms of aromatic amine (aromatic = C_6H_5 or C_6F_5) and alkyl amine (where alkyl = CH_3, C_2H_5, C_3H_7, C_6H_{13}, $C_{12}H_{25}$ or $C_{18}H_{37}$)

based naphthoxazine monomers (15-Na, 15Na-C1, 15Na-C2, 15Na-C3, 15Na-C6, 15Na-C12 and 15Na-C18) during curing

2) The thermal degradation products and mechanisms of the polynaphthoxazines (P-15-Na, P-15NaF, P-15Na-C1, P-15Na-C2, P-15Na-C3, P-15Na-C6, P-15Na-C12 and P-15Na-C18) prepared by curing, via direct pyrolysis mass spectrometry technique.
3) Furthermore, the effects of alkyl-chain length on curing mechanism and thermal characteristics are studied.

CHAPTER 2

EXPERIMENTAL

2.1. Materials

The aromatic and alkyl amine based naphthoxazine monomers and the corresponding polynaphthoxazines were synthesized and characterized by Tamer Uyar as described in the literature [75]. The formation of alkyl and aromatic amine based naphthoxazine monomers are shown in Scheme 3.

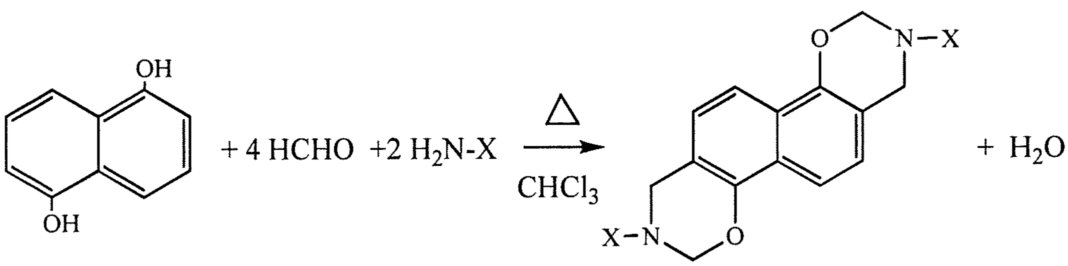

where X = C_6H_5, C_6F_5, CH_3, C_2H_5, C_3H_7, C_6H_{13}, $C_{12}H_{25}$ or $C_{18}H_{37}$

Scheme 3: Formation of alkyl and aromatic amine based naphthoxazines

In Table I heating profiles and thermal behavior of polynaphthoxazines determined by Differential Scanning Calorimetry (DSC) and Thermogravimetric analyses (TGA) are summarized [75].

Table 1. Heating profiles used in curing and thermal degradation behavior of polynaphthoxazines at a heating rate of 20 °C/min

Material	Monomer 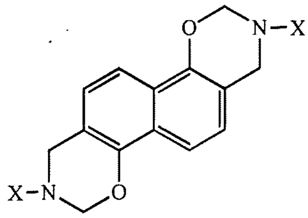	Curing Temperature	T_d[1] 5%	T_d[2] 10%	Char yield[3]
15Na-C18 MWt = 746	X=$C_{18}H_{37}$	150 °C -1hour 170 °C -1hour	188	212	19
15Na-C12 MWt = 578	X=$C_{12}H_{25}$	150 °C -1hour 170 °C -1hour	216	248	29
15Na-C6 MWt = 410	X=C_6H_{13}	150 °C -1hour 170 °C -1hour	223	248	36
15Na-C3 MWt = 326	X=C_3H_7	150 °C -1hour 170 °C -1hour	224	250	46
15Na-C2 MWt = 298	X=C_2H_5	170 °C -2hours	249	278	47
15Na-C1 MWt = 270	X=CH_3	210 °C -2hours	325	424	66
15Na MWt = 394	X=C_6H_5	210 °C -2hours			
15Na-F MWt = 574	X=C_6F_5	210 °C -2hours			

[1] The temperature at which 5% weight loss observed in TGA under nitrogen atmosphere

[2] The temperature at which 10% weight loss observed in TGA under nitrogen atmosphere

[3] The char yield at 800 ^{0}C under nitrogen atmosphere

2.2 Mass Spectrometry

In this study, 5973 HP quadruple mass spectrometry system coupled to a JHP SIS direct insertion probe was used for direct pyrolysis experiments. During the pyrolysis, mass spectra were recorded at a scan rate of 2 scan/s in the mass range of 10-800 Da. Mass spectrometers have three main parts which are operated in high vacuum. The mass spectrometer consists of four main components which are a sample inlet, an ion source, a mass analyzer and an ion detector.

1. *Sample inlet:* sample introduction to mass spectrometer is done by direct insertion probe.

   The direct insertion probe used in this study is a stainless steel pipe with a tip suitable to introduce the micro sample vial to the mass spectrometer. It consists of a thermocouple to measure the temperature at the tip of the probe. The heating profile is controlled by using probe's software.

2. *Ion source*: Electron impact (EI) ionization source is used to ionize the pyrolysis products. In electron impact ionization, the molecules are bombarded with high energy electrons and by the loss of electron from the sample molecule, molecular and/or fragment cations are generated. In this study, 70 eV EI mass spectra were recorded at a scan rate of 2 scans during the pyrolysis.

3. *Mass analyzer*: The mass analyzer sorts and separates the ions according to their mass to charge ratio (m/z) by using electric and/or magnetic fields. In this study a quadrupole mass analyzer, which is the most common one, is used. The quadrupole is a device which uses the stability of the trajectories in superimposed RF and DC fields to separate ions according to their m/z ratio.

4. *Ion detector*: separated ions are amplified and detected by a detector. In this study, high energy conversion dynode (HED) was used as an ion detector which is coupled to an electron multiplier.

5. *Vacuum System:* Mass spectrometers are operated under high vacuum to avoid scattering and collisions of ions and neutrals present in the medium and to

prevent condensation and secondary reactions. Furthermore it used to favor vaporization and to remove the background gases. The high vacuum necessary inside the mass spectrometer is provided by diffusion and rotary pumps. The background pressure is about 10^{-7} mbar.

During the direct pyrolysis analysis, the heating profiles used for the curing process were applied for the monomer samples (Table 1), while the polymers samples were heated from room temperature up to the maximum attainable temperature, 445 °C, at a heating rate of 20 °C/min and kept at that temperature for 10 minutes.

During the study, very small amount of samples (0.01mg) were pyrolyzed in flared glass sample vials.

CHAPTER 3

RESULTS AND DISCUSSION

Polymerization and thermal degradation of naphthoxazine monomers based on aromatic and alkyl amines were studied by direct pyrolysis mass spectrometry technique. The effect of amine group on polymerization and thermal degradation and crosslinking processes were investigated for each monomer.

In general, the presence of more than one peak in the total ion current (TIC) curve (the variation of ion yield as function of temperature) indicates either a multi-step thermal degradation mechanism or presence of more than one component. The peaks detected in the pyrolysis mass spectra are due to the dissociative ionization of the evolved species or thermal degradation products generated during the pyrolysis. Fragmentation pathways are determined by assuming that the products having the same evolution profiles are produced from the same thermal degradation pathways or by dissociative ionization of a high molecular mass thermal degradation product, parent fragment. Parent fragments can be assumed to be produced during pyrolysis. However, the products of the parent fragments may be produced during the heating and/or by dissociative ionization of the parent fragment. So, the data gained from pyrolysis mass spectra is inadequate to determine the structures. Thus, the assignments for the fragments are made by assuming that the fragments with the similar single ion evolution profile trend are produced from the same fragmentation pathway.

3.1 Polymerization and degradation mechanism of aromatic amine-based naphthoxazine (15-Na)

3.1.1 Curing of aromatic amine-based naphthoxazine monomer (15-Na)

The total ion current (TIC) curve, and the pyrolysis mass spectra at the peak maxima present in the TIC curve recorded during the curing of 15-Na are shown in Figure 1. A broad peak with a maximum at 4.1 min (at 110 °C) and a sharper and more intense peak were detected. The second peak showed two maxima at 8.5 (at 200 °C) and 9.0 min (at 210 °C) indicating that it was due to combination of two separate peaks. Yet, the pyrolysis mass spectra recorded in this region were almost identical. As expected, the molecular ion peak at m/z= 394 Da was quite noticeable indicating continuous evolution of the monomer during the heating process up to the curing temperature 210 °C. However, at around 210 °C, the relative intensity of the peak at 93 Da increased significantly pointing out evolution of aniline (Figure 1d).

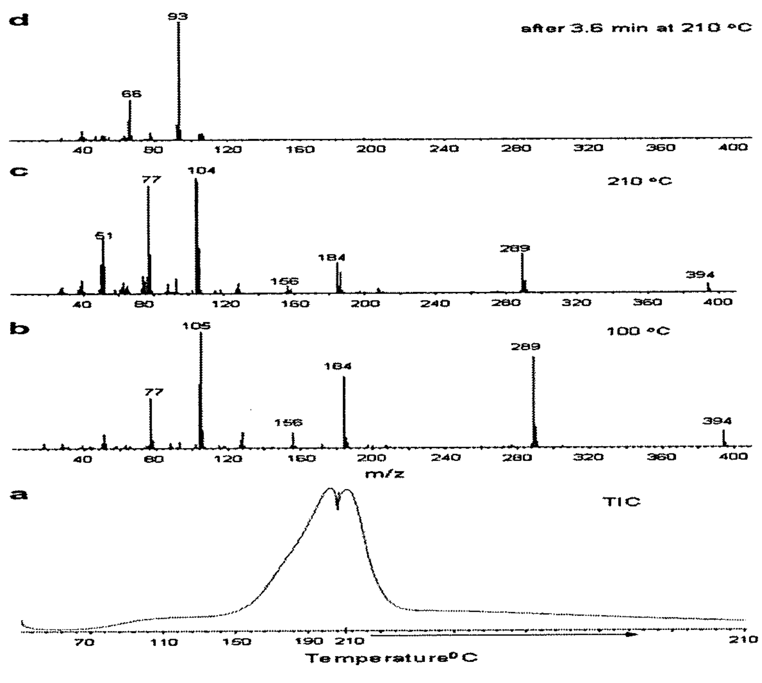

Figure 1: a. The total ion current (TIC) curve and the pyrolysis mass spectra recorded at b. 100 °C c. 210 °C and d. after 3.6 minute at 210 °C during the heating process of 15-Na

For the aromatic amine based naphthoxazine monomer (15-Na), the base peak was at 105 Da due to $CH_2NC_6H_5$ ion. Other intense peaks at 104 and 77 Da were attributed to the fragment ions produced by the loss of hydrogen and HCN from $CH_2NC_6H_5$ ion, respectively. Intense peaks at m/z=289 and 184 Da were due to fragment ions produced by the elimination of $CH_2=NC_6H_5$ and $[CH_2=NC_6H_5]_2$ groups from the molecular ion. By the elimination of CO from these fragment ions, products yielding quite intense peaks at 261 Da ($[M - CH_2=NC_6H_5 - CO]$), 156 Da ($[M - [CH_2=NC_6H_5]_2 - CO]$) and 128 Da ($[M - [CH_2=NC_6H_5]_2 - 2CO]$) were generated. Weak peaks at 274, 154, 260 and 126 Da due to fragments generated by loss of $O=CHNC_6H_5$, $[O=CHNC_6H_5]_2$, $O=CHN(CH_2)C_6H_5$ and $[O=CHN(CH_2)C_6H_5]_2$ from the molecular ion respectively, were also detected. Two possible fragmentation pathways during EI ionization of the aromatic amine-based naphthoxazine (15-Na) are shown in Scheme 4. The first one involves the production of $CH_2=NC_6H_5$ ion and the elimination of HCN from this ion (Scheme 4.1). The other involves the production of a resonance stabilized hydroxytropylium ion by the loss of $CH_2=NC_6H_5$ from the molecular ion and the elimination of CO from the hydroxytropylium ion (Scheme 4.2). As a result, intense peaks corresponding to the fragments consisting aromatic units are observed in the mass spectra.

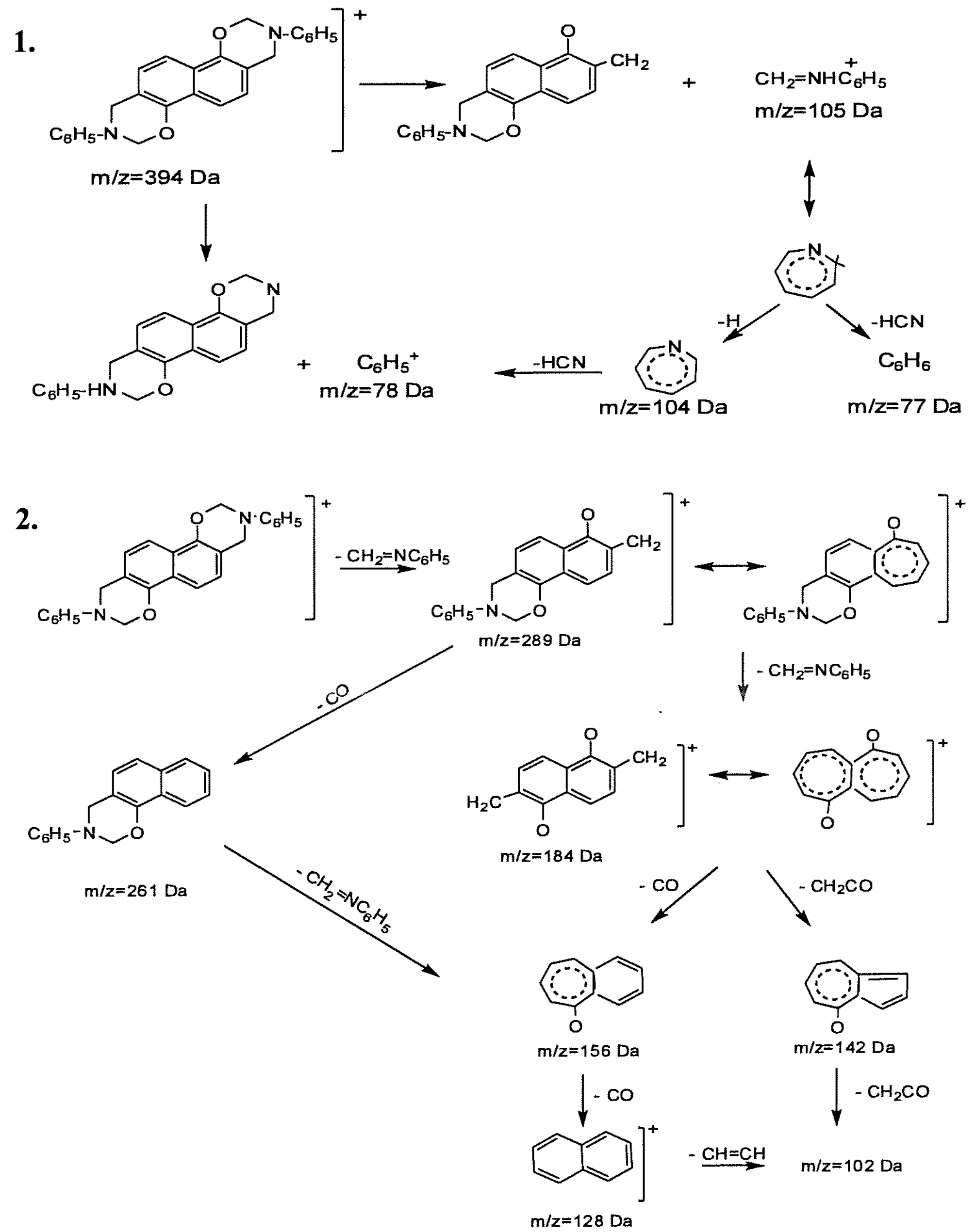

Scheme 4: The main fragmentation patterns proposed for 15-Na during EI ionization

It can be observed from the mass spectra that the evaporation of the monomer occurred at temperatures below the curing temperature, 210 °C. However, similar decomposition products might have also been produced when the decomposition of the monomer occurred during the curing. Generally, the similarity between the decomposition products' and the molecular ion's single ion evolution profiles is regarded as a proof for the evaporation before decomposition. Thus, to determine the fragmentation pathways during curing, single ion evolution profiles of each product detected in the pyrolysis mass spectra were evaluated and compared with each other and with the single ion evolution profile of the molecular ion. Single ion evolution profiles of some characteristic fragments detected during the curing process of 15-Na are shown in Figure 2.

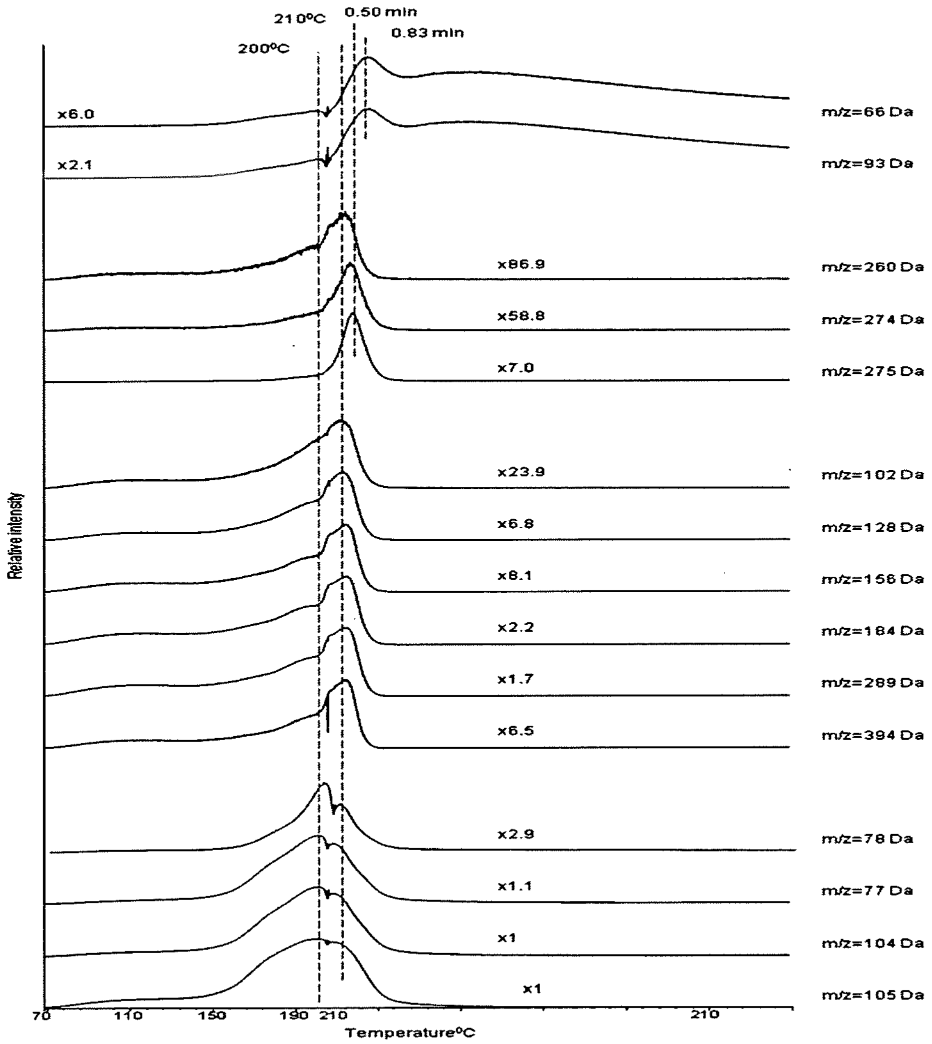

Figure 2: Single ion evolution profiles of some characteristic products detected during the curing process of 15-Na (Note: the intensities are normalized by a number factor as shown in the figure)

Evolution of products was mainly detected around two temperature regions, at around 100 °C and 210 °C. The peak at around 210 °C was divided into two maxima at around 199 °C and 208 °C. In this region, variations in the relative intensities of the fragments were detected. This information indicates that upon thermal excitation, the decomposition pathways were not changed very much. It is clear that the main evolved product up to the curing temperature, 210 °C, was the monomer. The maximum yield for the fragments which were generated by the loss of $CH_2N(CH_2)C_6H_5$ from the monomer was detected 0.45 min after the curing temperature, 210 °C. The yields of all the products were decreased drastically, shortly after the curing temperature has been reached. In the same period, evolution of aniline and its fragments were increased significantly. The maximum yield for these products was observed 0.9 min after the curing temperature has been reached. Aniline evolution decreased slowly and continued throughout the curing. Above the curing temperature, only the peaks related to aniline and its fragments were detected. It can be concluded that the dissociation of the monomer occurred around the curing temperature to a certain extend. The high vacuum inside the mass spectrometer prevents secondary reactions. Thus, shifts of H atoms to generate aniline were the only possibility within the naphthoxazine monomer. In the mass spectra, there was no peak which can be attributed to the decomposition product consisting naphthalene unit. Hence, it can be concluded that the evolution of aniline occurred during the ring opening polymerization of the monomer.

3.1.2. Pyrolysis of aromatic amine-based polynaphthoxazine

The TIC curve of the cured 15-Na showed two peaks (Figure 3). The first peak was at around 100 °C indicating evaporation of unreacted monomer and/or lower mass oligomers. The second peak had a shoulder at around 270 °C and a maximum at 410 °C. The pyrolysis mass spectra recorded at the peak maxima were dominated by peaks of aniline and related ions (93, 66, and 49 Da peaks) (Figure 3). Weak peaks belonging to fragments involving N-substituted anilines were detected in the pyrolysis mass spectra recorded at low (250 °C) and moderate temperatures (250- 400 °C) (Figure 3c).

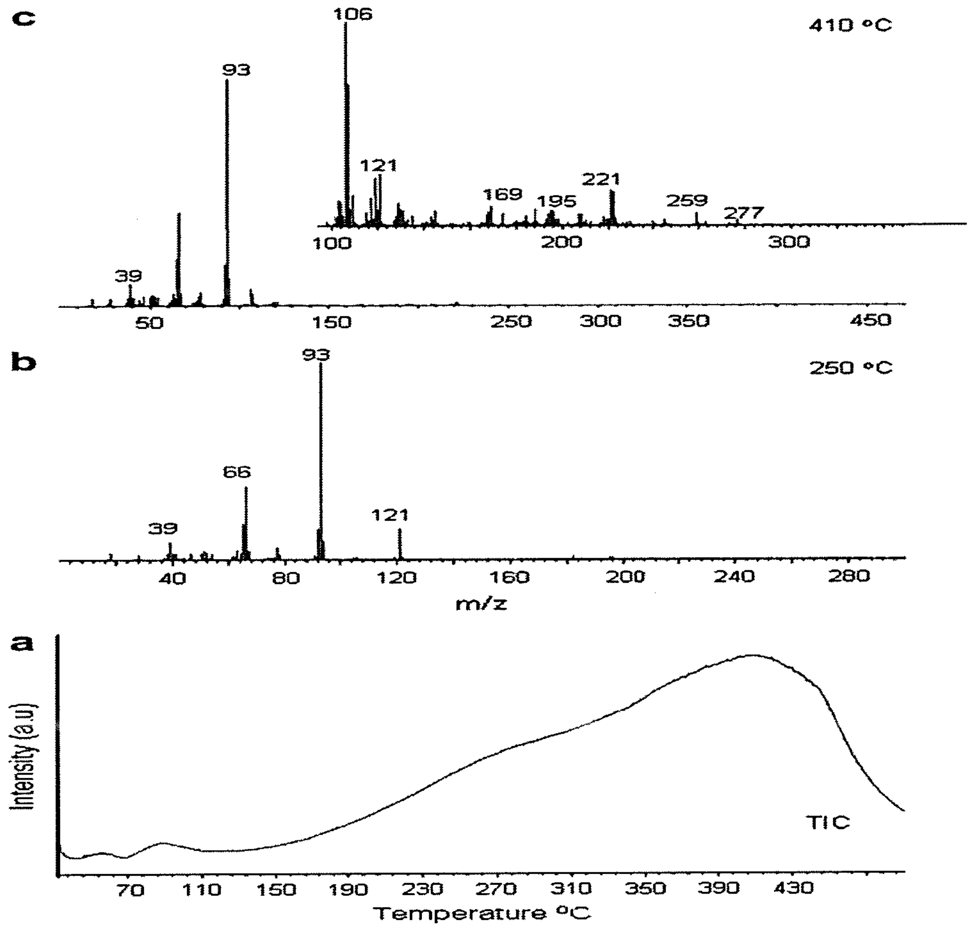

Figure 3: The TIC curve and the pyrolysis mass spectra recorded during the heating process of the cured monomer, poly15-Na

As a result of grouping and analyzing the identical evolution profiles of fragments it was determined that the main fragmentation product was aniline. Fragments involving N-substituted anilines and naphthoxazines were produced over a broad temperature range. Fragments involving N-substituted anilines evolved mainly at initial stages of pyrolysis as shown in the single ion evolution profiles given in Figure 4. In general, aliphatic amines are generated by the α-cleavage reaction due to loss of the largest radical. Decomposition products of aliphatic amines degrade due to loss of ethene and transfer of a β-H to the positive nitrogen. Similar fragmentation pathways can be estimated for N-alkyl anilines. The peaks detected in the pyrolysis mass spectra at low temperature ranges, below 400 °C, and their assignments are shown in Table 2. In this table, only the ortho substituted N-alkyl anilines are shown but, the production of the para substituted N-alkyl anilines have equal possibility. It was observed that at the initial period of pyrolysis the trends in the single ion evolution profiles of fragments having mass to charge ratio 182, 105 and 77 Da were identical. So these ions were assigned to N-benzyl aniline radical produced due to elimination of end groups or decomposition of thermally less stable linkages.

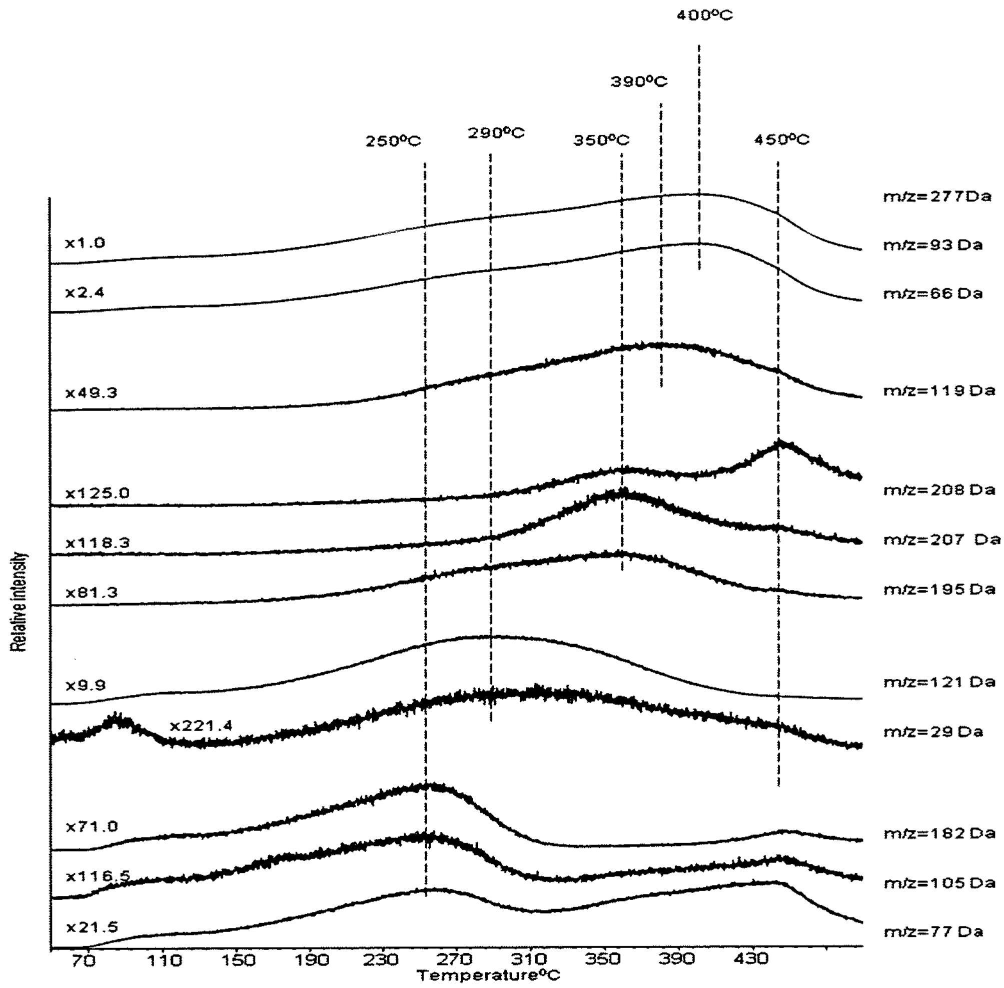

Figure 4: The single ion evolution profiles of fragments involving N-substituted anilines

Table 2. Peaks present in the low temperature pyrolysis mass spectra, the proposed structures and the temperatures at which the product yields were maximized

m/z (Da)	Assignment	Peak maxima (temperature, °C)
182	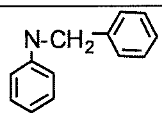	250, 450
105	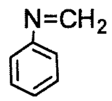	
77	C_6H_5	
119	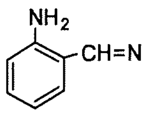 or 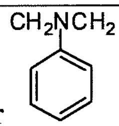	390
121	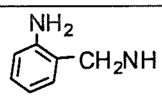	290
29	CH_2=NH	
93	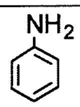	290, 400
66	C_5H_6	
195	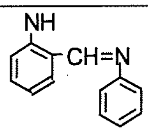	290, 350
207	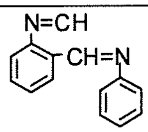	350, 450
208	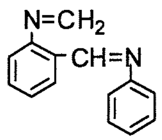	

A previous study made by Shen and Ishida showed that the increase in the room temperature density of 15-Na polynaphthoxazine is due to the increase of crosslink density [32]. Also, it was determined that to obtain fully cured 15-Na polynaphthoxazine the minimum post-cure temperature should be 260 °C or above. The results of our study showed that the loss of weak linkages and/or end groups occurred at temperatures below 270 °C. The elimination of these fragments from the monomer would produce radicals that can combine and form a highly crosslinked and/or high molecular weight chains with higher thermal stability.

The evolution of the main degradation product, aniline, took place in a broad temperature range. The single ion pyrograms of aniline, 93 Da, and 66 Da fragment has two maxima at around 290 °C and at 400 °C. The low temperature evolution of aniline can be associated with dissociative ionization of fragments involving aniline units, such as loss of CH_2NH group from 121 Da fragment. However, at high temperatures, single ion evolution profiles of aniline and other related fragments showed noticeable differences. Thus, it can be concluded that around 400 °C the main fragmentation pathway was the loss of aniline.

It was detected that aniline has very high yield throughout the pyrolysis. This information shows that $-NCH_2$ radicals recombined and formed thermally less stable linkages involving β Hs as shown in Scheme 5.1. Then, the naphthoxazines with unsaturated linkages were formed by loss of aniline. After that, crosslinked structure with higher thermal stability could be formed as a result of coupling of these naphthoxazines as shown in Scheme 5.2. A previous study showed that aniline was also the major decomposition product for the thermal degradation of polybenzoxazines based on aniline [76].

1.

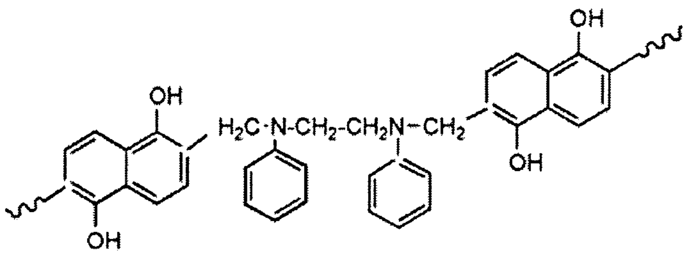

2.

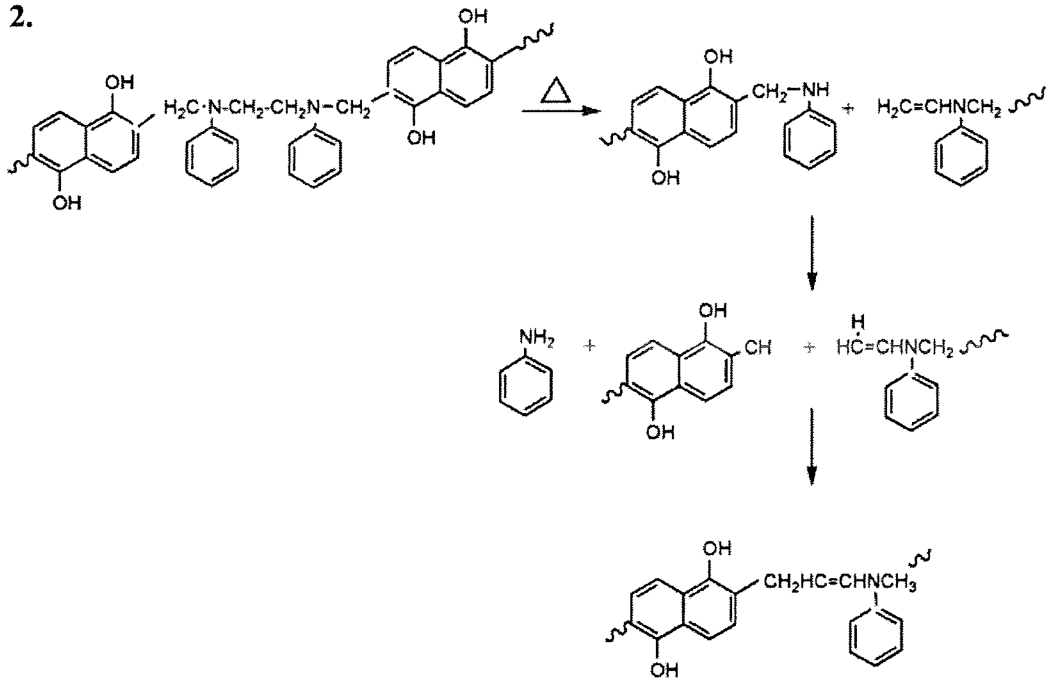

Scheme 5: 1. The linkages formed during the polymerization of aromatic amine-based bifunctional naphthoxazines 2. Generation of aniline and unsaturated linkages by thermal degradation of Poly15-Na

However, some of the products detected in the pyrolysis mass spectra cannot be generated if polymerization proceeded only by recombination of N–CH_2 radicals. The single ion evolution profiles of 91 and 221 Da fragments showed identical trends over a broad temperature range and the maximum yield for these products were detected at around 450 °C. Presence of 91 Da fragment in a mass spectrum, generally indicates presence of alkyl substituted benzene ring in the structure (Figure 3, Table 3). Thus, as decomposition of naphthalene ring is energetically unfavorable, the detection of 91 Da peak over a wide temperature range can be interpreted as a proof for alkyl substitution to the benzene ring of aniline. There is no free ortho position in bifunctional naphthoxazine monomers, unlike the corresponding monofunctional benzoxazines. In addition, there are OH groups at both of the para positions. Accordingly, polymerization by the attack of $-NCH_2$ radicals directly to the naphthoxazine ring has a lower probability compared to what was observed for benzoxazines. On the other hand, para and ortho positions of the benzene ring of aniline are potentially reactive, although less reactive compared to those of phenols. Consequently, detection of ortho (or para) substituted anilines confirmed that the polymerization proceeded by the attack of $-NCH_2$ radicals to the benzene ring attached to the nitrogen (Scheme 6).

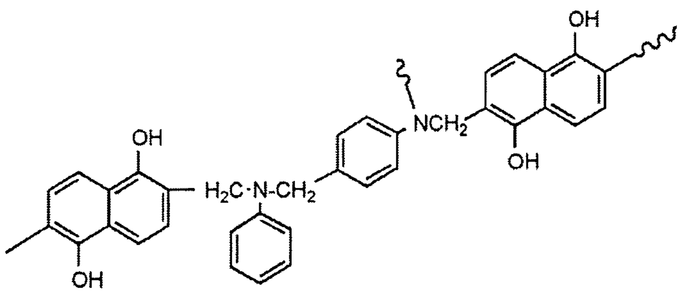

Scheme 6: The linkages formed during the polymerization of aromatic amine based bifunctional naphthoxazines

In a GC–MS study done by Hemvichian and Ishida on thermal and thermo-oxidative degradation of aromatic amine-based polybenzoxazines, not only aniline, the major degradation product, but also p-aminotoluene (may be also o-aminotoluene, having similar mass spectrum) was detected as a decomposition product [76]. In GC MS, as thermal degradation takes place outside the MS, secondary reactions cannot be avoided and only stable fragments can be detected. Accordingly, unstable radicals like alkyl or amine substituted aniline radicals cannot be detected. In contrast, in our study, Py-MS, both 221 Da fragment and the daughter fragments involving aniline ring, such as m/z=105 Da, produced by dissociative ionization of 221 Da fragment were detected at low and/or moderate temperatures. Thus, the trends observed in the single ion pyrograms were in accordance with the assignments made. Furthermore, the absorption band emerged at around 1670 cm^{-1} associated with C=N stretching for the Schiff base at 200 °C in FTIR was consistent with the mass spectral assignments.

In Figure 5, the evolution profiles of some of the thermal decomposition products with m/z= 106, 221, 245, 259, 273, and 330 Da, which include naphthoxazine units or N-alkyne anilines are shown. In addition, the assignments of these products are given in Table 3. No fragment involving naphthoxazine unit can be detected between 100 and 360 °C. The detection of these fragments below 100 °C was interpreted as the evolution of unreacted monomer and low molecular weight oligomers. The evolutions of these fragments at high temperatures, up to 450 °C, confirmed thermal degradation of a polymeric structure. The evolution of H_2O was detected at high temperatures indicating the presence of ortho substituted phenolic structure. The yield of aniline was decreased considerably in this region. On the other hand, the yield of N-alkyne anilines and methyl substituted N-alkyl anilines were increased steadily up to 450 °C indicating the higher stability of these linkages. It may be thought that the number of dangling groups of polynaphthoxazines should be decreased if the benzene attached to the nitrogen reacted during polymerization increasing the thermal stability of the polymer.

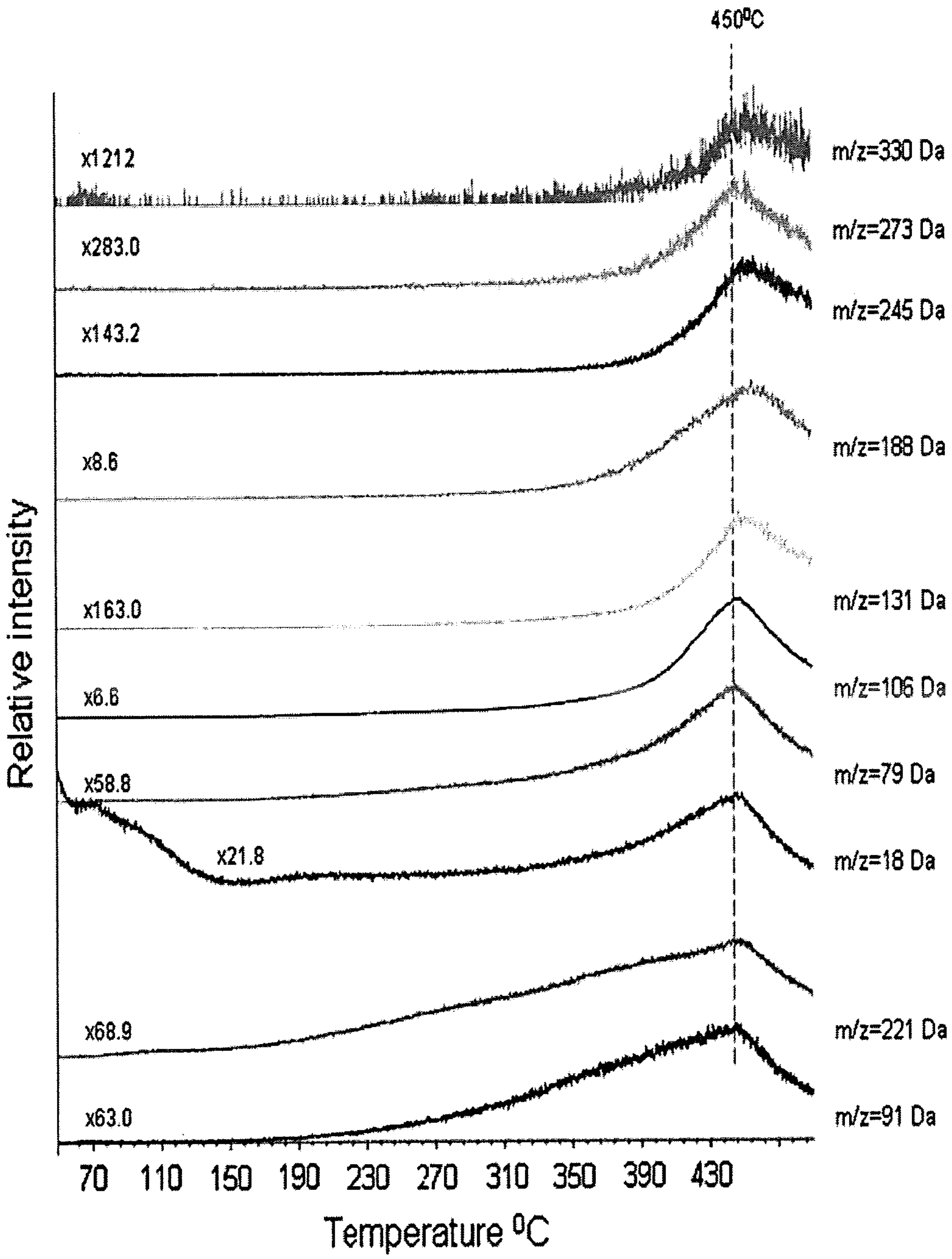

Figure 5: The evolution profiles of some of the products involving naphthoxazine units or N-alkyne aniline

Table 3. Peaks present in the high temperature pyrolysis mass spectra and the proposed structures

m/z	Assignments
18	H_2O
221	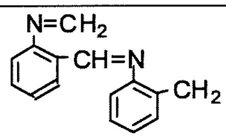
91	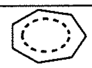
106	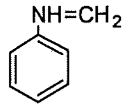
131	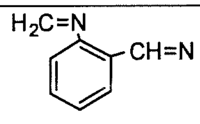
188	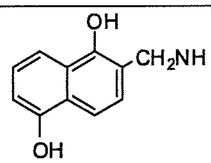
245	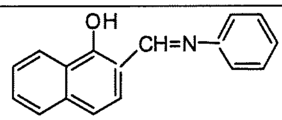
259	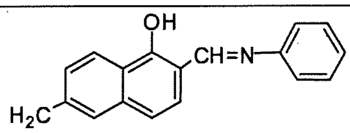
273	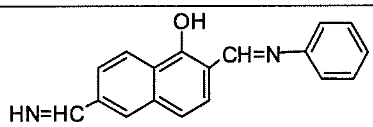
330	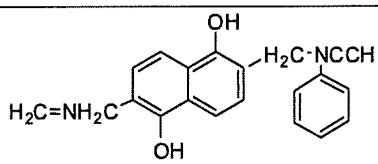

Additionally, pyrolysis mass spectrometry analysis of cured (at 240 °C) naphthoxazine monomer prepared by using pentafluoroaniline instead of aniline was performed for comparison. As expected, for this polymer, pentafluoroaniline was the main degradation product. In Figure 6, single ion pyrograms of some distinctive products such as $C_6F_5N(CH_2)_2$ (m/z = 209 Da), $C_6F_5NH_2$ (183 Da), CF=CH (44 Da), $C_{10}H_4(OH)_2CH{=}NH_2$ (186 Da), HF (20 Da), and H_2O (18 Da) are shown. For this sample, as all positions of benzene ring were substituted by F atoms no free position on benzene ring is present. Thus, as expected, no peak that can be attributed to a product generated by the attack of CH_2 radicals to the benzene ring was detected. The peaks attributed to the fragments generated by dissociative ionization of pentafluoroaniline dominated the pyrolysis mass spectra. Evolutions of HF, H_2O and the fragments including naphthoxazine units at high temperature (nearly at 450 °C) were interpreted as the presence of chains involving ortho substituted hydroxy naphthalene ring and pentafluoroaniline. In addition, it was detected that the yield of pentafluoroaniline (m/z = 183 Da) was very high so it may be interpreted as polymerization by coupling of N–CH_2 radicals which were produced by opening of the side chains.

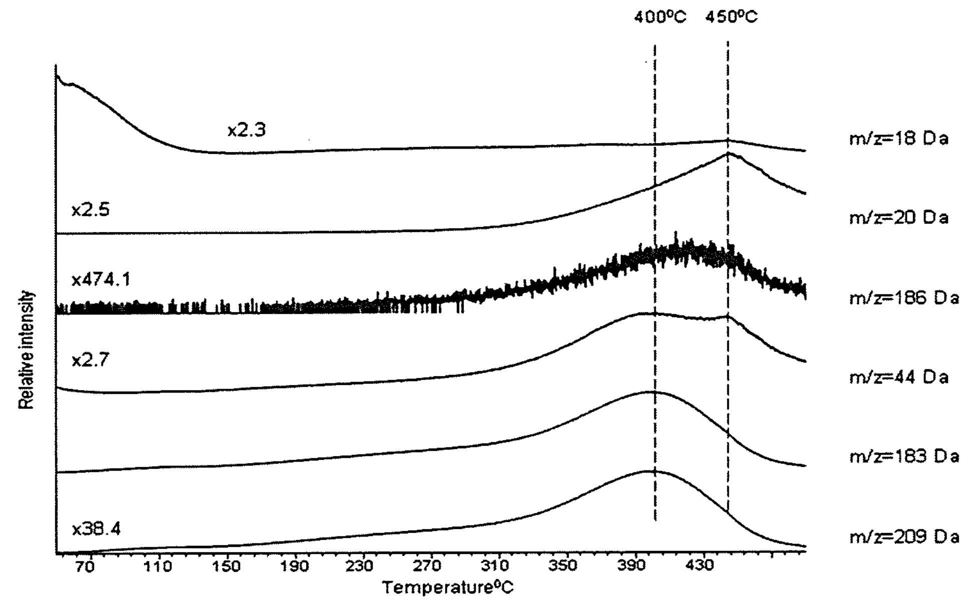

Figure 6: The single ion pyrograms of some characteristic products recorded during pyrolysis of cured naphthoxazine involving pentafluoroaniline

It can be concluded that polymerization of naphthoxazine based on aniline proceeded mainly through the aniline units, either by coupling of the radicals produced by the ring opening of the side chains or by substitution to benzene ring of aniline. However, even if no direct evidence to confirm polymerization by attack of $-NCH_2$ groups to naphthalene ring was detected, it is not possible totally to eliminate its existence.

3.2 Polymerization and degradation mechanism of alkyl-functional naphthoxazines

3.2.1 Curing of alkyl-functional naphthoxazine monomers

The naphthoxazine monomers based on alkyl amines RNH_2, where R is CH_3, C_2H_5, C_3H_7, C_6H_{13}, $C_{12}H_{15}$ or $C_{18}H_{37}$ (15Na-C1, 15Na-C2, 15Na-C3, 15Na-C6, 15Na-C12 and 15Na-C18) are discussed separately first and then compared with each other to investigate the effect of alkyl chain length on polymerization and thermal degradation characteristics.

3.2.1.1 Curing of 15Na-C1 monomer

The total ion current (TIC) curve and the pyrolysis mass spectra recorded at 210 °C and after 0.67 min. curing at 210 °C of 15Na-C1 monomer are shown in Figure 7. The TIC curve of 15Na-C1 showed two maxima at the curing temperature of 210 °C and at around 150 °C and a shoulder at around 90 °C. The mass spectra recorded up to curing temperature were quite similar. The molecular ion peak at m/z = 270 Da was detected before the curing temperature was reached which indicates the evolution of the monomer before decomposition. Other peaks detected in the pyrolysis mass spectra recorded at 210 °C are at m/z = 42, 128, 156, 184 and 227 Da that can be associated readily with C_2H_4N, [M – $2(CH_2NCH_3)$ - 2CO], [M – $2(CH_2NCH_3)$ - CO], [M – $2(CH_2NCH_3)$] and [M – (CH_2NCH_3)] respectively, indicating that during dissociative EI ionization of the monomer, decomposition of cyclic side chains took place. The same peaks were also present in the mass spectra recorded after the curing temperature, but the intensities of the peaks were different. Single ion evolution profiles of some characteristic products detected during the curing process of 15Na-C1 monomer are shown in Figure 8. The evolution profile of C_2H_4N (m/z = 42) fragment showed significant differences. Its relative intensity increased above 130 °C pointing out that it was also generated directly during the curing process, besides the EI ionization of the evaporated monomer.

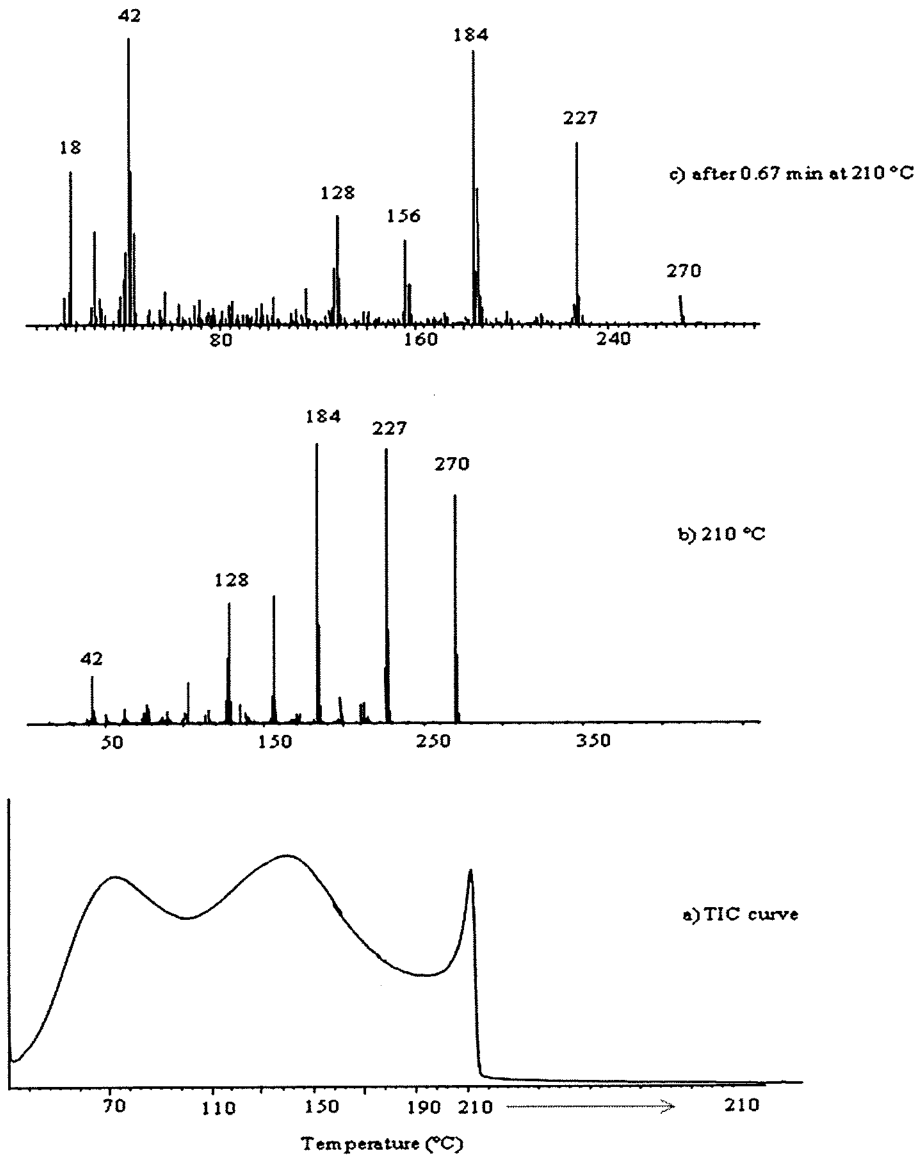

Figure 7: a. The total ion current curve and the mass spectra recorded at b. 210 °C and c. after 0.67 minute at 210 °C for 15Na-C1 monomer

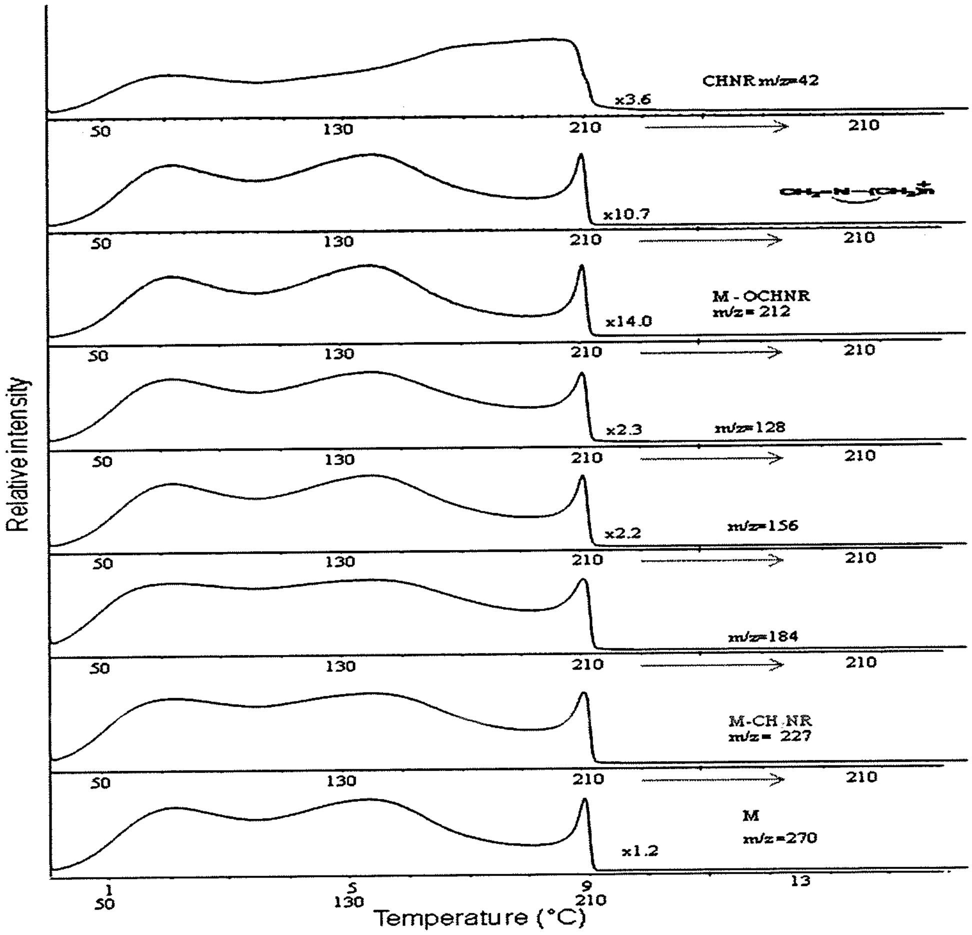

Figure 8: Single ion evolution products of some characteristic products detected during the curing process of 15Na-C1 monomer

3.2.1.2 Curing of 15Na-C2 monomer

The total ion current (TIC) curve and the pyrolysis mass spectra recorded at the curing temperature, 170 °C, and at after 1 min. the curing temperature has been reached during the curing of 15Na-C2 monomer are shown in Figure 9. Up to the curing temperature, the mass spectra were almost identical. The detection of the molecular ion peak, at m/z= 298 Da, before the curing temperature has been reached indicated the evolution of the monomer before decomposition. Other intense peaks detected up to 170 °C were at m/z = 42, 56, 128, 156, 184 and 241 Da that can be associated with C_2H_4N, $CH_2NC_2H_4$ [M – 2($CH_2NC_2H_5$) - 2CO], [M – 2($CH_2NC_2H_5$) - CO], [M – 2($CH_2NC_2H_5$)] and [M – ($CH_2NC_2H_5$)]

respectively, pointing out that the decomposition of cyclic side chains took place. However, after the curing temperature, the mass spectra recorded were dominated with the peaks with m/z values 30, 42 and 57 Da which were due to fragments CH_2=NH_2, C_2H_4N and C_3H_7N respectively, indicating the decomposition of oxazine ring and degradation of the monomer. In Figure 10, single ion evolution profiles of some characteristic products detected during the curing process of 15Na-C2 monomer are shown. It can be observed from the evolution profiles that the relative yields of low mass alkyl amines at m/z = 30, 42 and 57 Da were increased above 130 °C whereas the yields of other ions involving aromatic ring were decreased indicating that they were also produced during the curing process. Additionally, the generation of product with m/z = 30 was continued in the region where no other fragment was detected, so it should be produced by some rearrangement reactions.

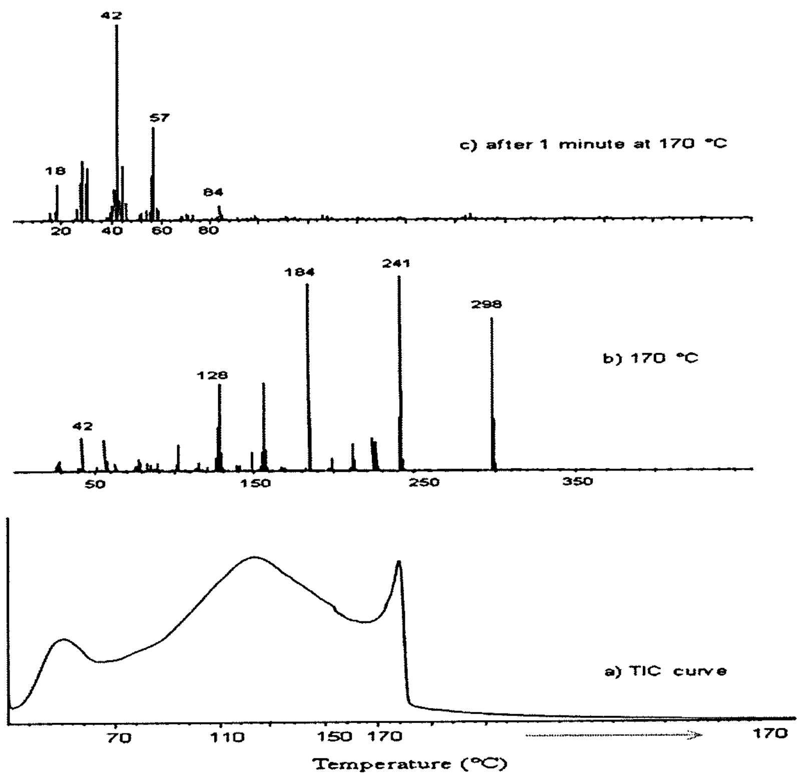

Figure 9: a. The total ion current curve and the mass spectra recorded at b. 170 °C and c. after 1 minute at 170 °C for 15Na-C2 monomer

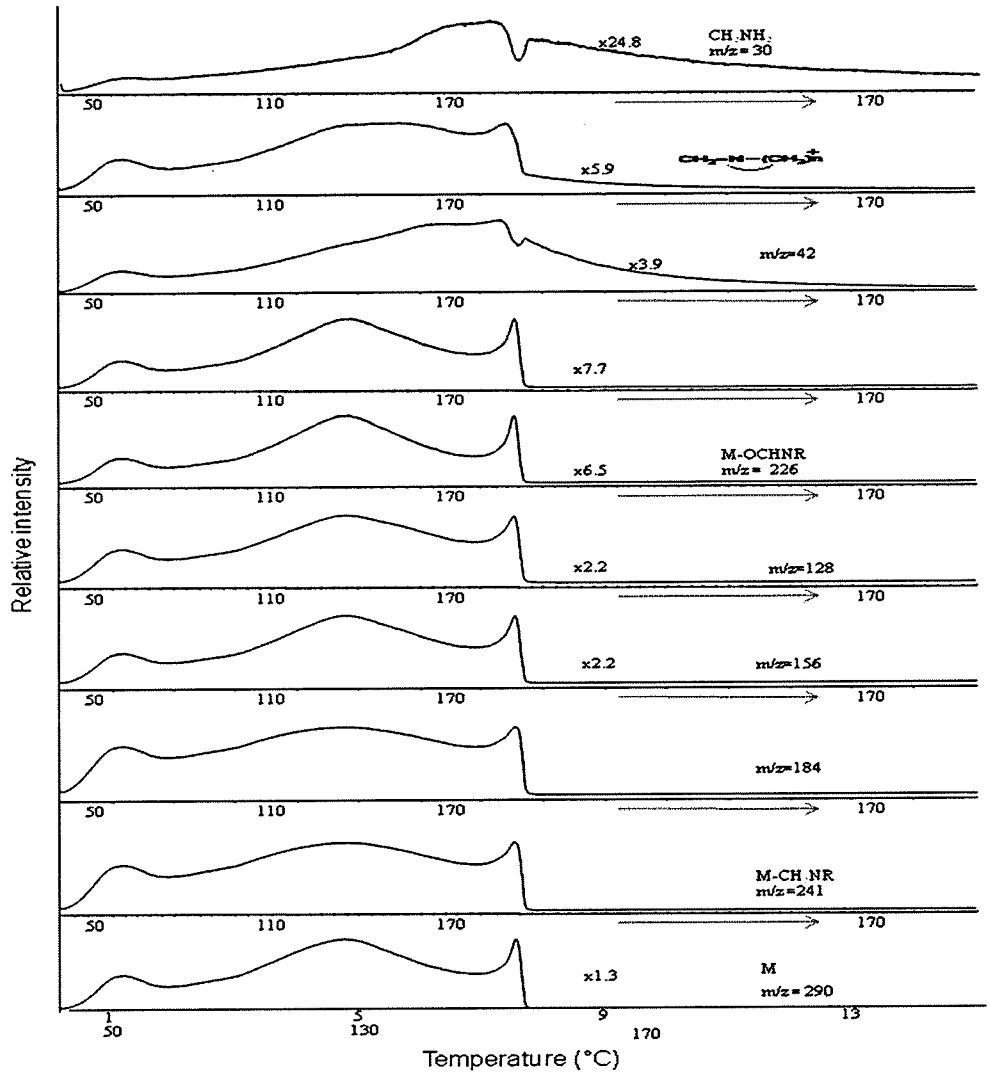

Figure 10: Single ion evolution products of some characteristic products detected during the curing process of 15Na-C2 monomer

3.2.1.3 Curing of 15NaC3 monomer

In Figure 11, the total ion current (TIC) curve and the pyrolysis mass spectra recorded at 150 °C, the first curing temperature, and after 2 min. curing at 150 °C during the curing of 15NaC3 monomer are shown. The TIC curve of 15NaC3 has maxima at around 50, 110 °C and at 150 °C. It was observed that the mass spectra recorded up to 150 °C were almost similar. Below the curing temperature, the molecular ion peak at m/z = 326 Da was detected indicating the evolution of the monomer before decomposition. Other intense peaks detected in the mass spectra recorded below 150 °C are at m/z = 42, 128, 156, 184, 226 and 255 Da that can be associated with C_2H_4N, [M – 2($CH_2NC_3H_7$) - 2CO], [M – 2($CH_2NC_3H_7$) - CO], [M – 2($CH_2NC_3H_7$)], [M – $OCHN(C_3H_7)CH_2$] and [M – ($CH_2NC_3H_7$)] indicating the decomposition of the cyclic side chains during ionization. The mass spectra recorded upon further heating at 150 °C, were dominated by the peaks at m/z = 30, 42 and 70 Da belonging to fragments CH_2=NH_2, C_2H_4N and $CH_2N(CH_2)_3$ again, pointing out the degradation of the monomer. Single ion evolution profiles of some products detected during the curing process of 15Na-C3 monomer are shown in Figure 12 showed that CH_2=NH_2, C_2H_4N and $CH_2N(CH_2)_3$ were produced in the region where the evolution of no other fragment was detected. Thus, it can be concluded that they were produced during the curing process. The detection of only CH_2=NH_2, 8 minutes after the curing temperature has been reached, revealed that it should be generated by some other rearrangement reactions as in case of 15Na-C1 and C2.

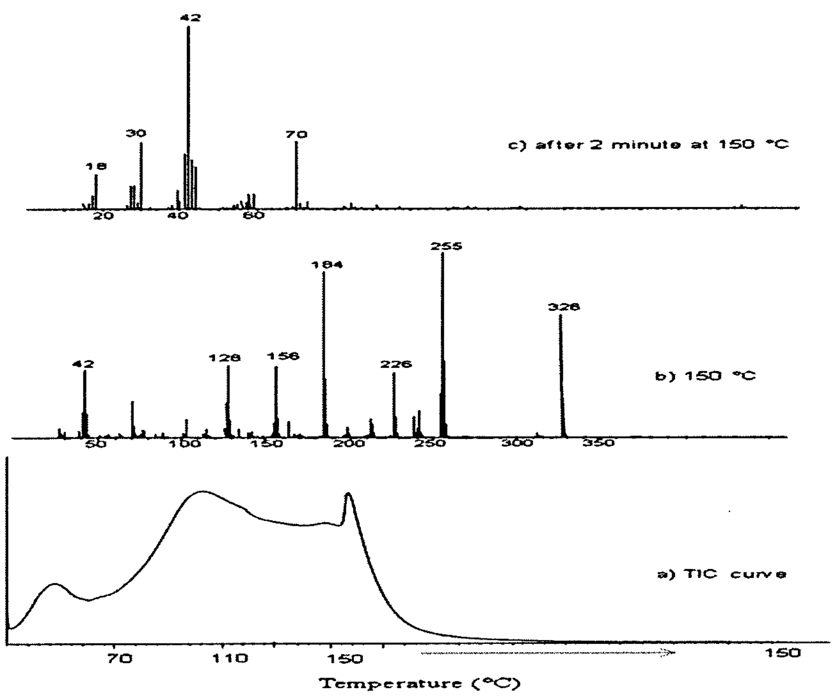

Figure 11: a. The total ion current curve and the mass spectra recorded at b. 150 °C and c. after 2 minute at 150 °C for 15Na-C3 monomer

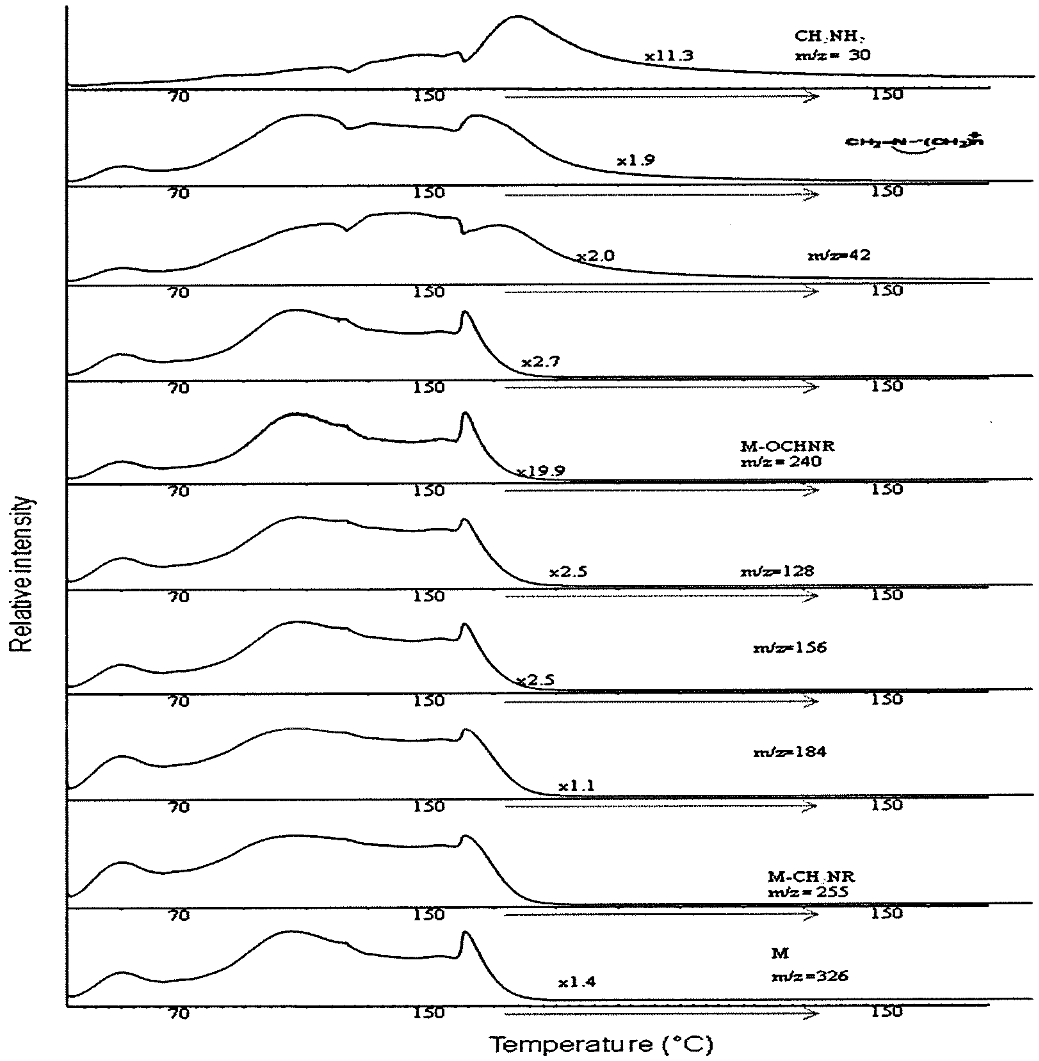

Figure 12: Single ion evolution products of some characteristic products detected during the curing process of 15Na-C3 monomer

3.2.1.4 Curing of 15Na-C6 monomer

In Figure 13, the TIC (total ion current) curve and the pyrolysis mass spectra at 125 °C and at the first curing temperature, 150 °C, recorded during the curing of 15Na-C6 monomer are shown. The presence of molecular ion peak, at m/z = 410 Da, indicated the evolution of the monomer before decomposition. The mass spectra recorded at 125 °C involved also the peaks at m/z = 30, 42, 84, 112, 128, 156, 184, 226 and 297 Da due to the products $CH_2{=}NH_2$, C_2H_4N, $CH_2N(CH_2)_4$, $CH_2N(CH_2)_6$, [M – 2($CH_2NC_6H_{13}$) - 2CO], [M – 2($CH_2NC_6H_{13}$) - CO], [M –

$2(CH_2NC_6H_{13})]$, $[M - CH_2NC_6H_{13} - C_5H_{11}]$ and $[M - (CH_2NC_6H_{13})]$ respectively, signifying the decomposition of the cyclic side chains. On the other hand, the mass spectrum recorded at 150 °C was dominated with the peaks at m/z = 30, 44, 70, 84 and 112 Da that can be associated with the fragments $CH_2{=}NH_2$, $C_2H_4NH_2$, $CH_2N(CH_2)_3$, $CH_2N(CH_2)_4$ and $CH_2N(CH_2)_6$ respectively. Thus, degradation of the monomer was again confirmed around the curing temperature. In Figure 14, the single ion evolution profiles of some products detected during the curing process of 15Na-C6 are shown. It can be observed from the figure that the evolution profiles of $CH_2{=}NH_2$, C_2H_4N, $CH_2N(CH_2)_4$ had different trends compared to others. Their relative intensities increased above 130 °C indicating that they were also generated during the polymerization process. Among the fragments involving nitrogen, evolution of $CH_2{=}NH_2$ was continued in the region where no other product evolution was observed.

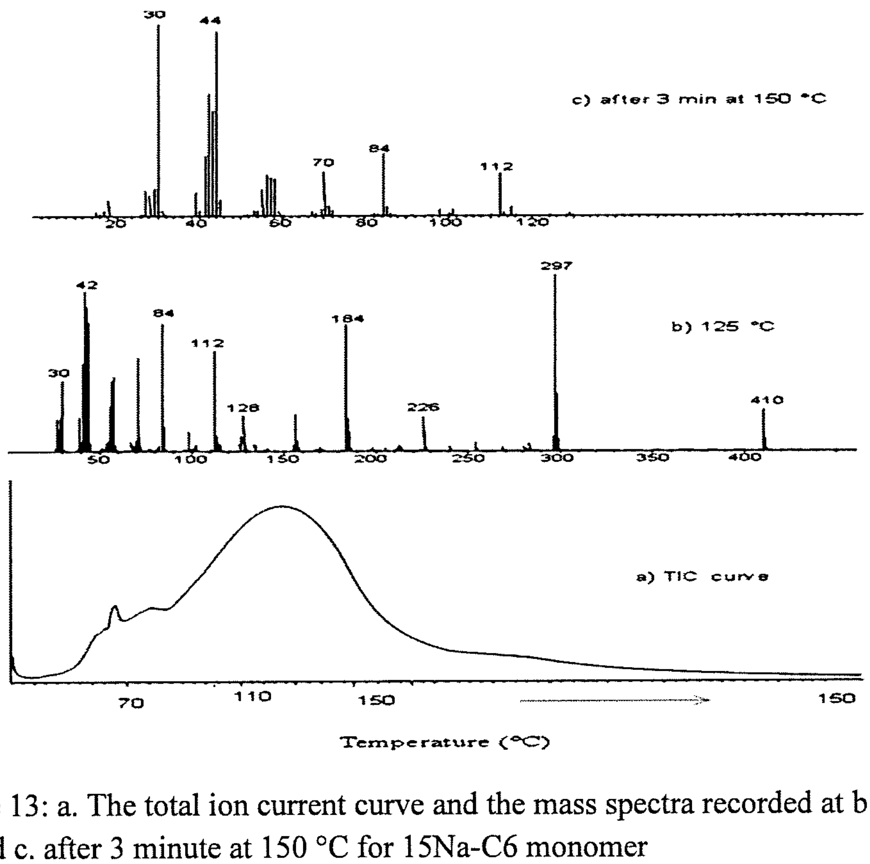

Figure 13: a. The total ion current curve and the mass spectra recorded at b. 125 °C and c. after 3 minute at 150 °C for 15Na-C6 monomer

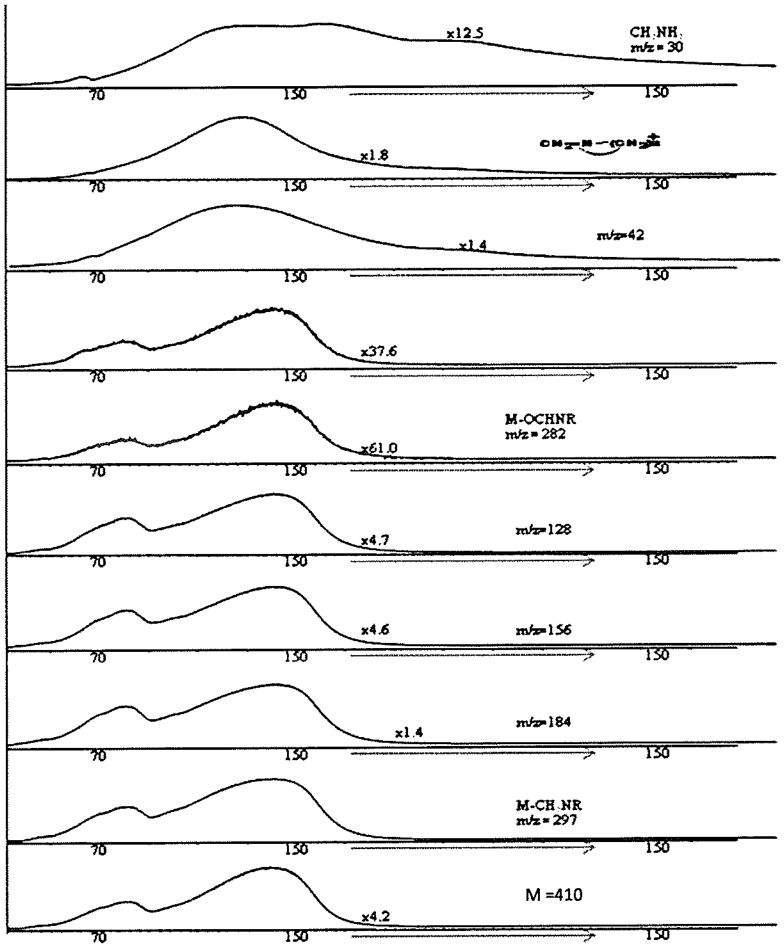

Figure 14: Single ion evolution products of some characteristic products detected during the curing process of 15Na-C6 monomer

3.2.1.5 Curing of 15Na-C12 monomer

The total ion current (TIC) curve and the pyrolysis mass spectra recorded at 120 °C, and 8 min. after the first curing temperature has been reached, at 150 °C, during the curing of 15Na-C12 monomer are shown in Figure 15. The intense peaks dominated in the mass spectrum at 120 °C were at m/z = 30, 43, 84, 98, 112, 126, 156, 184 and 196 Da that can be associated with CH_2NH_2, C_3H_7, $CH_2N(CH_2)_4$, $CH_2N(CH_2)_5$, $CH_2N(CH_2)_6$, $CH_2N(CH_2)_7$, [M – $2(CH_2NC_{12}H_{25})$ - CO], [M – $2(CH_2NC_{12}H_{25})$] and $CH_2N(CH_2)_{12}$ respectively, indicating that the decomposition of the cyclic side chains took place during ionization. The same peaks were detected in the mass spectra recorded after the first curing temperature has been reached, but the relative intensities of the peaks at 30 and 44 Da were increased significantly, where the intensity of the other peaks decreased. The single ion evolution profiles of some characteristic products detected during the curing process of 15Na-C12 monomer are given in Figure 16 showing that the generations of the products at m/z = 30, 42, 56, 128, 156 and 184 were continued in the region where the evolution of high mass products such as the fragment ions at m/z= 381 [M - $CH_2NC_{12}H_{25}$] and 366 Da [M - $OCHNC_{12}H_{25}$] were not detected. Thus, it can be concluded that degradation of the monomer has taken place. Similar to other monomers involving alkyl chains up to C6, evolution of fragments involving aromatic ring was also detected for 15Na-C12. However, the evolution profile of CH_2=NH_2 followed almost a similar trend with those of other monomers.

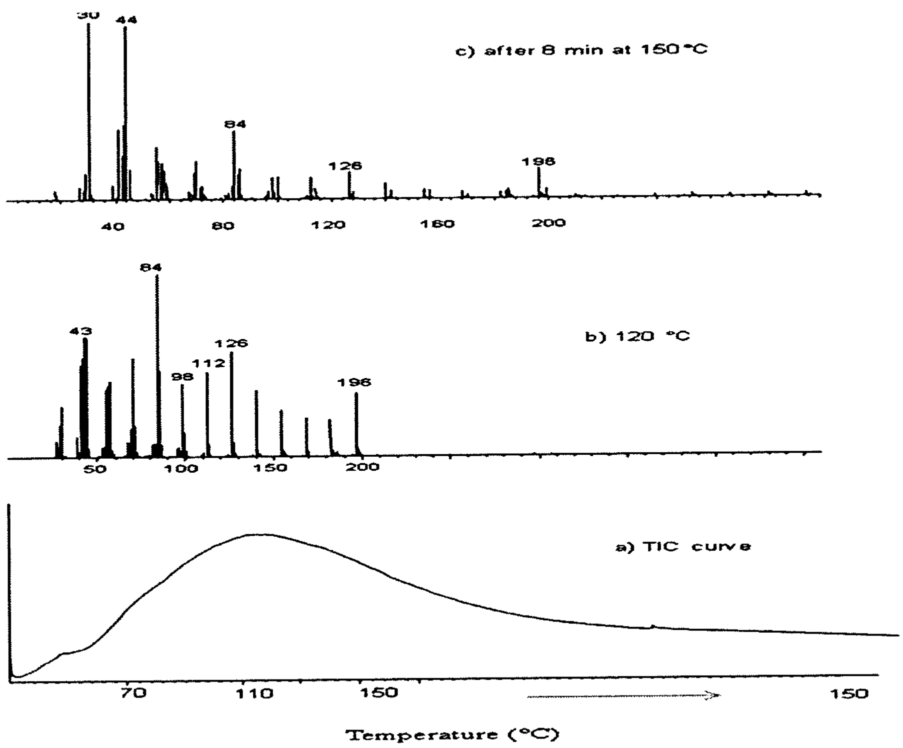

Figure 15: a. The total ion current curve and the mass spectra recorded at b. 120 °C and c. after 8 minute at 150 °C for 15Na-C12 monomer

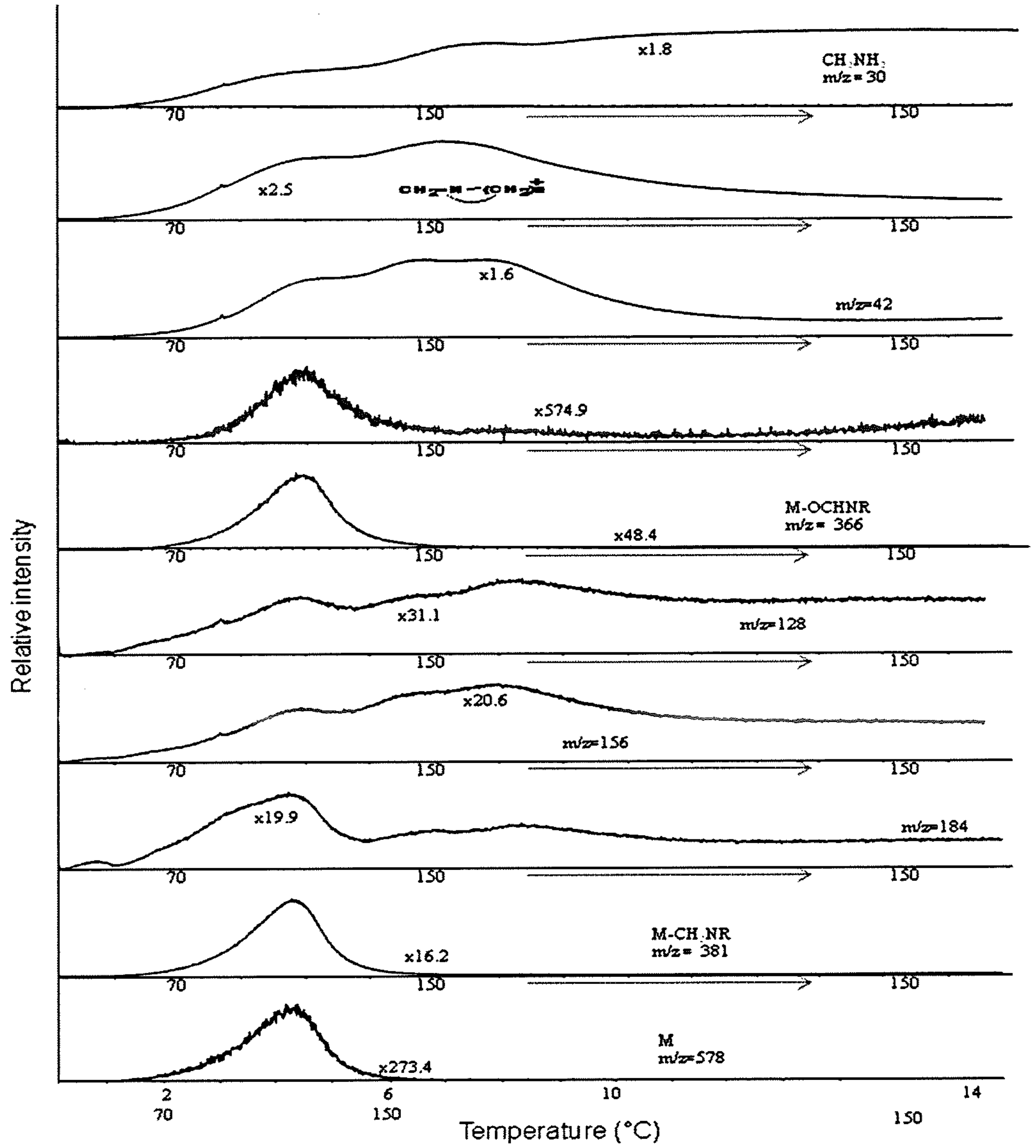

Figure 16: Single ion evolution products of some characteristic products detected during the curing process of 15Na-C12 monomer

3.2.1.6 Curing of 15Na-C18 monomer

In Figure 17, the TIC curve and the pyrolysis mass spectra at 130 °C and at the first curing temperature, 150 °C, recorded during the heating of 15Na-C18 monomer are shown. As expected, the molecular ion peak was not detected. The mass spectrum recorded at 130 °C involved the peaks at m/z = 30, 44, 84, 98, 126, 156, 182, 238 and 280 Da that can be associated with CH_2=NH_2, $C_2H_4NH_2$,

$CH_2N(CH_2)_4$, $CH_2N(CH_2)_5$, $CH_2N(CH_2)_6$, [M – $2(CH_2NC_{18}H_{37})$ - CO], $CH_2N(CH_2)_{11}$, $CH_2N(CH_2)_{15}$ and $CH_2N(CH_2)_{18}$ respectively, indicating again the decomposition of the cyclic side chains. Identical peaks were detected at 150 °C, but the relative intensities of the peaks changed significantly. Single ion evolution profiles of some characteristic products detected during the curing process of 15Na-C18 monomer are shown in Figure 18. Evolution of fragments involving aromatic ring continued in the region where the yield of alkyl amine fragments decreased significantly. On the other hand evolution of CH_2NH_2 followed a completely different path; its evolution continued for a longer period of time, even in the region where the yield of all other fragments diminished significantly.

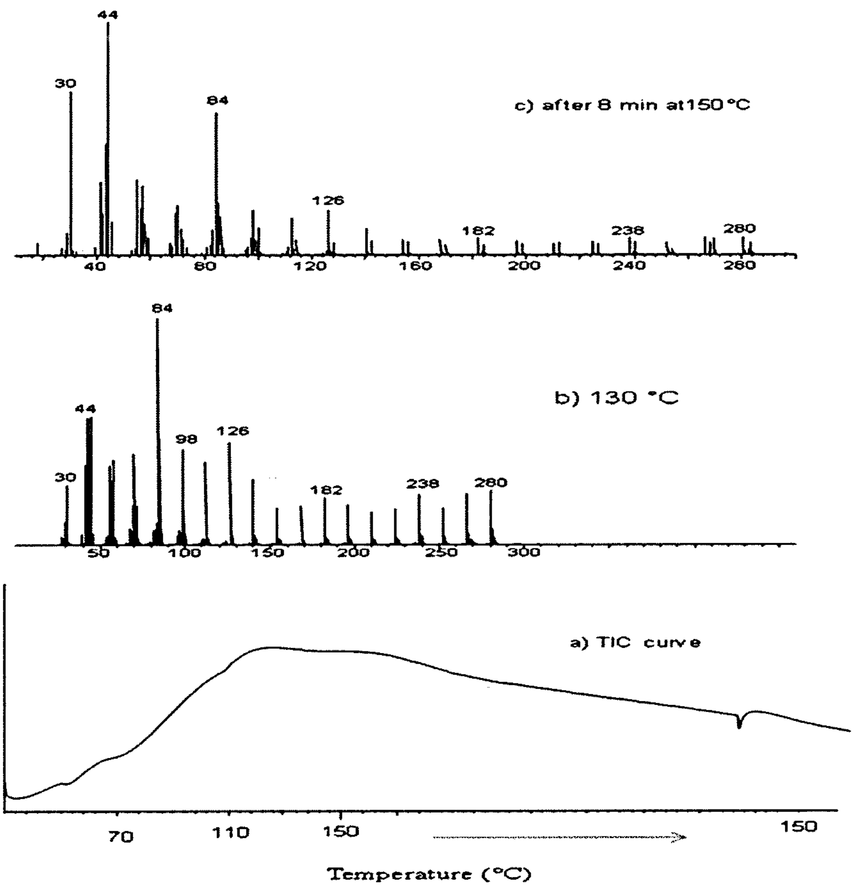

Figure 17: a. The total ion current curve and the mass spectra recorded at b. 130 °C and c. after 8 minute at 150 °C for 15Na-C18 monomer

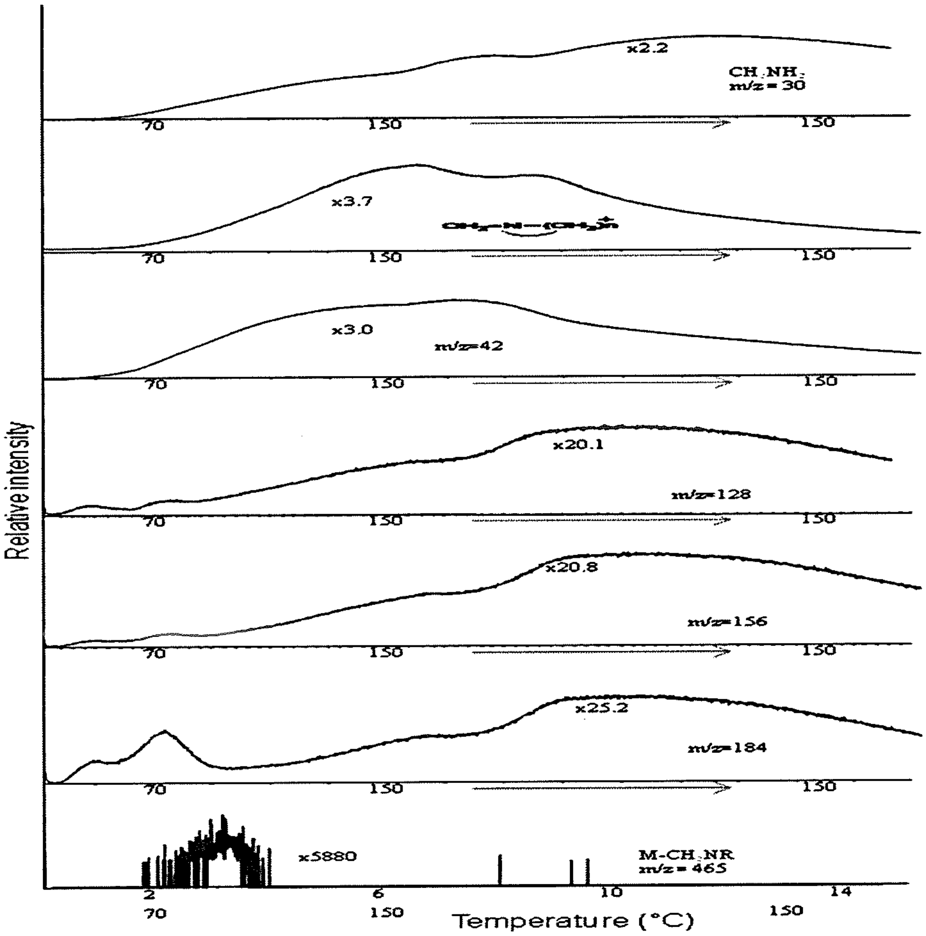

Figure 18: Single ion evolution products of some characteristic products detected during the curing process of 15Na-C18 monomer

The single ion evolution profiles of the peaks detected in the pyrolysis mass spectra for all alkyl-functional naphthoxazine monomers are grouped and analyzed. To understand the effect of the alkyl chain length on the fragmentation of the monomers, both the differences and the similarities of the single ion evolution profiles of all products were analyzed.

The TIC curves of all alkyl-functional naphthoxazine monomers have more than one peak (Figure 19). The pyrolysis mass spectra of the monomers detected at the temperatures up to the curing temperatures were very similar to each other, but the pyrolysis mass spectra detected around the first curing temperature were quite different. The molecular ion peaks were detected for all the monomers, except 15Na-C18, before the curing temperature indicating the evaporation of the monomers before decomposition. In addition, the relative intensity of the molecular ion peak decreased as the chain length of the alkyl substituent on N increased and for 15Na-C18, the molecular ion peak was undetectable as expected for molecules involving long alkyl chains.

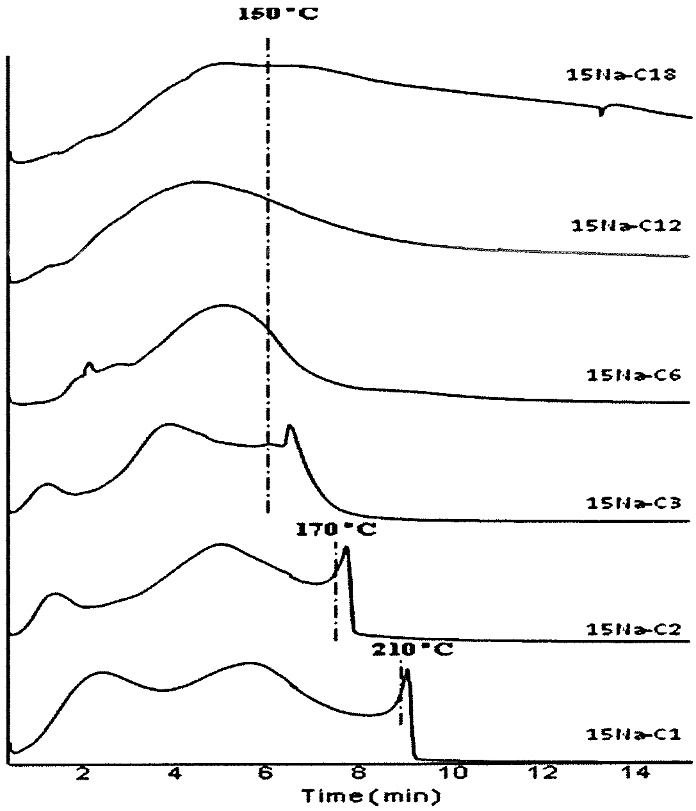

Figure 19: TIC curves of alkyl amine based naphthoxazines

If a molecule contains a heteroatom, the molecule ionizes generally by the removal of an electron from a nonbonding orbital of the heteroatom and ∝-cleavage is one of the main fragmentation patterns. This fragmentation pattern is favored most in amines. Yet, if the molecule contains two heteroatoms, fragmentation pattern depends on the heteroatom and stability of the ions generated.

To determine all the possible fragmentation pathways during EI ionization of the naphthoxazine monomers, the single ion evolution profiles of each product detected in the pyrolysis mass spectra were analyzed and compared with each other (Figure 20).

The first group of fragments were produced by loss of one or two CH_2=NR groups from the monomers producing a resonance stabilized hydroxytropylium ion which further eliminates CO (Scheme 7).

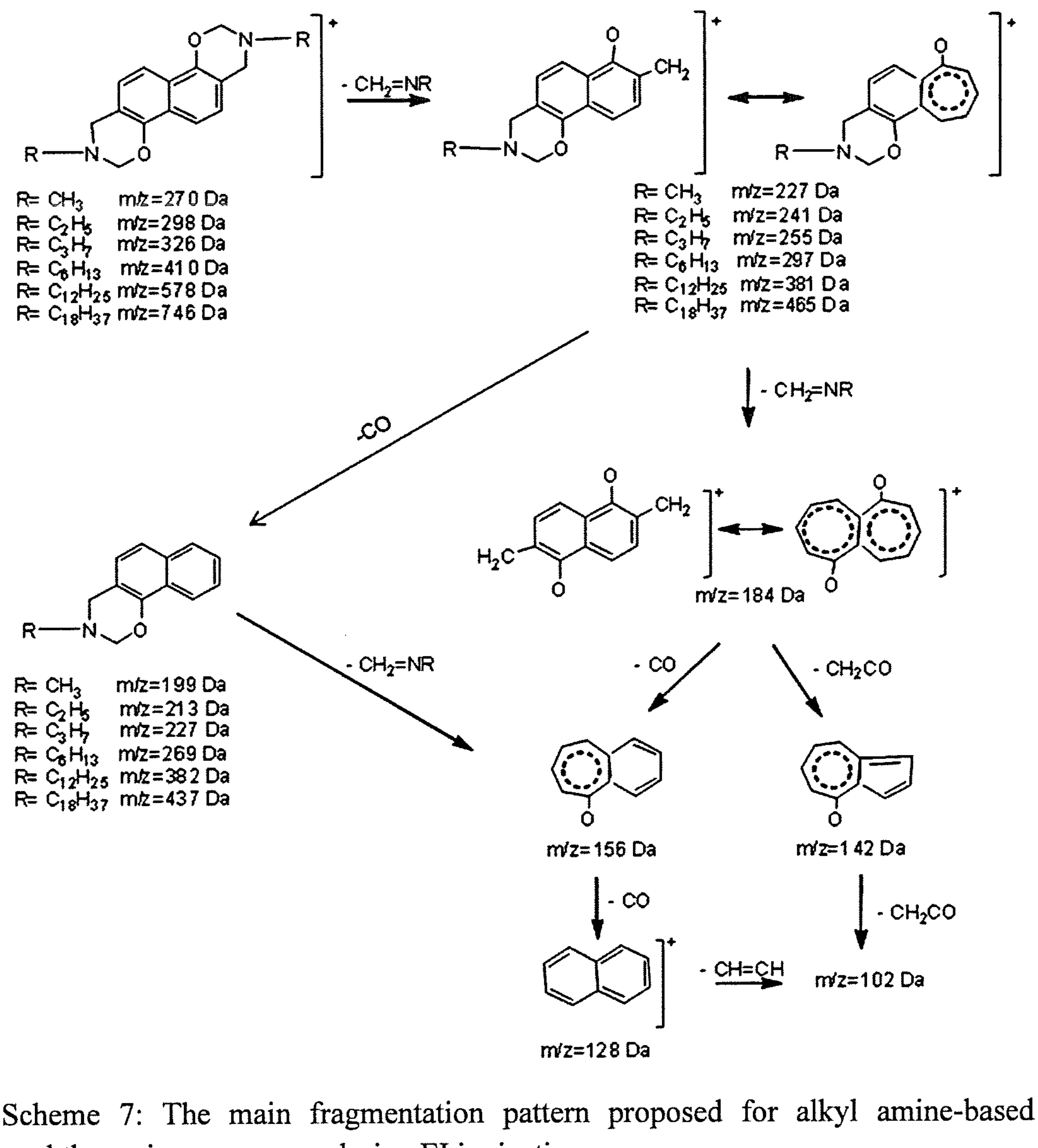

Scheme 7: The main fragmentation pattern proposed for alkyl amine-based naphthoxazine monomers during EI ionization

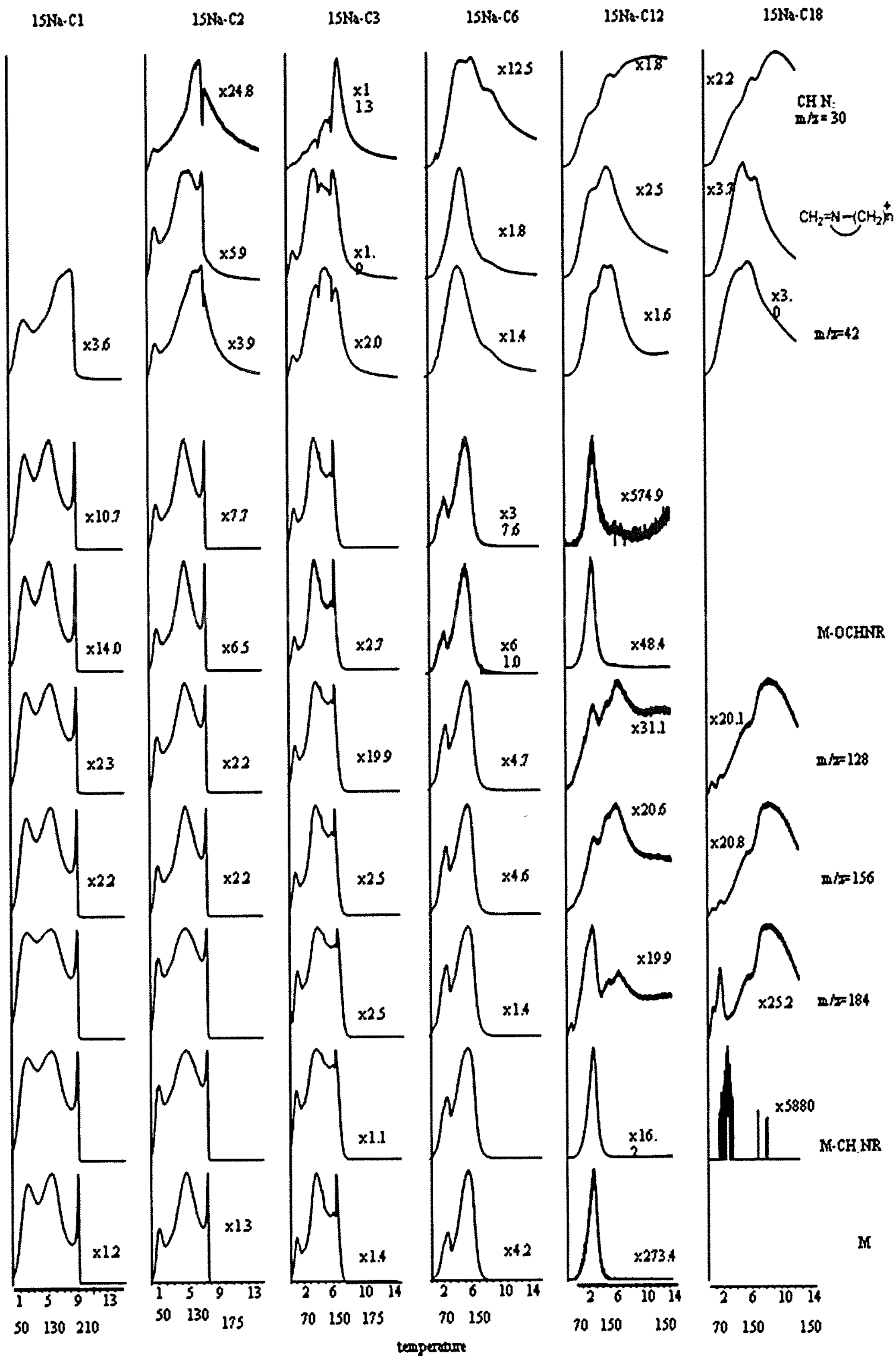

Figure 20: Single ion evolution profiles of some products generated during EI ionization of alkyl amine based naphthoxazine monomers

Another fragmentation pathway is the elimination of one or two O=CHNR groups from the monomers, except for 15Na-C18 (Scheme 8). However, the relative intensities of the peaks detected due to elimination of O=CHNR groups from the monomer were less than the peaks detected due to elimination of CH_2=NR groups from the monomer.

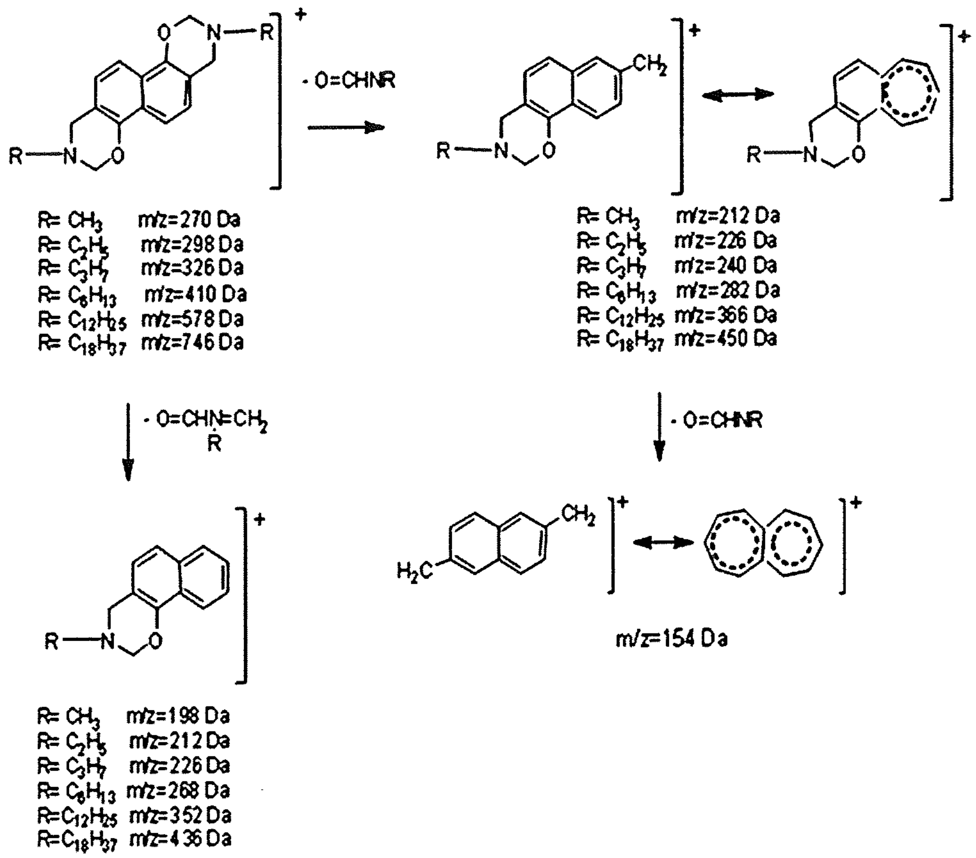

Scheme 8: Fragmentation patterns proposed for alkyl amine-based naphthoxazine monomers during EI ionization

The third group of fragments were cyclic CH_2=N$(CH_2)_n$ ions (where $n \geq 2$) (Scheme 9). The related peaks were not detected in the mass spectra of 15Na-C1. It was also detected that the relative intensity of the peaks due to CH_2=N$(CH_2)_n$ ion increased as the length (n) of the alkyl chain increased as expected.

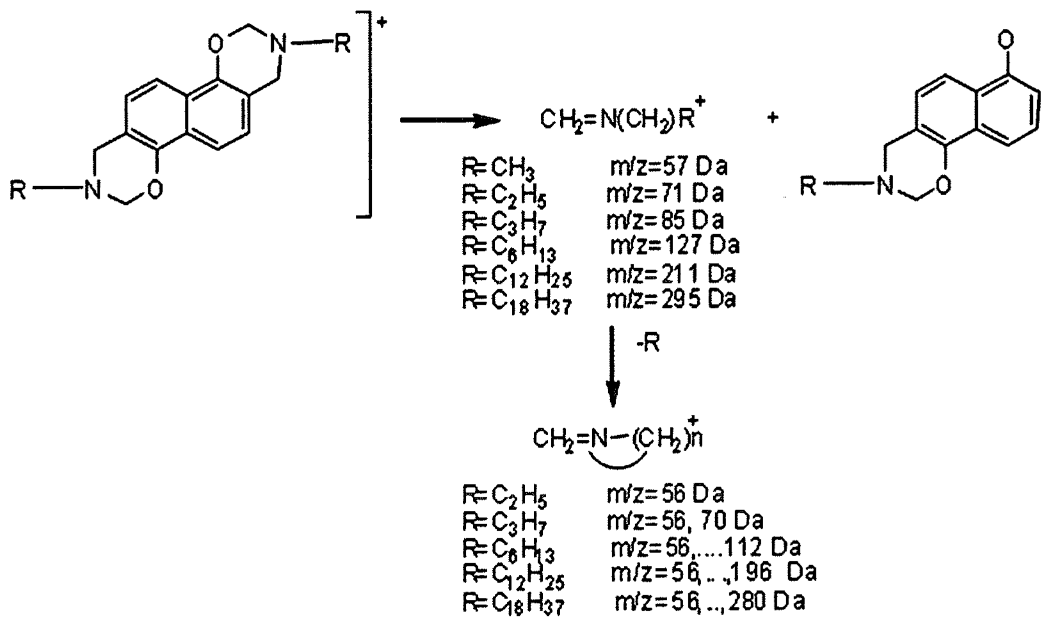

Scheme 9: Fragmentation patterns proposed for alkyl amine-based naphthoxazine monomers during EI ionization

The base peak in the pyrolysis mass spectra of 15Na-C1, 15Na-C2, 15Na-C3 and 15Na-C6 was at m/z = 227, 241, 255 and 297 Da, respectively, due to [M - CH_2=NR] (Scheme 7). The pyrolysis mass spectra of 15Na-C12 and 15Na-C18 were quite different than those of the other monomers. The base peak in the pyrolysis mass spectra of 15Na-C12 and 15Na-C18 was 84 Da (CH_2=N-$(CH_2)_4$ ion), produced as shown in Scheme 9. However, the peaks corresponding to the fragments produced by the classical fragmentation of the monomers were also detected.

All the product ions detected in the mass spectra of naphthoxazines, except imonium $CH_2=\overset{+}{N}(CH_2)_n$ and other related ions, were aromatic and thus, resonance stabilized (Schemes 7 and 8). The intense peaks detected in the mass spectra of short chain alkyl amine based naphthoxazines belong to aromatic products. On the other hand, besides the peaks due to alkyl fragments, intense peaks due to amines were detected in the mass spectra of longer chain alkyl amine based naphthoxazines. The relative intensities of the peaks due to molecular ion and high mass fragments decreased as the molecular weight of the naphthoxazine increased, in accordance with expectations.

In general, the detection of molecular ion peak and/or the peaks due to the products produced by the possible fragmentation pathways indicates the evaporation of the monomers before decomposition. On the other hand, similar fragments might have also been produced if the decomposition of the monomers took place during the curing of the monomers. Consequently, to understand all possible processes taking place during curing, for each sample, single ion evolution profiles of each product detected in the pyrolysis mass spectra were analyzed and compared with each other and with that of the molecular ion (Figure 20). The single ion evolution profiles of molecular ion and fragment ions generated during ionization show identical trends (Figure 20). This similarity is generally the indication of the evaporation of the monomer before decomposition.

For all the monomers, except 15Na-C12 and 15Na-C18, the single ion evolution profiles of the series of products having an aromatic structure, generated as shown in Schemes 7 and 8, show identical trends with the corresponding molecular ion. Yet, the trends of the single ion evolution profiles of imonium $CH_2{=}\overset{+}{N}(CH_2)_n$ and other N involving ions were significantly different than those of the molecular and aromatic fragment ions. The single ion evolution profiles showed that the yield of the molecular ion and the aromatic fragment ions decreased almost exponentially above the first curing temperature (Figure 20). On the other hand, the yield of the imonium ions was maximized near to the first curing temperature where the yield of other products was relatively low.

The single ion evolution profiles of the fragment ions of 15Na-C12 and C18 showed noticeable differences (Figure 20). For 15Na-C12, single ion evolution profiles of the molecular ion and the fragment ion with m/z = 381 Da showed a single peak with a maximum at around 120 °C. However, products with m/z = 128, 156 and 184 Da involving aromatic rings produced by further fragmentation of the molecular ion were detected also above 150°C. For 15Na-C18, the evolution of the fragments was continued in a broad temperature range. At low temperatures during the curing, the yield of fragments involving aromatic structure was very low. However, around 70°C, the yield of 184 Da fragment, involving aromatic structure, increased sharply. The peaks due to molecular ion and high molecular weight fragment ions were not detected above the first curing temperature, 150°C. Conversely, at this region, the yield of low molecular weight aromatic fragments, m/z=184, 156 and 128 Da, increased significantly up to 150°C as in the case of 15Na-C12. The yield of cyclic amines and N involving fragments also increased in a broad temperature range up to the first curing temperature and decrease at 150 °C.

Thus, it can be concluded that alkyl-substituted naphthoxazine monomers evaporated below the curing temperature. Up to the curing temperature, the mass spectra were dominated with products generated by the main fragmentation pathways as shown in Scheme 7. But, around the curing temperature, the relative yields of imonium ions were increased. The yield of these fragments could be increased either due to an increase in the probability of removal of an electron from N and fragmentation through the mechanism shown in Scheme 9 or due to decomposition of the cyclic side chains and elimination of nitrogen containing fragments during the curing process at higher temperatures. Both possibilities can be explained by the activation of lone pair electrons on N around the curing temperatures.

The yields of molecular ion and the fragment ions involving aromatic structure were decreased sharply in the region where the evolution of fragments involving nitrogen was observed during the curing of all monomers. In addition, for 15Na-C12 and C18, low mass aromatic fragments were also detected in the region where evolution of fragments involving nitrogen nearly completed. These observations confirmed the decomposition of cyclic side chains and elimination of N containing fragments. The generation of alkyl amines was occurred up to the curing temperature. For all the monomers, except 15Na-C1, the production of $CH_2{=}NH_2$ was continued in the region where no other fragment was detected so it can be concluded that CH_2=NH_2 was produced by some rearrangement reactions due to the polymerization of the monomers just above the curing temperature.

3.2.2 Pyrolysis of alkyl-functional polynaphthoxazines

Direct pyrolysis analyses of the polynaphthoxazines prepared by applying the curing programs given in Table 1 were performed to investigate the thermal degradation characteristics.

3.2.2.1 Pyrolysis of 15Na-C1 polymer (P15Na-C1)

In Figure 21, the total ion current (TIC) curve and the pyrolysis mass spectra at 310, 390 and 440 °C recorded during the pyrolysis of P15Na-C1 polymer are shown. The TIC curve of P15Na-C1 has two maxima at 440 and 270 °C. The mass spectra showed noticeable differences indicating a complex degradation mechanism. The intense peaks at 310 °C at m/z = 28 (C_2H_4), 30 (CH_2NH_2), 44 ($C_2H_4NH_2$), 57 (C_3H_7N), 70 ($C_3H_6N_2$), 73 ($C_3H_8N_2$), 97 ($C_5H_9N_2$) and 125 Da ($C_7H_{13}N_2$) and at 390 °C at m/z = 28, 30, 44, 57, 70 and 83 ($C_4H_7N_2$) Da and those dominant at 440 °C, at m/z = 28, 30, 44, 70 and 83 Da are attributed to alkyl amine fragments. The detection of products involving more than one N indicated coupling of the alkyl amine radicals that were generated by ring-opening polymerization during curing. Single ion evolution profiles of some characteristic products detected during the pyrolysis of P15Na-C1 polymer are shown in Figure 22. Evolution of alkyl amines and diamines at around 300 °C confirmed that the degradation of the polymer started by loss of these groups. Furthermore, the trends in the evolution profiles of low mass alkyl amines with m/z = 30 (CH_2NH_2), 44 (C_2H_6N), 70 ($C_3H_8N_2$ or C_4H_8N) and 72 Da ($C_4H_{10}N$ or $C_3H_8N_2$) were different confirming that they were produced as a result of different degradation pathways. It can also be observed from Figure 22 that the peak at m/z = 188 Da due to $C_{10}H_4(OH)_2CH_2NH_2$) ion involving naphthoxazine ring started to appear in the pyrolysis mass spectra at around 300 °C indicating the degradation of polymer chains with naphthoxazine units were started at this region.

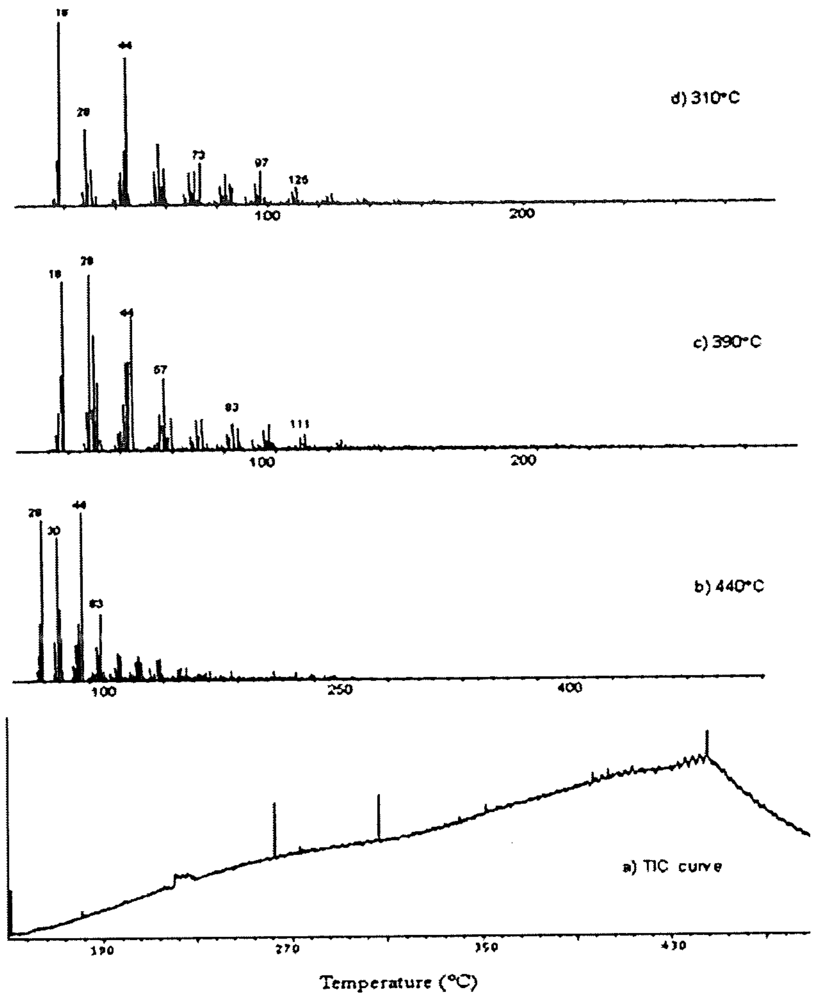

Figure 21: a. The total ion current curve and the mass spectra recorded at b. 440 °C and c. 390 °C d. 310 °C recorded during the pyrolysis of P15Na-C1 polymer

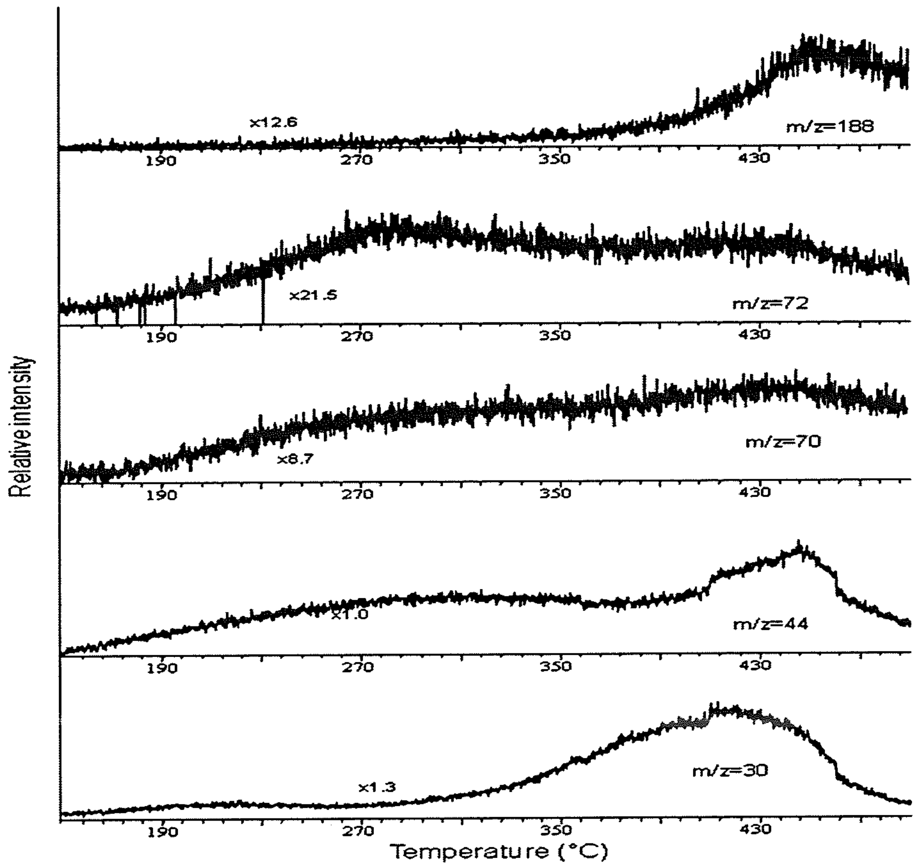

Figure 22: Single ion evolution products of some characteristic products detected during the curing process of P-15Na-C1 polymer

3.2.2.2 Pyrolysis of 15Na-C2 polymer (P15Na-C2)

The total ion current (TIC) curve of P15Na-C2 shows two peaks with maxima at around 310 and 430 °C. The TIC curve and the pyrolysis mass spectra recorded at 310 and 430 °C during the pyrolysis of P15Na-C2 polymer are shown in Figure 23. The intense peaks in the pyrolysis mass spectrum recorded at 310 °C and 430 °C are at m/z = 28 (C_2H_4), 44 ($C_2H_4NH_2$), 57(C_3H_7N) , 73 (C3H8N2) and 97 Da (C5H9N2) and at m/z = 115 ($C_6H_4C_3H_3$), 131 ($C_6H_3(OH)C_3H_3$), 145 ($C_9H_6(OH)CH_2$), 174 ($C_{10}H_5(OH)_2CH_3$), 188 ($C_{10}H_4(OH)_2CH_2NH$) and 226 Da ($C_{10}H_{10}N(OH)_2$) (Table 4). Detection of ions involving naphthoxazine ring (at m/z = 174, 188) pointed out the degradation of the polymer. Single ion evolution profiles of some products detected during the pyrolysis of P15Na-C2 polymer are shown in Figure 24. The low mass alkyl amines with m/z = 30 (CH_2NH_2), 44 ($C_2H_6N_2$) and 72 Da ($C_4H_{10}N$ or $C_3H_8N_2$) had almost identical evolution profiles. They were produced around 200 °C signifying that the polymer started to degrade by loss of these groups. However, evolution of other alkyl amines at ($C_3H_8N_2$ or C_4H_8N) followed a different trend indicating that its generation occurred by a different degradation pathway. In addition, the products involving naphthoxazine ring such as 188 Da fragment started to evolve at around 350 ° C. Thus, it can be concluded that degradation of the polymer chains involving aromatic rings started at around this temperature.

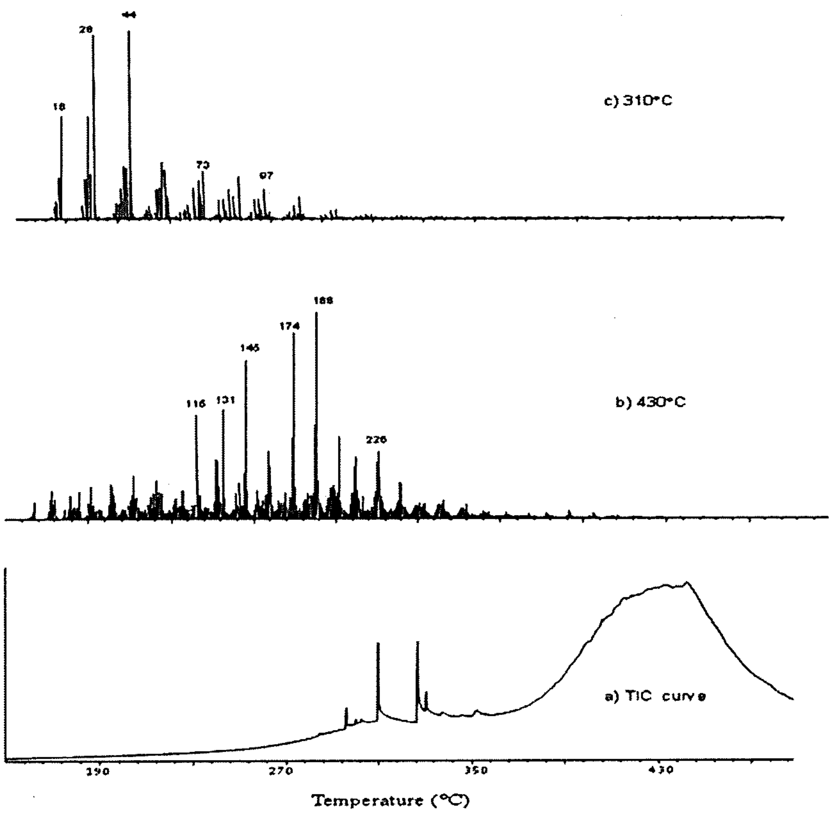

Figure 23: a. The total ion current curve and the mass spectra recorded at b. 430 °C and c. 310 °C during the pyrolysis of P15Na-C2 polymer

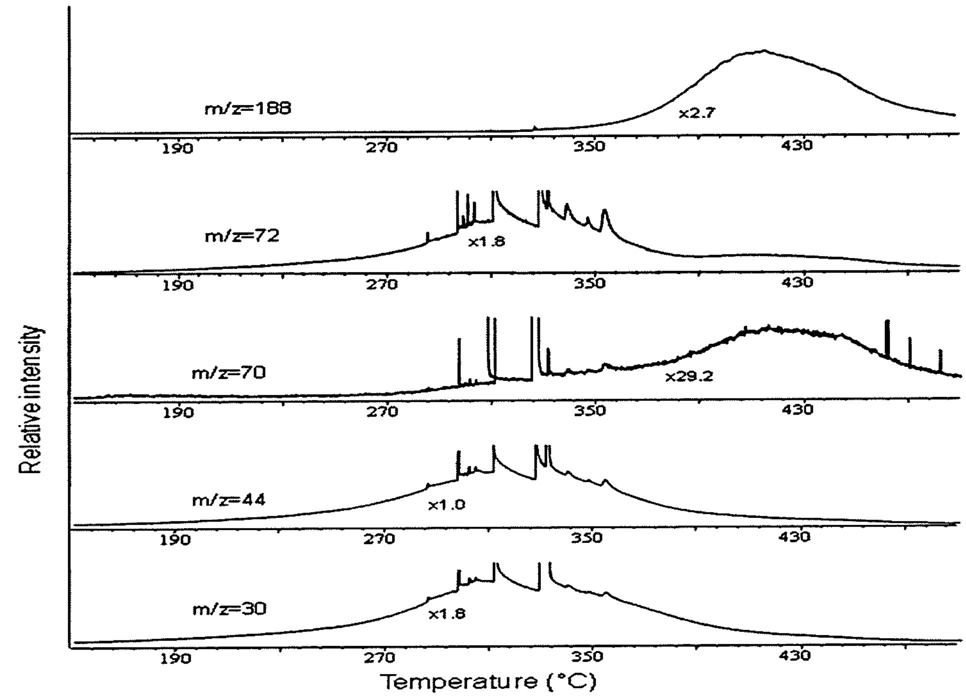

Figure 24: Single ion evolution products of some characteristic products detected during the curing process of P-15Na-C2 polymer

3.2.2.3 Pyrolysis of 15Na-C3 polymer (P15Na-C3)

The total ion current (TIC) curve and the pyrolysis mass spectra at 440, 320 and 270 °C recorded during the pyrolysis of P15Na-C3 polymer are given in Figure 25. The TIC curve of P15Na-C3 shows two peaks the first being weaker with a shoulder at 270 °C. The peaks detected at 270 °C at m/z = 30 (CH_2NH_2), 44 ($C_2H_4NH_2$), 58 (C_3H_8N) and 72 Da ($C_4H_{10}N$) were attributed to low mass alkyl amines. Around 320 °C, the evolution of alkyl amines and diamines were continued. However, around 440 °C peaks that can readily be associated with fragments involving aromatic ring were detected. In this region relative intensities of alkyl amine peaks were quite weak. In Figure 26, single ion evolution profiles of some products detected during the pyrolysis of P15Na-C3 were shown. The trends observed in the evolution profiles pointed out presence of polymer chains with different thermal stabilities that decompose through a multi step thermal degradation process.

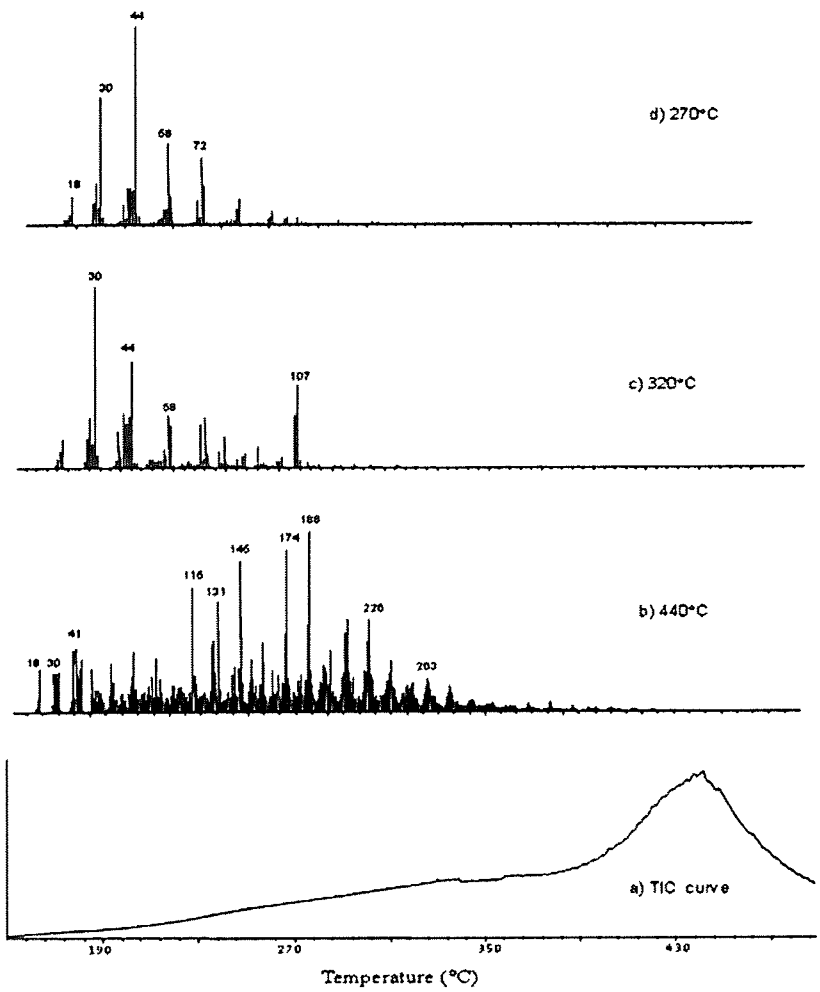

Figure 25: a. The total ion current curve and the mass spectra recorded at b. 440 °C and c. 320 °C and d. 270 °C during the pyrolysis of P15Na-C3 polymer

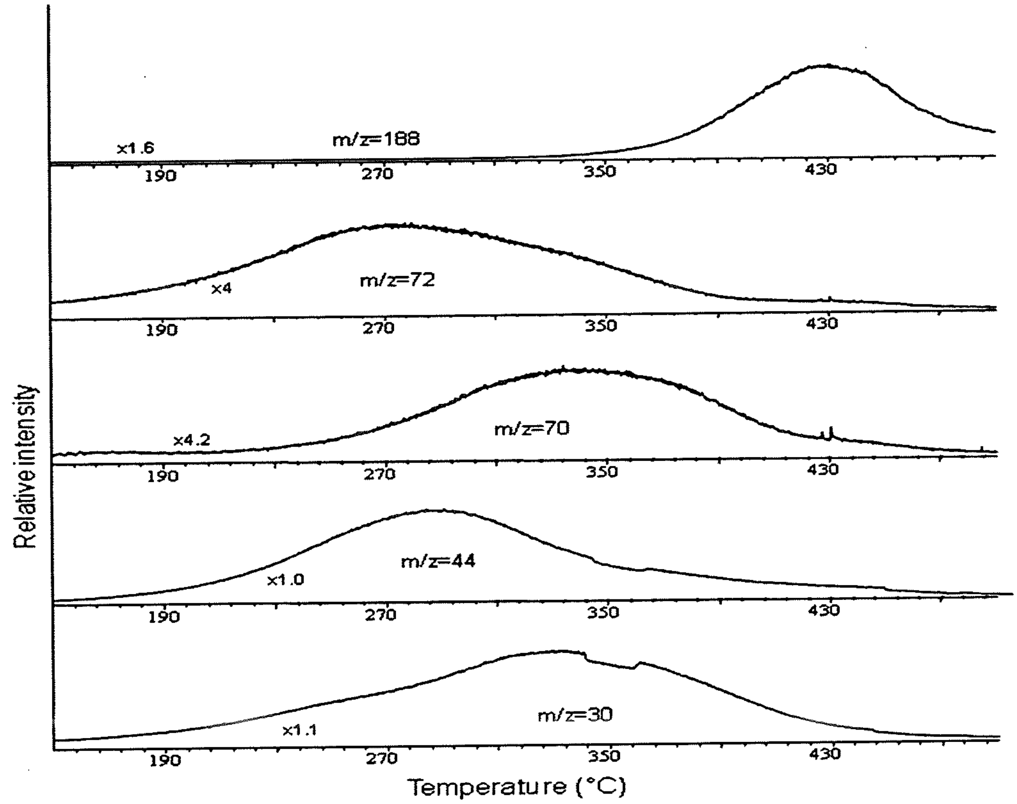

Figure 26: Single ion evolution products of some characteristic products detected during the curing process of P-15Na-C3 polymer

3.2.2.4 Pyrolysis of 15Na-C6 polymer (P15Na-C6)

The total ion current (TIC) curve and the pyrolysis mass spectra at 270, 320 and 450 °C recorded during the pyrolysis of P15Na-C6 polymer are given in Figure 27. The TIC curve of P15Na-C6 showed a broad weak peak around 320 °C and an intense peak with a maximum at 450 °C. The peaks detected at 270 °C were at m/z = 30, 44, 58, 72, 86 and 112 Da attributed to CH_2NH_2, $C_2H_4NH_2$, C_3H_8N, $C_3H_8N_2$, $C_4H_{10}N_2$, $C_7H_{14}N$ respectively. The mass spectra recorded around 320 °C were again dominated with peaks that can be attributed to alkyl amines. In this region relative intensities of the peaks due to high mass alkyl amines such as 112 Da fragment were increased. Weak peaks that can be associated with aromatic fragments such as 149 ($C_{10}H_4C{\equiv}CH$) and 191 Da ($C_{10}H_4(OH)(C{\equiv}CH)_2$) were also appeared in this region. Single ion evolution profiles of some products detected during the pyrolysis of P15Na-C6 are shown in Figure 28. The evolution profiles of N involving fragments showed different trends. Thus, it can be concluded that alkyl amines were produced through different degradation pathways. Additionally, the fragments involving naphthoxazine ring were maximized at around 440 °C indicating the degradation of the polymer units involving naphthoxazine units in the final stages of pyrolysis.

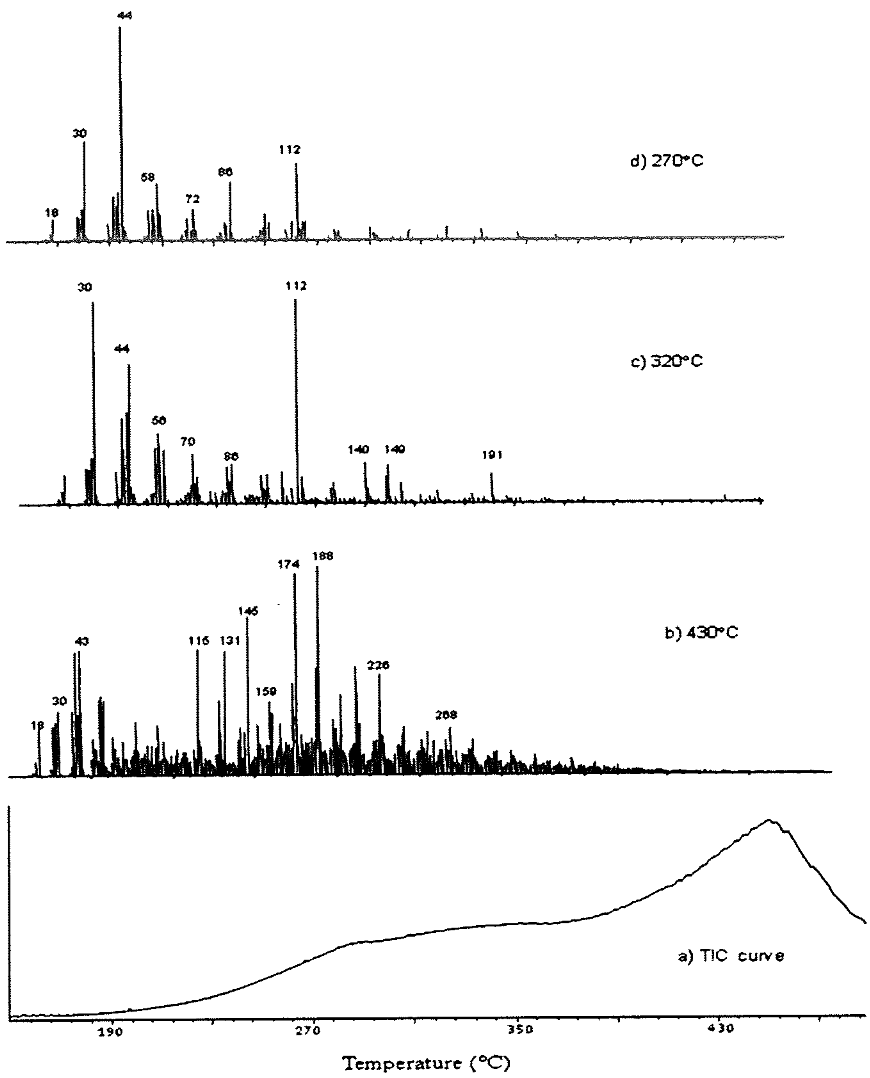

Figure 27: a. The total ion current curve and the mass spectra recorded at b. 430 °C and c. 320 °C and d. 270 °C during the pyrolysis of P15Na-C6 polymer

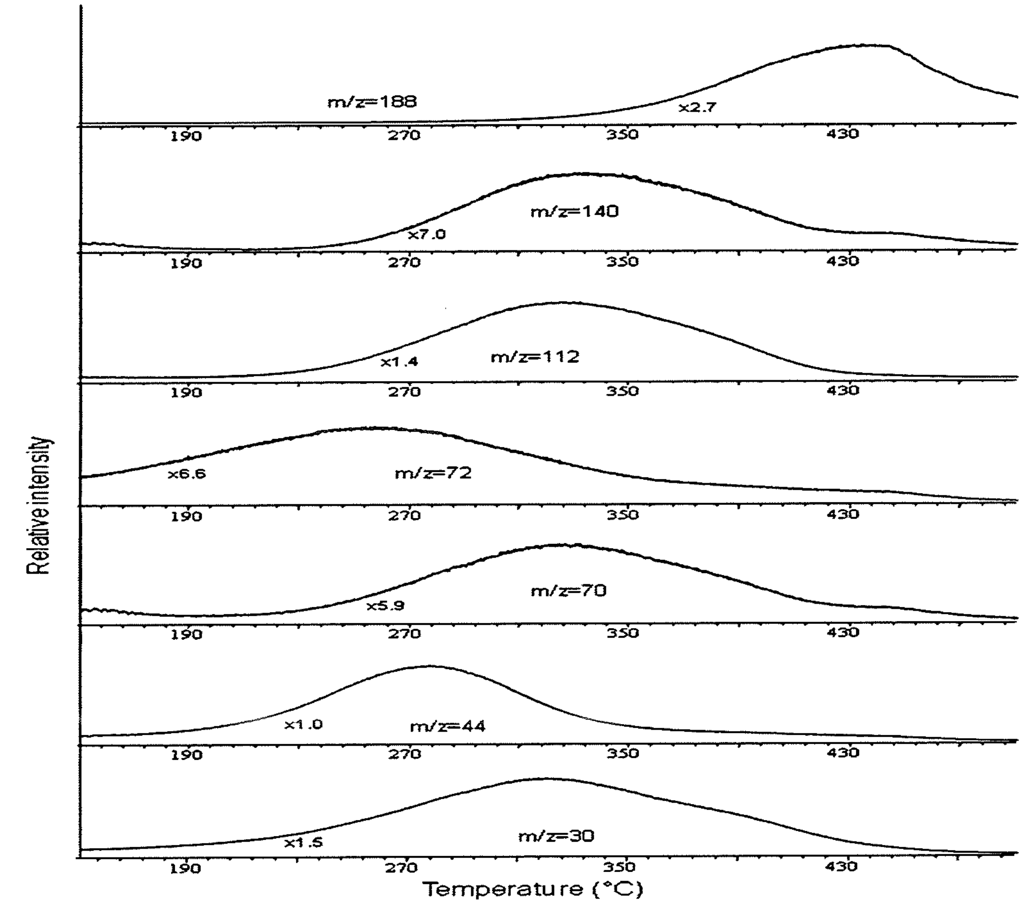

Figure 28: Single ion evolution products of some characteristic products detected during the curing process of P-15Na-C6 polymer

3.2.2.5 Pyrolysis of 15Na-C12 polymer (P15Na-C12)

The TIC curve of P15Na-C12 shows two broad peaks with maxima at around 325 and 440 °C and a shoulder at around 240 °C (Figure 29). Again at low temperature ranges below 350 °C alkyl amines and diamines peaks were detected as in case of other polynaphthoxazines. Besides the alkyl amine and diamine peaks, intense 280 Da peak was detected in this temperature range. The significantly intense 280 Da peak can be associated with two naphthoxazine rings connected by an acetylene unit, with a highly stable structure (Table 4). Evolution of this product at low temperatures indicated that this unit was generated during the curing process as alkyl amines were eliminated and connected to the polymer backbone by weak linkages. Single ion evolution profiles of some products detected during the pyrolysis of P15Na-C12 are presented in Figure 30 pointing out again different evolution profiles for alkyl amine fragments. Again, the yield of the products involving naphthoxazine units increased in the region where the yield of alkyl amine fragments decreased. Thus, it can be concluded that P15Na-C12 degrades through a multi-step degradation process.

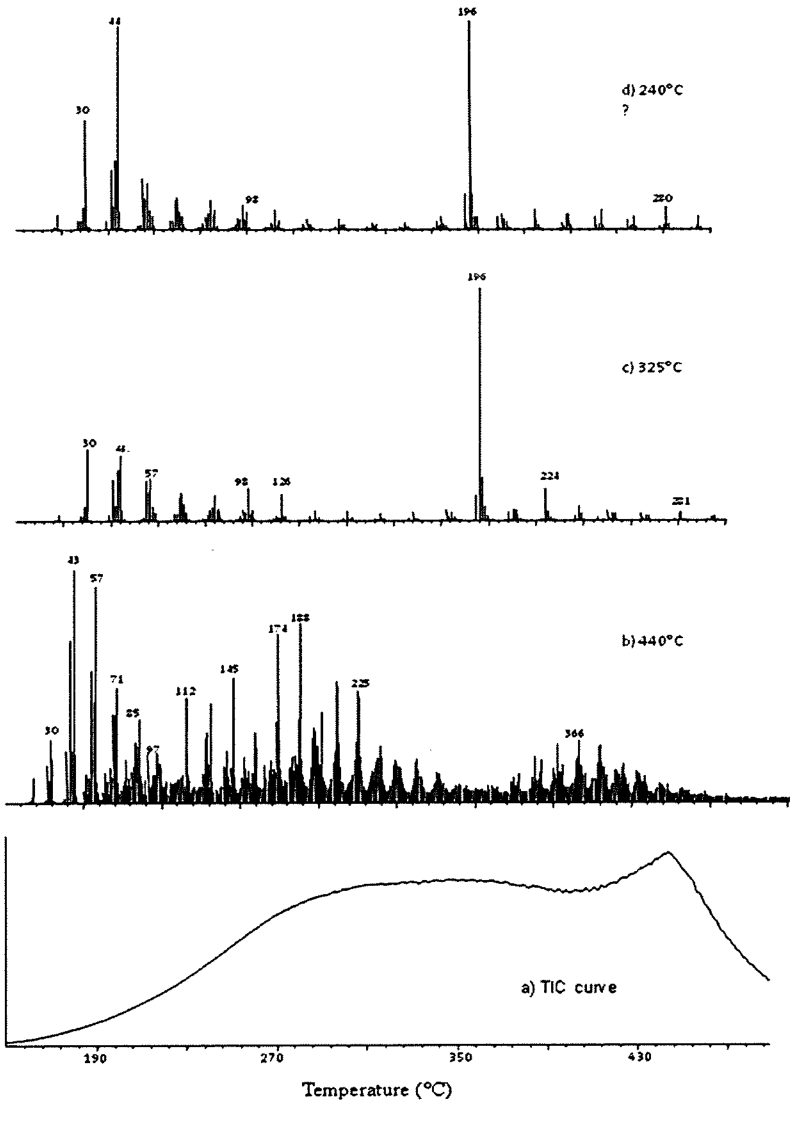

Figure 29: a. The total ion current curve and the mass spectra recorded at b. 440 °C and c. 325 °C and d. 240 °C during the pyrolysis of P15Na-C12 polymer

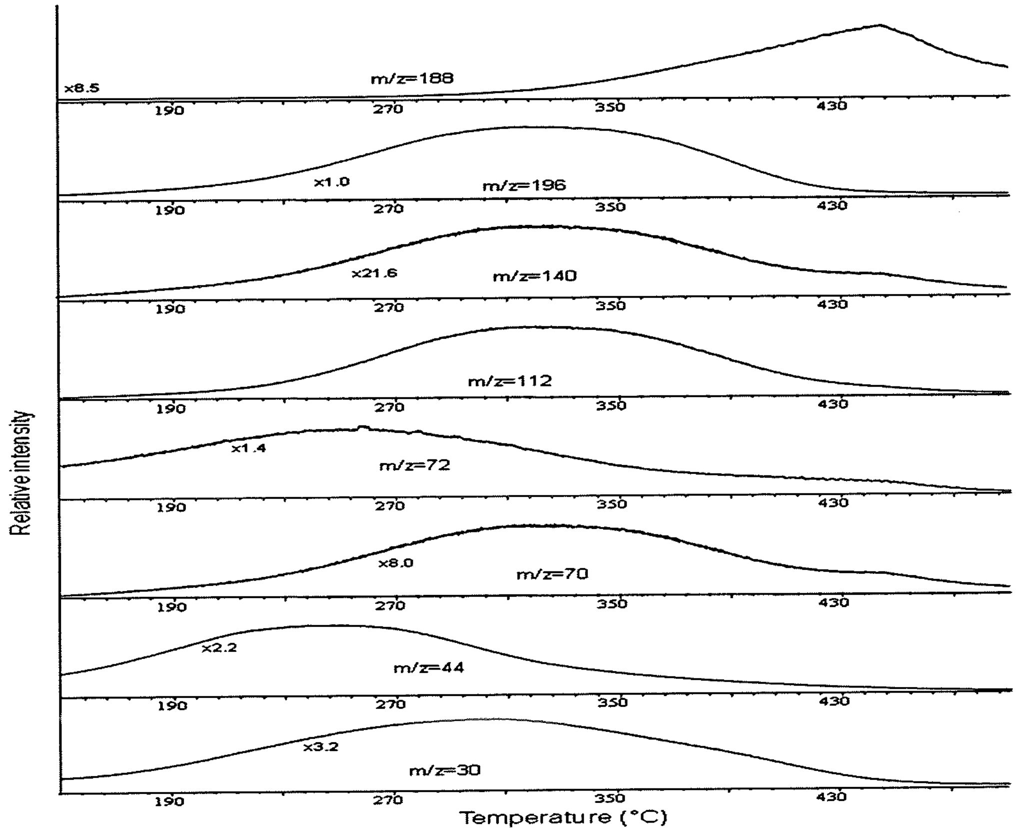

Figure 30: Single ion evolution products of some characteristic products detected during the curing process of P-15Na-C12 polymer

3.2.2.6 Pyrolysis of 15Na-C18 polymer (P15Na-C18)

In Figure 31, the TIC curve and the pyrolysis mass spectra at around the peak maxima in the TIC curve of P15Na-C18 polymer are shown. The mass spectra were dominated with similar peaks. Again intense 280 Da peak was present as in case of P15NaC-12. However, for this polymer its generation was continued over a broader temperature range. Furthermore, intense peaks due to alky amine and alkyl fragments were observed even at around 440 °C. The single ion evolution profiles of some products detected during the pyrolysis of P15Na-C18 are given in Figure 32. The trends in the evolution profiles of products showed significant differences indicating polymer chains with different thermal stability. Thus, it can be inferred that P15Na-C18 has a multi-step degradation process as in case of P15Na-C1 to C12.

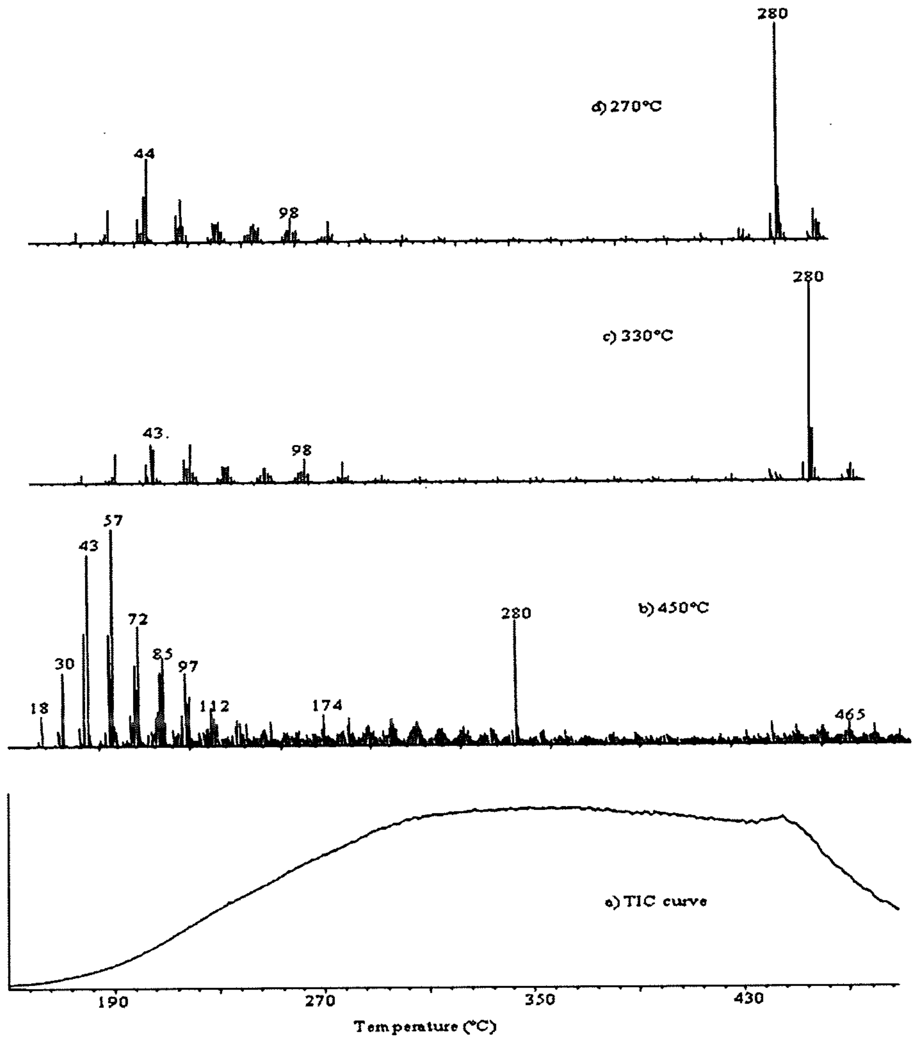

Figure 31: a. The total ion current curve and the mass spectra recorded at b. 440 °C and c. 330 °C and d. 270 °C during the pyrolysis of P15Na-C18 polymer

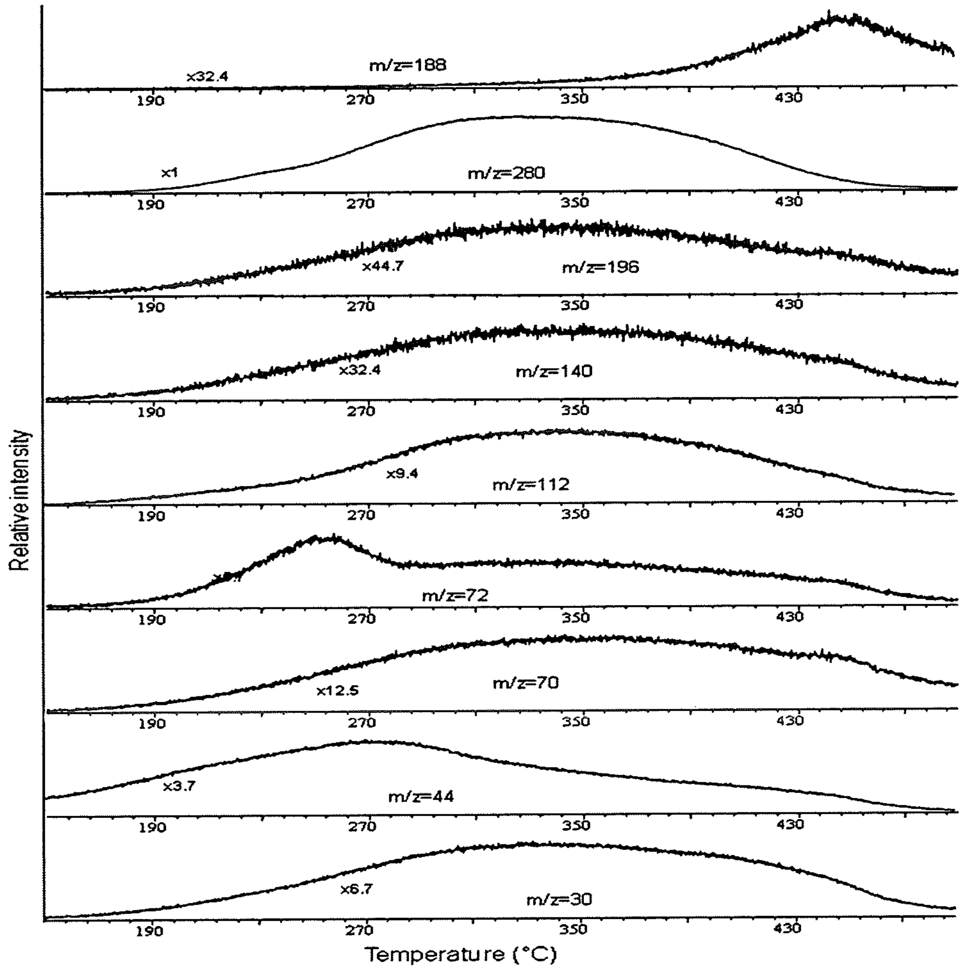

Figure 32: Single ion evolution products of some characteristic products detected during the curing process of P-15Na-C18 polymer

The pyrolysis mass spectra of the alkyl-functional polynaphthoxazines have some similarities. Thus, the interpretations can be done by making comparisons to investigate the effect of the alkyl chain length on the thermal stability of polynaphthoxazines.

The trends of the TIC curves of all polynaphthoxazines were quite similar. These curves showed two broad overlapping peaks at around 270 and 445°C indicating a complex decomposition mechanism. The intensity of the first peak in the TIC curves of polynaphthoxazines around 270 °C, increased as the alkyl chain length increased (Figure 33).

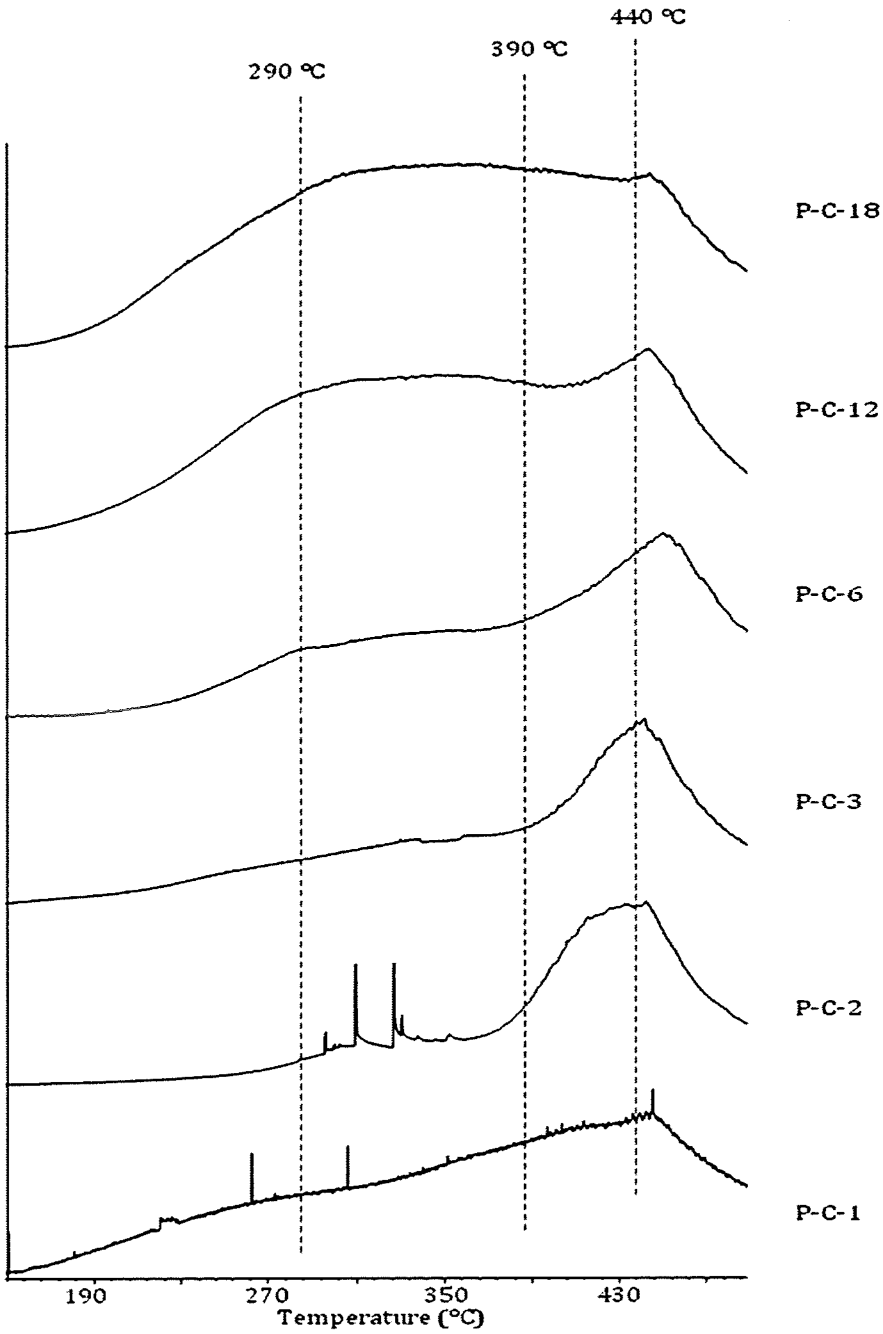

Figure 33: TIC curves of alkyl amine based polynaphthoxazines

The peaks, at around 270 °C, were attributed to loss of alkyl amine fragments such as at m/z=30Da ($CH_2{=}NH_2$), 44 Da (CH_3CH_2NH or C_2H_6N), 57 Da (C_3H_7N), 72 Da ($C_4H_{10}N$) and 97 Da ($C_6H_{11}N$). Alkyl amine peaks with relatively high m/z values compared to those of the related $CH_2N(R)CH_2$ groups were detected for all the polymers, even for P-15Na-C1. One of the examples is the presence of 70 Da (C_4H_8N or $C_3H_6N_2$) peak in the mass spectra of P-15Na-C1. Above 400°C, the intense peaks due to the fragments involving naphthoxazine ring, such as the peaks at m/z= 174 ($C_{10}H_5(OH)_2CH_3$) and 188 Da ($C_{10}H_4(OH)_2CH_2NH$), were detected indicating the degradation of the polymer chains involving naphthoxazine units. The intensities of these peaks were relatively low in the mass spectra of P-15Na-C1 (Figure 21) pointing out that the loss of naphthoxazine ring was not very likely in the temperature range studied. In Table 4 intense and/or characteristic peaks detected during the curing of alkyl amine based polynaphthoxazines are summarized.

To understand the thermal degradation and polymerization mechanisms, single ion evolution profiles of some products compared with each other (Figure 34). The trends in the evolution profiles of fragments involving alkyl amines showed significant differences, thus, alkyl amines are grouped considering these differences. In the first group, the maximum yield of fragments $C_2H_4NH_2$ (m/z=44) and $C_4H_{10}N$ or $C_3H_8N_2$ (more probable) (m/z=72 Da) were detected at around 270 °C. However, the maximum yield of the second group of the fragments such as CH_2NH_2 (m/z=30 Da), C_4H_8N or $C_3H_6N_2$ (m/z=70 Da), $C_7H_{14}N$ or $C_6H_{12}N_2$ (m/z=112 Da) etc were detected at around 330 °C. The relative yields of alkyl amine fragments were similar for all the polymers pointing out that the alkyl chain length had no effect on lose of alkyl amines. On the other hand, the relative intensity of the peaks due to high mass amines increased as the alkyl chain length increased. Additionally, for P15Na-C1 and P15Na-C2, the single ion pyrograms of alkyl amine fragments showed a second peak with a maximum at around 440 °C for P15Na-C1 (Figure 34). These findings indicated that they were generated through two different degradation pathways.

Table 4. Peaks present in the pyrolysis mass spectra of polynaphthoxazines, the proposed structures and the temperatures at which the product yields were maximized

m/z (Da)	Assignment	Alkyl amine based polynaphtoxazines and peak maxima temperature (°C)					
		C1	C2	C3	C6	C12	C18
28	C_2H_4	310, 450	310, 330	330, 400	65, 300	290, 450	360
30	CH_2NH_2	210, 390	310, 330	340	320	310	340
41	CH_2NCH or C_3H_5	410	310, 330	360	340	310	440
42	C_2H_4N	390	310, 330	360	320	300	440
43	C_2H_4NH or C_3H_7	400	310, 330	360	340	330	440
44	$C_2H_4NH_2$ or C_2H_5NH	310, 440	310, 330	290	280	250	270
56	C_3H_6N or $C_2H_4N_2$	440	310, 330	360	350	330	440
57	C_3H_6NH or C_3H_7N or $C_2H_5N_2$ or C_4H_9	430	310, 330	290	340	350	440
58	$C_3H_6NH_2$ or C_3H_7NH or $C_2H_6N_2$	310	310, 330	255	110, 280	290	330
70	$C_4H_6NH_2$ or C_4H_7NH or $C_3H_6N_2$	430	300, 310, 430	340	330	330	350
71	$C_4H_7NH_2$ or $C_3H_7N_2$ or C_5H_{11}	270	310, 330	320	320	370	440
72	$C_4H_{10}N$ or $C_3H_8N_2$	280, 430	310, 430	280	260	260	255
73	$C_3H_6NH_2$ or C_3H_7NH or $C_2H_5N_2$	280	310, 330	280	110, 250	300	250
83	$C_5H_7NH_2$ or C_5H_8NH or $C_4H_7N_2$	270	310, 330, 450	440	310	340	440

Table 4. cont'd

85	$C_5H_9NH_2$ or $C_4H_9N_2$ or C_6H_{13}	290	310, 330	440	150, 310	445	440
86	$C_4H_{10}N_2$	275	310, 330	270, 440	280	280	280
97	$C_5H_9N_2$ or C_7H_{13}	270, 440	430	440	310, 440	370	445
98	$C_5H_{10}N_2$ or C_7H_{14}	440	430	440	150, 330	320	340
107	$C_6H_7N_2$ or C_7H_9N or C_8H_{11}	440	330, 450	350	350	380	385
112	$C_6H_{12}N_2$ or $C_7H_{14}N$ or C_8H_{16}	440	330, 450	170, 440	330	330	340
115	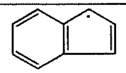	440	450	440	280, 440	445	450
126	$C_7H_{14}N_2$ or $C_8H_{16}N$ or C_9H_{18}	440	450	440	150, 290, 440	320	355
131	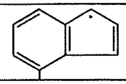	440	450	440	440	445	450
140	$C_8H_{16}N_2$	440	450	440	330	330	340
145	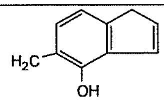	440	415	430	440	445	450
149	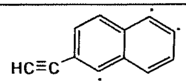	—	445	170, 440	350	445	—
174	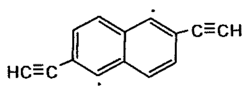 or 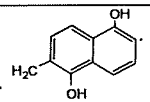	450	430	445	440	445	450

Table 4. cont'd

188	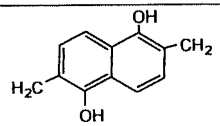	440	415	430	440	445	450
191	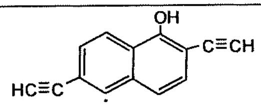	440	445	445	350, 440	445	450
226	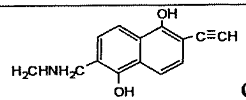 or 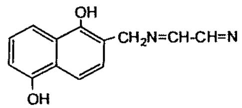	—	445	445	440	445	450
268	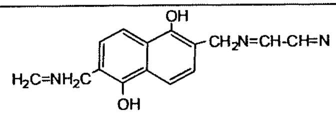	–	445	445	440	240, 450	250, 320
280	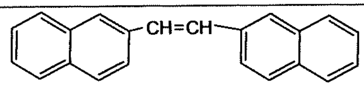	–	445	445	440	360, 450	330

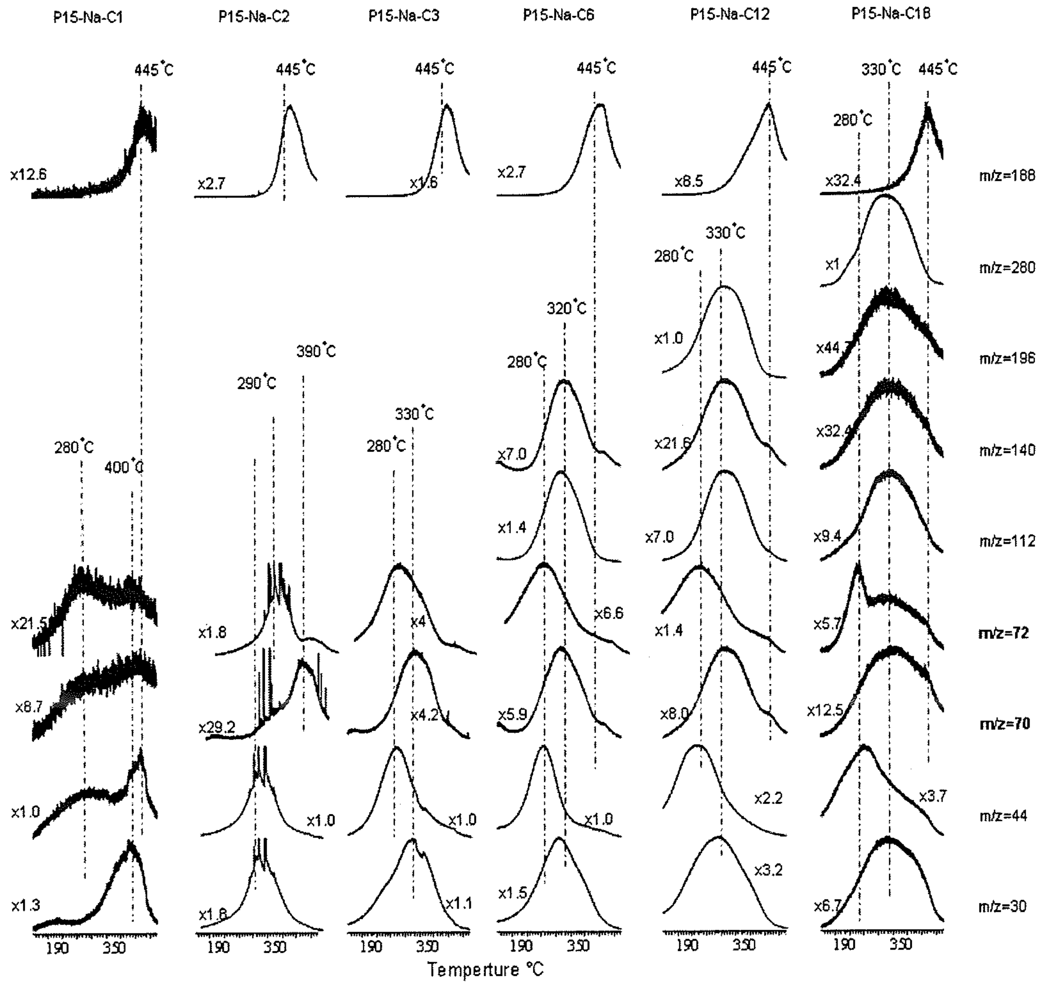

Figure 34: Single ion evolution profiles of some products detected during pyrolysis of alkyl amine based polynaphthoxazines

The bifunctional naphthoxazine monomers do not have a free ortho position and both of the para positions are deactivated due to the presence of the other OH group. Consequently, polymerization by the attack of $-NCH_2$ radicals directly to the naphthoxazine ring is less probable. In addition, as mentioned above, the detection of the peaks due to fragments produced by lose of long alkyl and/or alkyl amine chains, even for 15Na-C1, indicates the coupling of alkyl amine radicals produced by the ring opening of side chains of alkyl functionalized naphthoxazine monomers during the curing process as presented in Scheme 10.

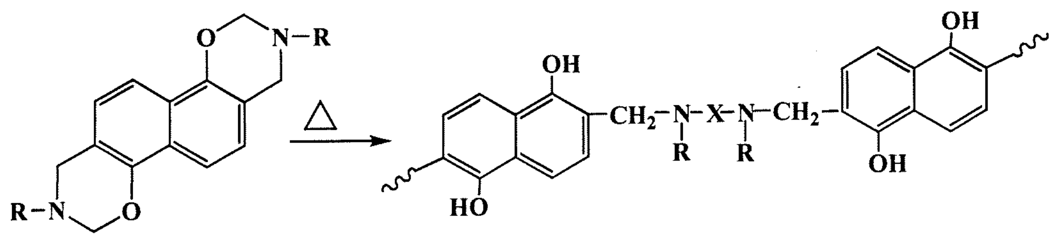

where R = CH_3, C_2H_5, C_3H_7, C_6H_{13}, $C_{12}H_{25}$ or $C_{18}H_{37}$ X = CH_2-CH_2 or CH=CH

Scheme 10: Proposed polymerization mechanism for alkyl amine based naphthoxazines

Consequently, it can be concluded that the polynaphthoxazines generated, as a result of this coupling, involved linkages with different thermal stabilities. Degradation of the polynaphthoxazines involving saturated alkyl chains started by loss of $CH_2CH_2NH_2$ (m/z= 44 Da) and $CH_2NCH_2CH_2NH_2$ (m/z= 72 Da). However, evolution of linkages involving hydrocarbon chains observed at higher temperatures around 330 °C. The radicals generated by loss of alkyl amines can further couple to generate a more stable polymer structure as summarized in Scheme 11.

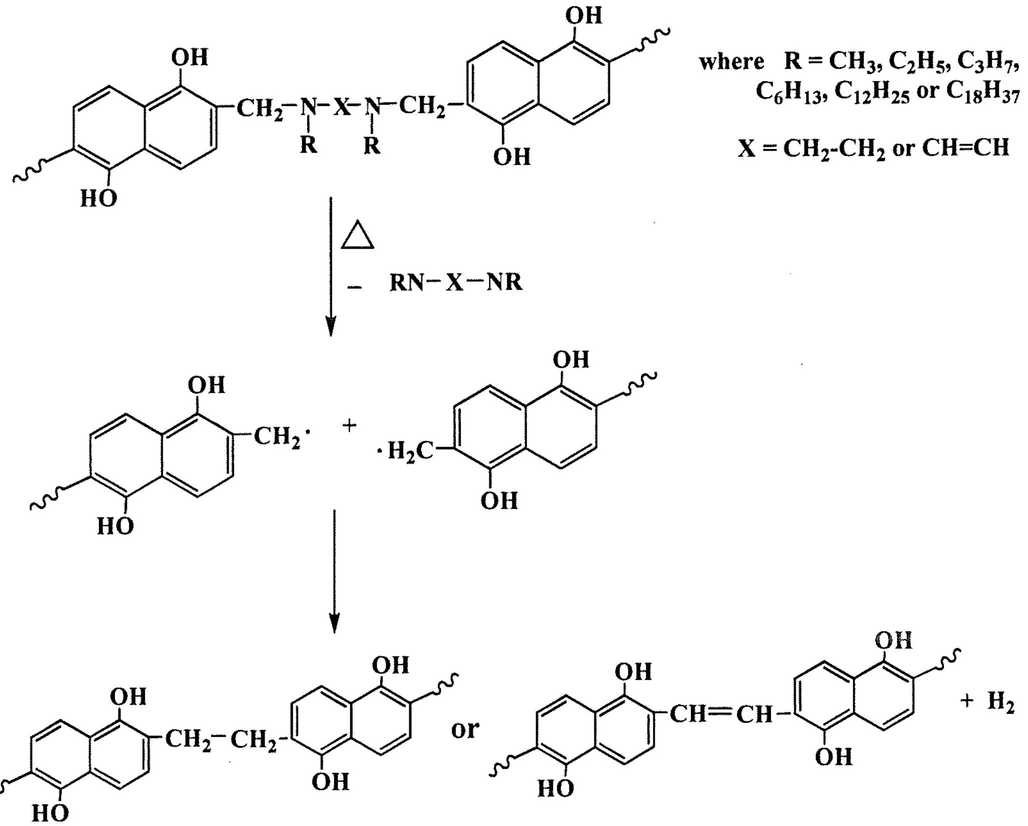

Scheme 11: Coupling of the radicals generated by lose of alkyl amines from polynaphthoxazines

The increase in char yield determined by TGA analyses with the decrease in alkyl chain length can directly be attributed to generation of crosslinked structures upon loss of alkyl amines. The mass percentages of naphthoxazine units in the monomers were 25, 32, 45, 57, 62 and 69 for R= C18, C12, C6, C3, C2 and C1 respectively. On the other hand, the char yields given in the same order were 19, 29, 36, 46, 47 and 66. Thus, it can be concluded that more than 75% of the naphthoxazine units present in the monomer were crosslinked upon loss of alkyl amines and converted to char.

CHAPTER 4

CONCLUSIONS

In this work, polymerization mechanisms of aromatic (C_6H_5 or C_6F_5) and alkyl (CH_3, C_2H_5, C_3H_7, C_6H_{13}, $C_{12}H_{25}$ or $C_{18}H_{37}$) amine based naphthoxazine monomers (15-Na, 15Na-C1, 15Na-C2, 15Na-C3, 15Na-C6, 15Na-C12 and 15Na-C18) and thermal degradation mechanisms of polynaphthoxazines (P-15-Na, P-15NaF, P-15Na-C1, P-15Na-C2, P-15Na-C3, P-15Na-C6, P-15Na-C12 and P-15Na-C18) were investigated by direct pyrolysis mass spectrometry.

The results of this study can be summarized as;

Evolution of monomer and low mass aromatic or alkyl amines below the curing temperature indicated that the monomer was subjected not only to evaporation and degradation but also to polymerization during the curing process.

For 15-Na the polymerization proceeded through the aniline units, either by coupling of the radicals produced by the ring opening of the side chains or by substitution to the benzene ring of aniline. However, even if no direct evidence to confirm polymerization by attack of $-NCH_2$ groups to naphthalene ring was detected, it is not possible totally eliminate its existence.

The high yield of aniline throughout the pyrolysis indicated the decomposition of the polynaphthoxazines by elimination of aromatic amine involving linkages. Coupling of $-CH_2$ groups generated by loss of aniline, yielded naphthoxazines with unsaturated linkages that can recombine and form a crosslinked structure with higher thermal stability.

The polymerization of naphthoxazines based on alkyl amines followed opposing paths yielding some thermally less stable linkages. The main polymerization pathway was the coupling of alkyl amine radicals.

Thermal decomposition of alkyl amine based naphthoxazines was started by loss of alkyl amines and diamines. The crosslinked structures produced by coupling of the radicals generated by lose of alkyl amines decomposed at relatively high temperatures.

In general, it can be concluded that the polynaphthoxazines analyzed in this study suffer from low thermal stability so they may not be regarded as a very good candidate to be used as resins for composite preparation for the replacement of polybenzoxazines.

REFERENCES

1. Ghosh N.N., Kiskan B., Yagci Y., *Prog. Polym. Sci.,* 2007,32:1344–1391
2. Ning X., Ishida H., *J. Polym Sci, Polym Chem Ed.,* 1994;32:1121
3. Kim H. J., Brunovska Z., Ishida H., *Polymer*, 1999;40:1815
4. Ishida H., Low H. Y., *Macromolecules,* 1997;30 (4):1099-1106
5. Agag T., Takeichi T., *Macromolecules,* 2003;36 (16):6010-6017
6. Nair C. P. R., *Progress in Polymer Science*, 2004;29 (5):401-498
7. Holly F. W., Cope A. C., *J. Am. Chem. Soc.*, 1944;66:1875
8. Burke W. J., *J. Am. Chem. Soc.,* 1949;71:609
9. Burke W. J., Kolbezen M. J., Stephens C.W.J., *J. Am. Chem. Soc.,* 1952;74:3601-5
10. Burke W. J., Nurdock K. C., *J. Am. Chem. Soc.,* 1954;76:1677
11. Burke W. J., Smith R. P., Weatherbee C., *J. Am. Chem. Soc.,* 1952;74:602
12. Burke W. J., Glennie E. L. M., Weatherbeee C., *J. Org. Chem.,* 1964;29:909
13. Burke W. J., Hammer C. R., Weatherbee C., *J. Org. Chem.,* 1961;26:4403
14. Burke W. J., Nasutuvicus W. A., Weatherbee C., *J. Org. Chem.,* 1964;29:407
15. Burke W. J., Weatherbee C., *J. Am. Chem. Soc.,* 1950;72:4691-4
16. Burke W. J., Reynolds R. J., *J. Am. Chem. Soc.,* 1954;76:1291-3
17. Schreiber H., German Patent 2 255 504; 1973
18. Schreiber H, Saur W., Chem. Abst. 1990; 113: 41934c, European Patent EP 356 379
19. Riess G., Schwob J. M., Guth G., Roche M., Lande B.; Culbertson BM, McGrath JE. *Advances in Polymer Synthesis.* New York: Plenum; 1985
20. Ishida H., Allen D., *ACS Polym. Mat. Sci. Eng.,* 1995;73:496
21. Ishida H., Roduriguez Y., *Polymer*, 1995;36:3151

22. Jang J., Seo D., *J. Appl. Polym. Sci.,* 1998;67:1

23. Agag T., Takeichi T., *Macromolecules*, 2001;34:7257

24. Kimura H., Matsumoto A., Hasegawa K., Ohtsuka K., Fukuda A., *J. Appl. Polym. Sci.,* 1998;68:1903

25. Agag T., Takeichi T., *High Perform. Polym.,* 2001;13:327

26. Ishida H., Lee Y., *Polymer,* 2001;42:6971

27. Espinosa M. A., Ca'diz V., Galia M., *J. Appl. Polym. Sci.,* 2003;90:470

28. Espinosa M. A., Ca'diz V., Galia M., *J. Polym. Sci. Part A: Polym. Chem.* 2004; 42:279

29. Kim H. J., Brunovska Z., Ishida H., *J. Appl. Polym. Sci.,* 1999;73:857

30. Brunovska Z., Ishida H., *J. Appl. Polym. Sci.,*1999;73:2937

31. Kim H. J., Brunovska Z., Ishida H., *Polymer,* 1999;40:6565

32. Shen S., Ishida H., *J. Appl. Polym. Sci.,* 1996; 61:1595-1605

33. Ishida H., Sanders D. P., *J. Polym. Sci. Part B: Polym. Phys.,* 2000;38:3289

34. Allen D. J., Ishida H., *J. Polym. Sci. Part B: Polym. Phys.,* 1996;34:1019

35. Shen S. B., Ishida H., *Polym. Compos.,* 1996;17:710

36. Ishida H., Ohba S., *Polymer,* 2005;46:5588

37. Choi S. W., Ohba S., Brunovska .Z, Hemvichian K., Ishida H., *Polym. Degrad. Stab.,* 2006;91:1166

38. Kiskan B., Colak D., Muftuoglu A. E., Cianga I., Yagci Y., *Macromol. Rapid Commun.,* 2005;26:819

39. Kiskan B., Yagci Y., *Polymer,* 2005;46:11690-11697

40. Tasdelen M. A., Kiskan B., Yagci Y., *Macromol. Rapid Commun.,* 2006; 27:1539

41. Yildirim A., Kiskan B., Demirel A. L., Yagci Y., *Eur. Polym. J.,* 2006;42(11):3006-3014

42. Kiskan B., Yagci Y., Ishida H., *J. Polym. Sci. Part A: Polym. Chem.,* 2008;46:414

43. Nagai A., Kamei Y., Wang X.S., Omura M., Sudo A., Nishida H., Kawamoto E., Endo T., *J. Polym. Sci. Part A: Polym. Chem.,* 2008;46:2316

44. Oci, K., Tuboi T., Kageyama H., Shimbo M. J., *Adhesion Soc. Jpn,.* 1989;25:222

45. Kaji M., Endo T., *J. Polym. Sci. Part A: Polym. Chem.,* 1999;37:3063

46. Wang C. S., Hwang H. J., *J. Polym. Sci. Part A: Polym. Chem.,* 1996;34:1493

47. Sirkecioglu O., Andresen J. M., Mcrae C., Snape C. E., *J. Appl. Polym. Sci.,* 1997; 66: 663

48. Ho T. H., Wang C. S., *J. Appl. Polym. Sci.,* 1999;1905:74

49. Sun Y. M., Wang C. S., *J. Polym. Sci. Part A: Polym. Chem.,* 1996;34:1783

50. Yang C. P., Lin J. H., *J. Polym. Sci. Part A: Polym. Chem.,* 1996;34.341

51. Chen C. P., Chang T. C., *J. Polym. Sci. Part A: Polym. Chem.,* 1996;34:2857

52. Hsiao S. H., Liou G. S., Chen S. H., *J. Polym. Sci. Part A: Polym. Chem.,* 1998;36:1657

53. Leu T. S., Wang C. S., *Polymer,* 2002;43:7069

54. Hsiao S. H., Yang C. P., Chung C. L., *J. Polym. Sci. Part A: Polym. Chem.,* 2001;2003:41

55. Yang C. P., Hsiao S. H., Yang C. C., *J. Polym. Sci. Part A: Polym. Chem.,* 1998;36:919

56. Chen J. A., Yang C. P., J. *Appl. Polym. Sci.,* 2000;77:217

57. Yang C. P., Yang C. C., Chen R. S., *J. Polym. Sci. Part A: Polym. Chem.,* 2001;39:2591

58. Mercer F. W., Fone M. M., Mckenzie M. T., *J. Polym. Sci. Part A: Polym. Chem.,* 1997;35:521

59. Burke W. J., Murdock K.C., Ec G., J. Am. Chem. Soc., 1954;76:1677–9

60. Burke W. J., Nasutavicus W. A., Weatherbee C., *J. Org. Chem.* 1964;29:407–10

61. Agag T., *J. Appl. Polymer Science*, 2006;100:3769–3777

62. Shen S. B., Ishida H., *Journal of Materials Science*, 1996;31:5945-5952

63. Qian K., Killinger W. E., Casey M., *Anal. Chem.*, 1996;68:1019-1027

64. Blazso M., *J. Anal. Appl. Pyrolysis,* 1997;39:1-25

65. Tsuge S., Ohtani H., *Polym. Deg. Stab.,* 1997;58:109-130

66. Parsi Z., Górecki T., Poerschmann J., *J. Anal. Appl. Pyrolysis,* 2005;74:11-18

67. Lehrle R.S., *J. Anal. Appl. Pyrolysis,* 1997;40-41: 3-19

68. Richardson S.D., *Chem. Rev.,* 2001;101:211-254

69. Wapler T. P., *J. Anal. Appl. Pyrolysis*, 2004;71:1-12

70. The encyclopedia of mass spectrometry volume 6 ionization methods (2007); Michael L. Gross, Richard M. Caprioli pg: 926-927

71. Lattimer R. P., *J. Anal. Appl. Pyrolysis,* 1997;39:115

72. Meruva N. K., Metz L. A., Goode S. R., Morgan S. L., *J. Anal. Appl. Pyrolysis,* 2004;71:313-325

73. Oguri N., Onishi A., Uchino S., *Mass Spec.* 1992;40:41-46

74. Concetto Puglisi C., Sturiale L., Montaudo G., *Macromolecules,* 1999;32(7):2194 -2203

75. Uyar T., Koyuncu Z., Ishida H., Hacaloglu J., *Polym. Deg. Stab.,* 2008;93:2096-2103

76. Hemvichian K., Ishida H., *Polymer,* 2002;43:4391